

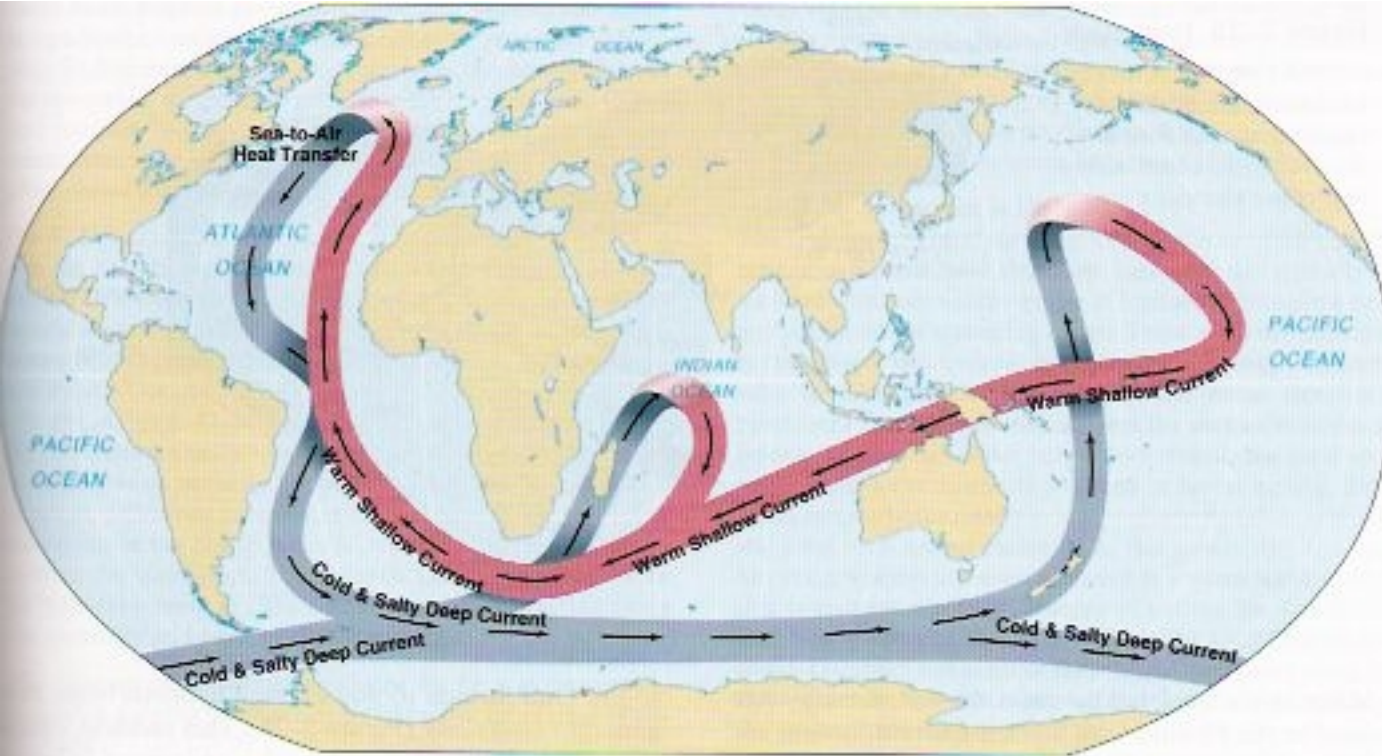
AMOC

EPS 131 intro to physical oceanography

EPS 231 Climate dynamics

Eli Tziperman

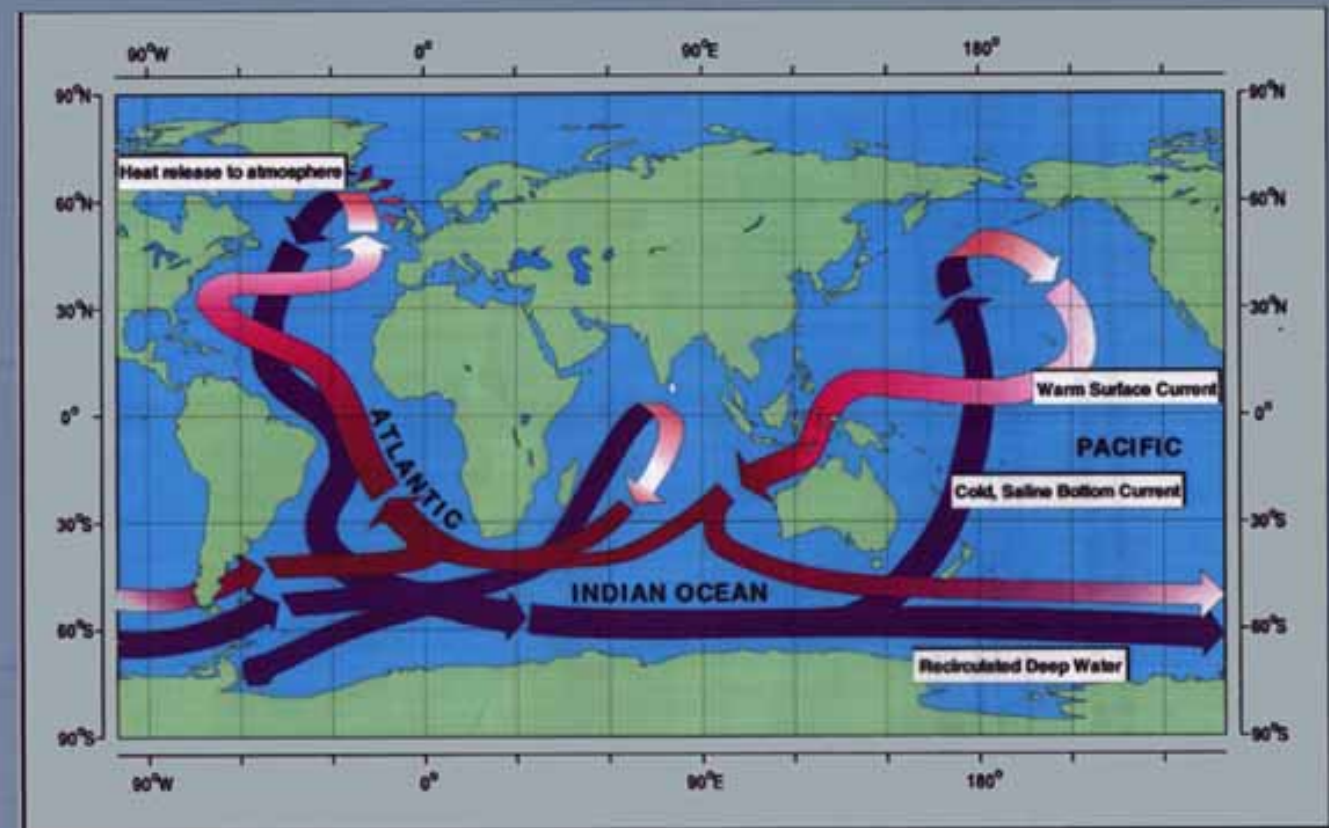
The Atlantic Meridional Overturning Circulation (AMOC)



AMOC schematics: the sinking occurs over very small high-latitude areas in the ocean. the upwelling back to the surface is very broad, over entire ocean basins, not as depicted.

The Atlantic Thermohaline Circulation

- A key Element of the Global Oceanic Circulation -



Schematic diagram of the global ocean circulation pathways, the 'conveyor' belt (after W. Broecker, modified by E. Maier-Reimer).

The Atlantic Meridional Overturning Circulation (AMOC)

Plate 9. A 2-layer thermohaline conveyor belt. Blue: abyssal water (deep & bottom layers), red: uppermost layer flow (thermocline & intermediate water); transports in Sverdrup circled.

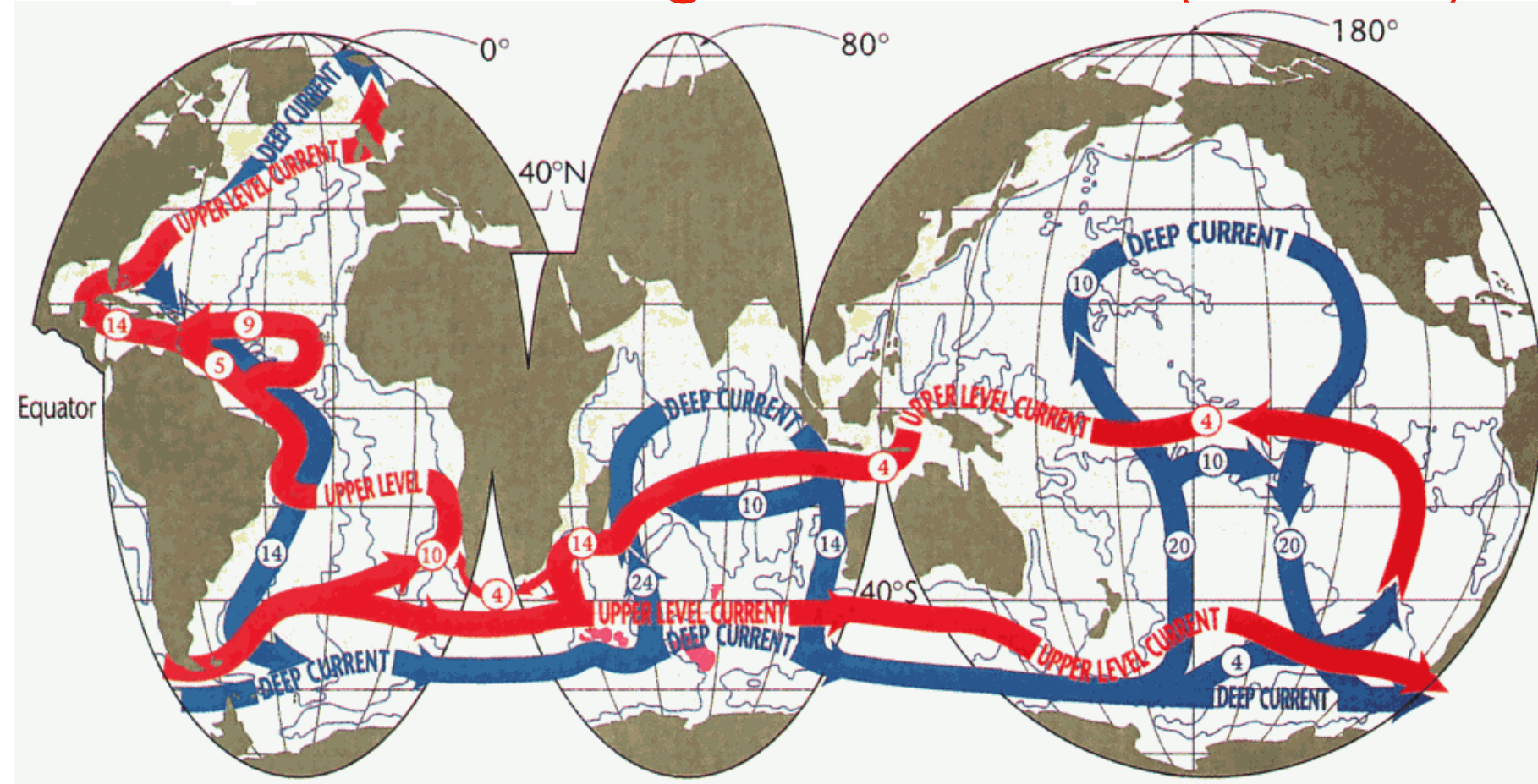
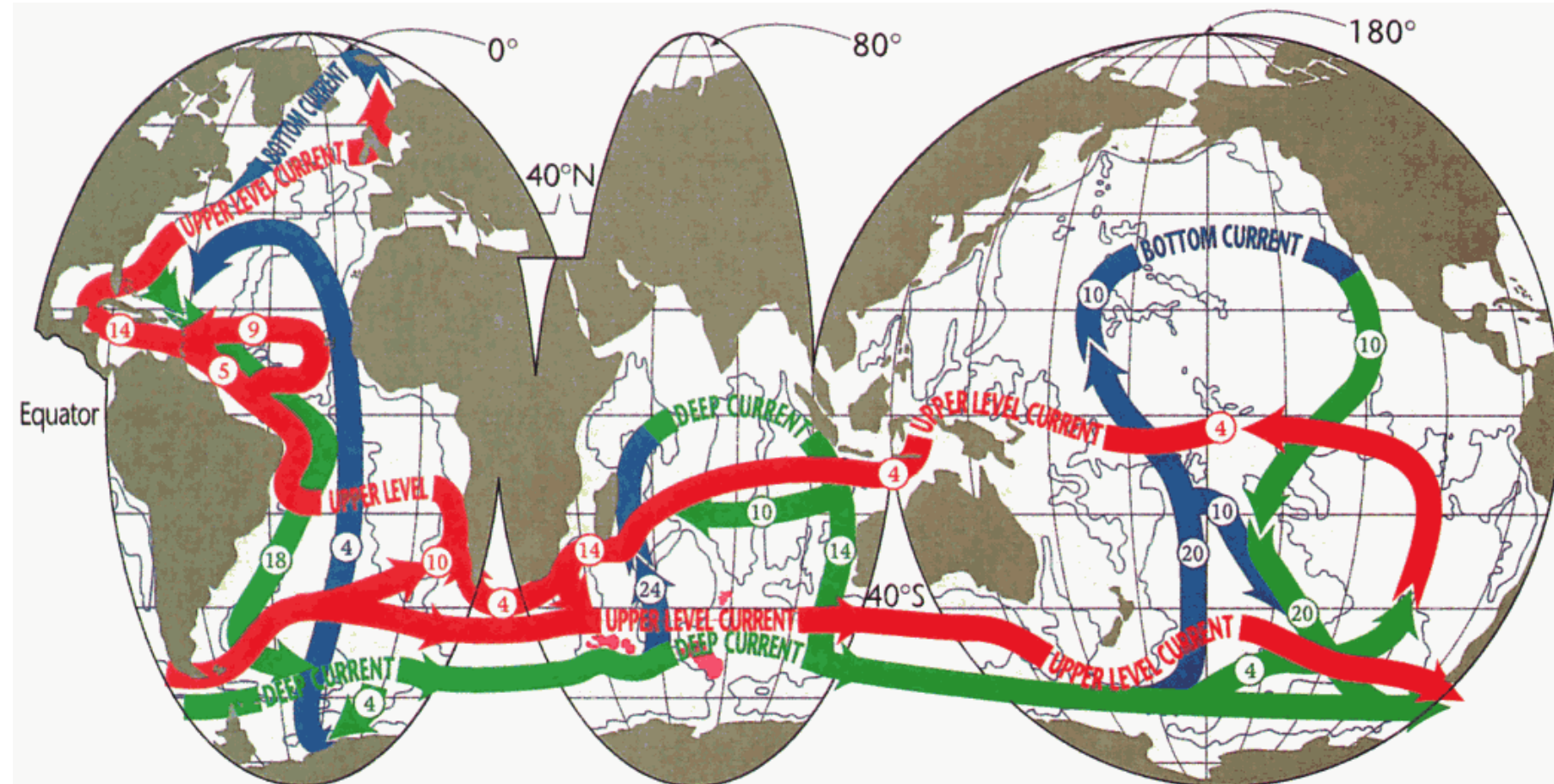
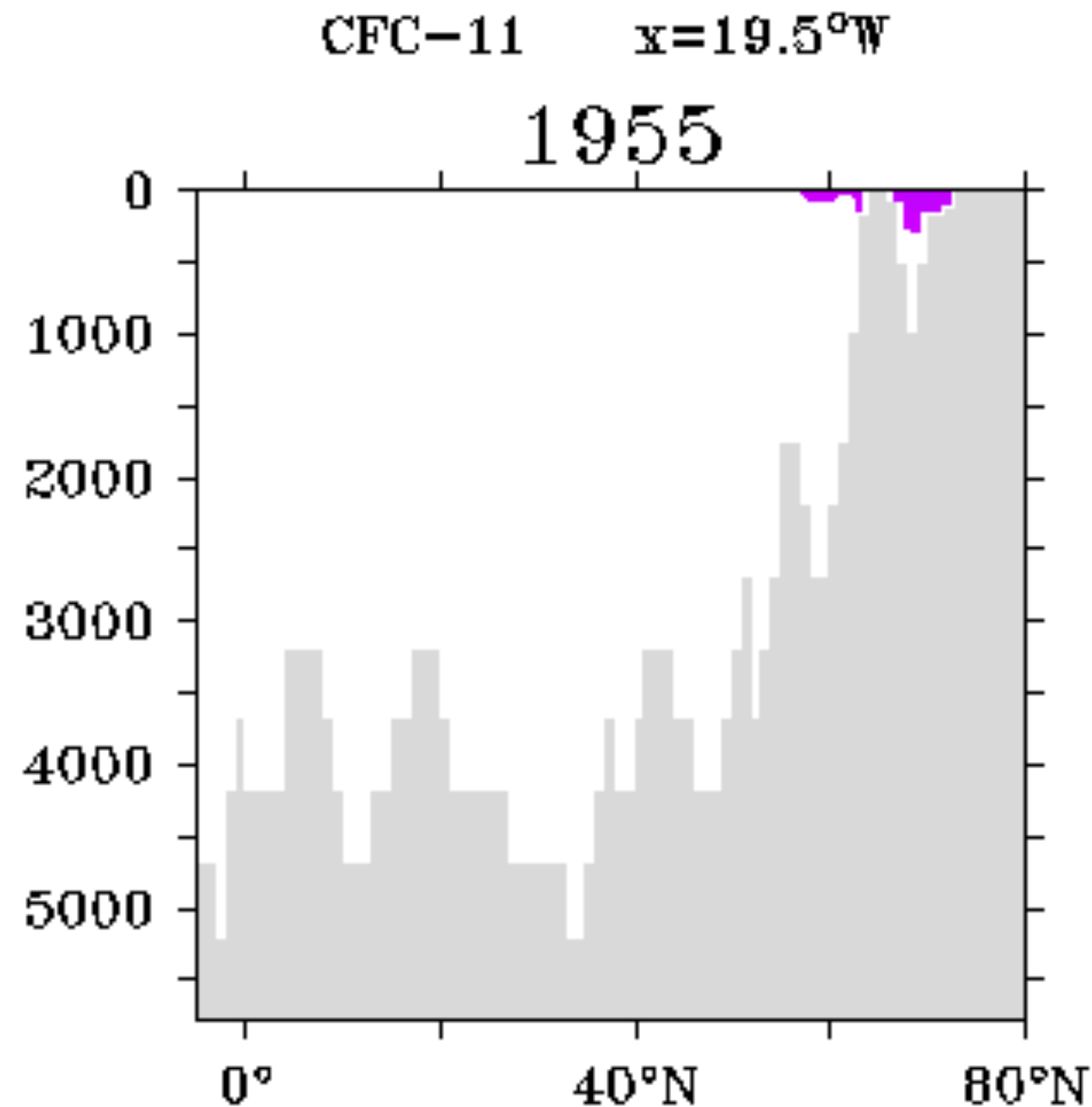


Plate 10. A 3-layer thermohaline conveyor belt. red: thermocline & intermediate layers, green: deep flow, blue: bottom circulation.



Schmitz 1995

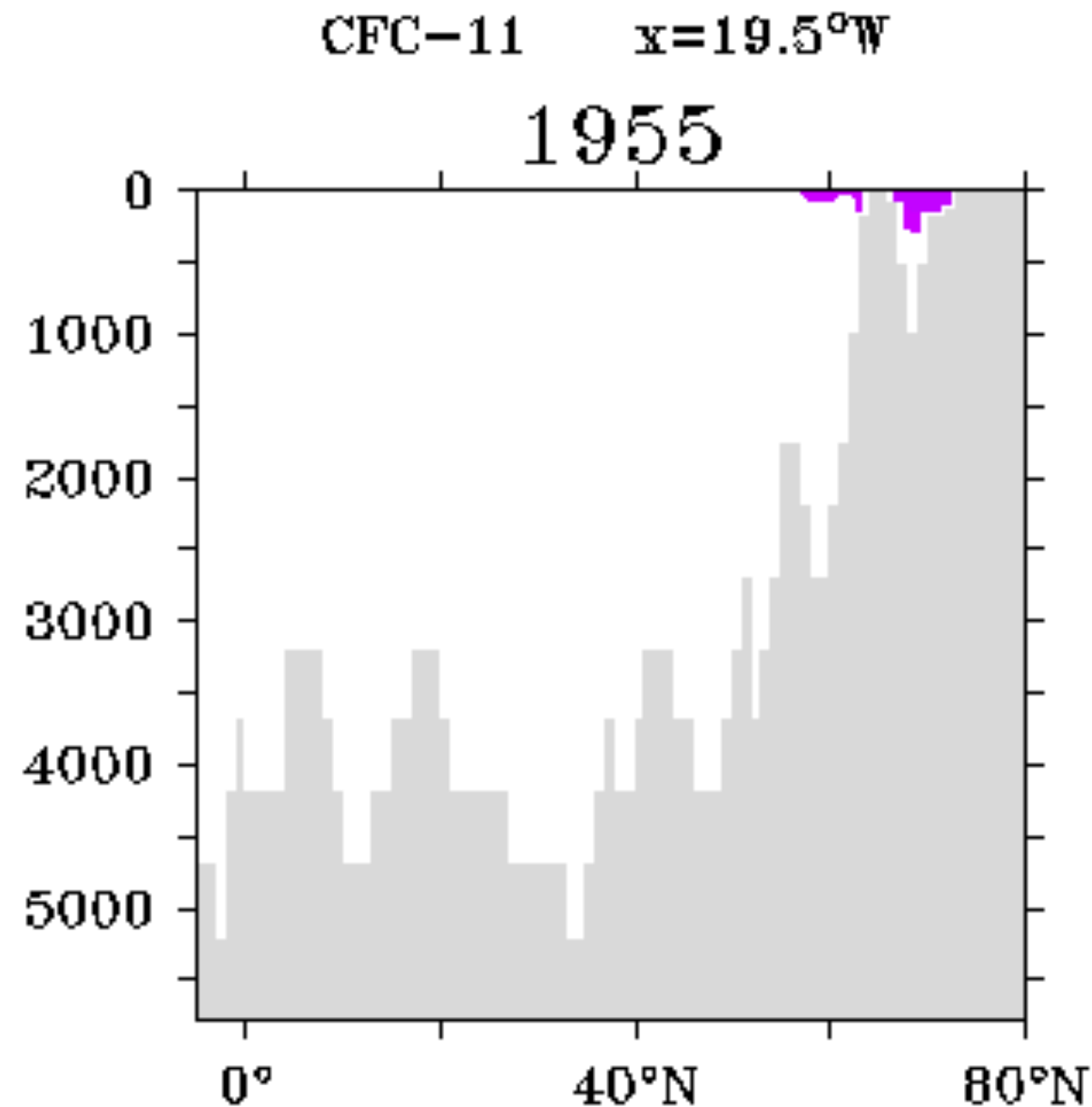
The Atlantic Meridional Overturning Circulation (AMOC)



Observations of CFC spreading in the North Atlantic Ocean, showing the sinking of deep water there.

<http://puddle.mit.edu/~mick/cfcsec.html>
(link does not work anymore?)

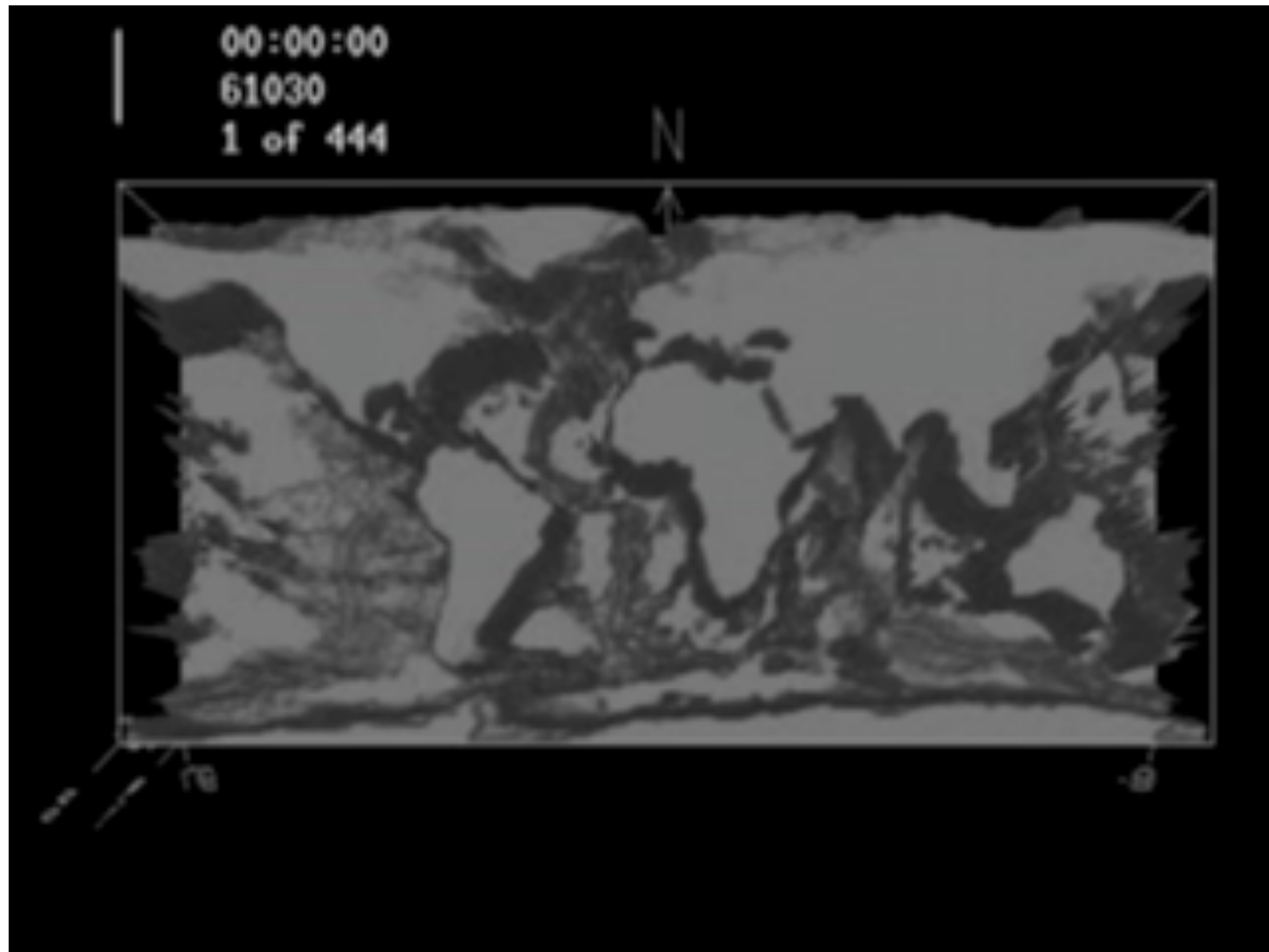
The Atlantic Meridional Overturning Circulation (AMOC)



Observations of CFC spreading in the North Atlantic Ocean, showing the sinking of deep water there.

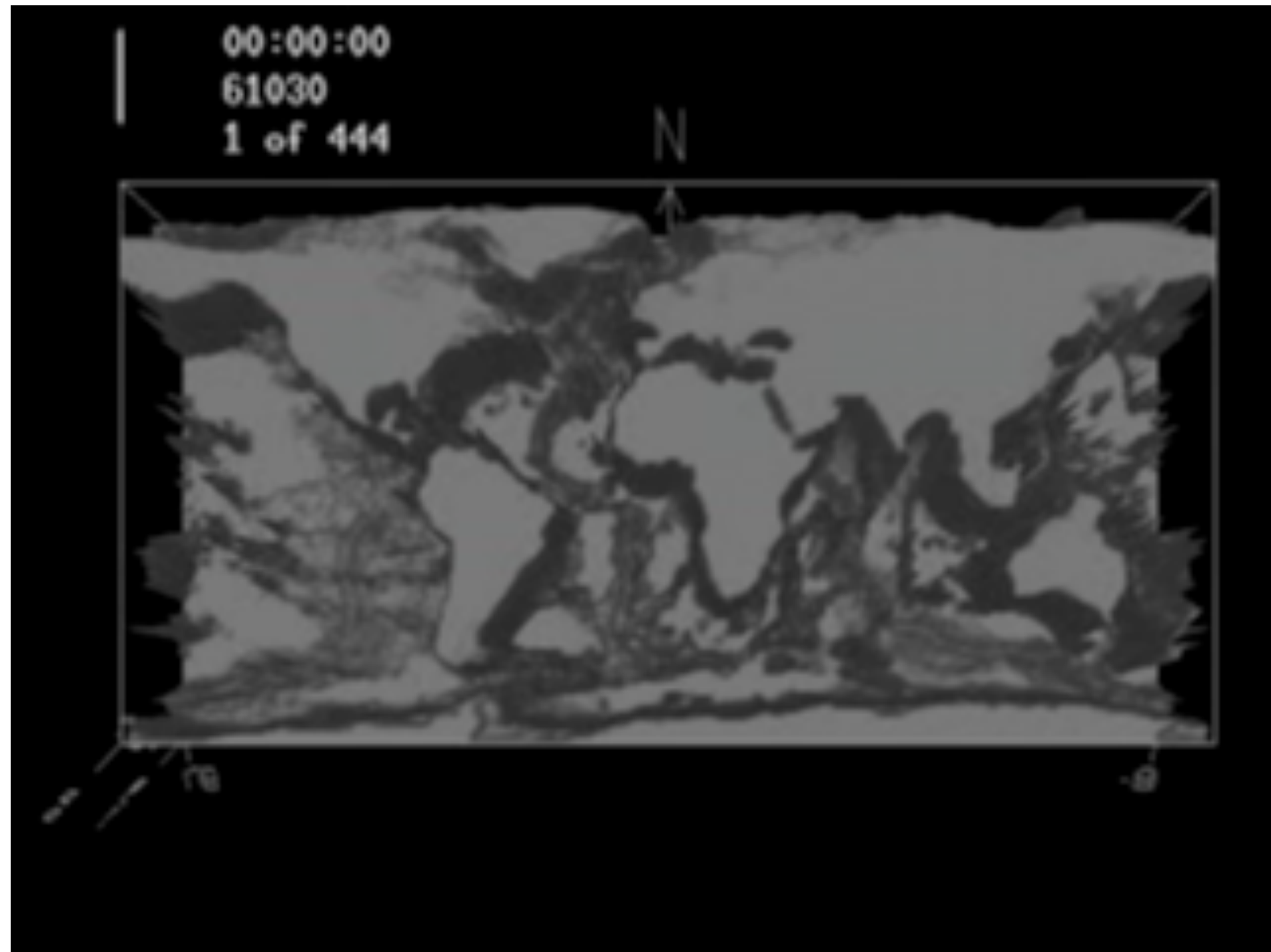
<http://puddle.mit.edu/~mick/cfcsec.html>
(link does not work anymore?)

The Atlantic Meridional Overturning Circulation (AMOC)



Simulation of tracer spreading in deep ocean

The Atlantic Meridional Overturning Circulation (AMOC)



Simulation of tracer spreading in deep ocean

The Atlantic Meridional Overturning Circulation in the news

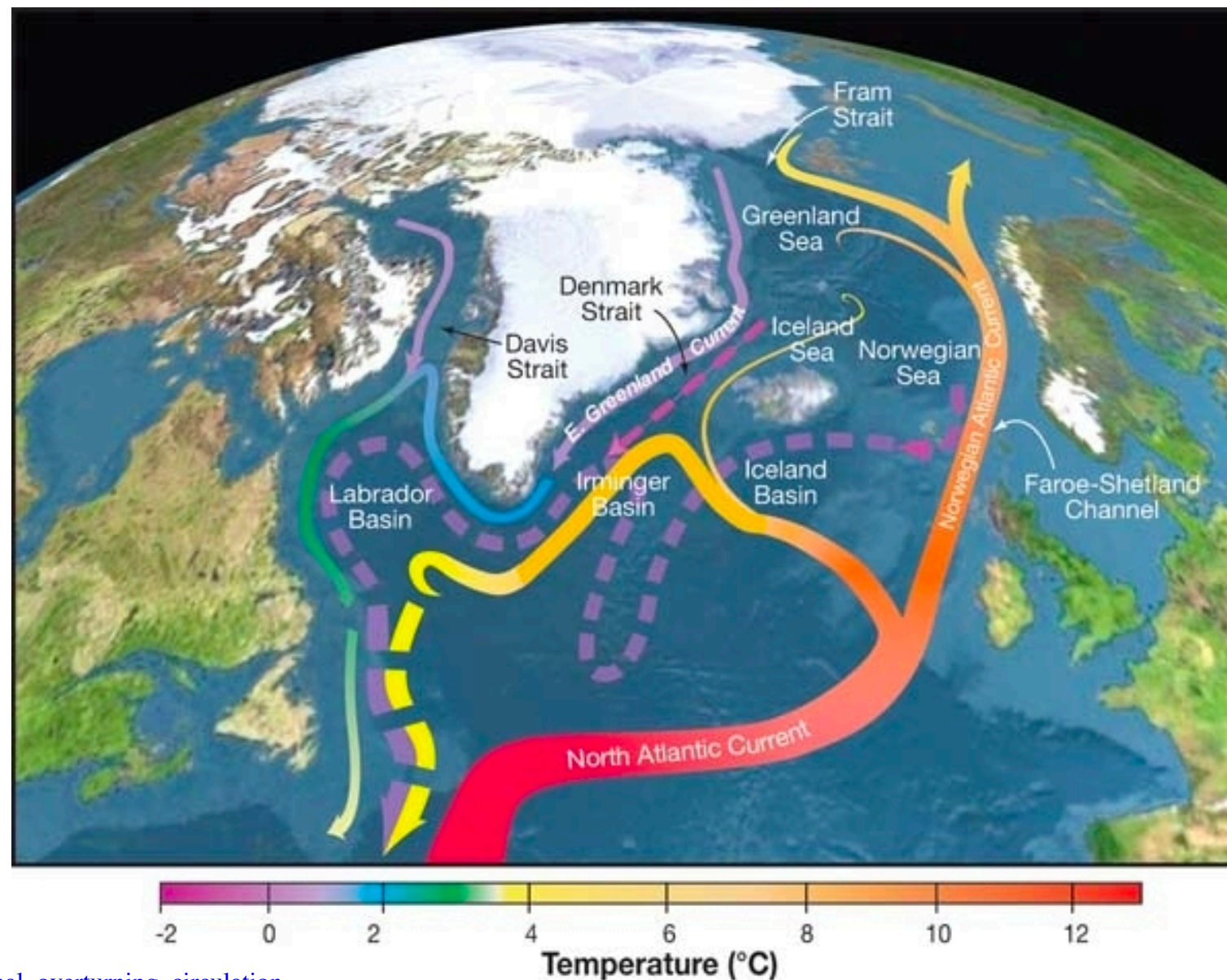
The New York Times

Atlantic Ocean current shows weakening signs

By Andrew C. Revkin

Nov. 30, 2005

NEW YORK — Atlantic Ocean currents that make Northern Europe warmer than it would otherwise be have weakened by about a third over the last 50 years, British oceanographers are reporting.



The day after tomorrow (2004)

https://www.youtube.com/watch?v=Ku_lseK3xTc

The day after tomorrow (2004)

https://www.youtube.com/watch?v=Ku_lseK3xTc

A news update about AMOC

The New York Times

Atlantic Ocean current shows weakening signs

By Andrew C. Revkin

Nov. 30, 2005



NEW YORK — Atlantic Ocean currents that make Northern Europe warmer than it would otherwise be have weakened by about a third over the last 50 years, British oceanographers are reporting.

A news update about AMOC

The New York Times

Atlantic Ocean current shows weakening signs

By Andrew C. Revkin

Nov. 30, 2005



NEW YORK — Atlantic Ocean currents that make Northern Europe warmer than it would otherwise be have weakened by about a third over the last 50 years, British oceanographers are reporting.

The New York Times

Scientists Back Off Theory of a Colder Europe in a Warming World

May 15, 2007



Gradual melting of the Greenland ice sheet, above left, might weaken the North Atlantic Current, which bathes parts of Europe with equatorial water. But any cooling effect in Europe would be overwhelmed by a general warming of the atmosphere.

Is the Atlantic Meridional Overturning Circulation collapsing already due to global warming??

Table 1 | Meridional transport in depth classes across 25° N

	1957	1981	1992	1998	2004
Shallower than 1,000 m depth					
Gulf Stream and Ekman	+35.6	+35.6	+35.6	+37.6	+37.6
Mid-ocean geostrophic	-12.7	-16.9	-16.2	-21.5	-22.8
Total shallower than 1,000 m	+22.9	+18.7	+19.4	+16.1	+14.8
1,000-3,000 m	-10.5	-9.0	-10.2	-12.2	-10.4
3,000-5,000 m	-14.8	-11.8	-10.4	-6.1	-6.9
Deeper than 5,000 m	+2.4	+2.1	+1.2	+2.2	+2.5

Values of meridional transport are given in Sverdrups. Positive transports are northward.

(Bryden et al 2005)

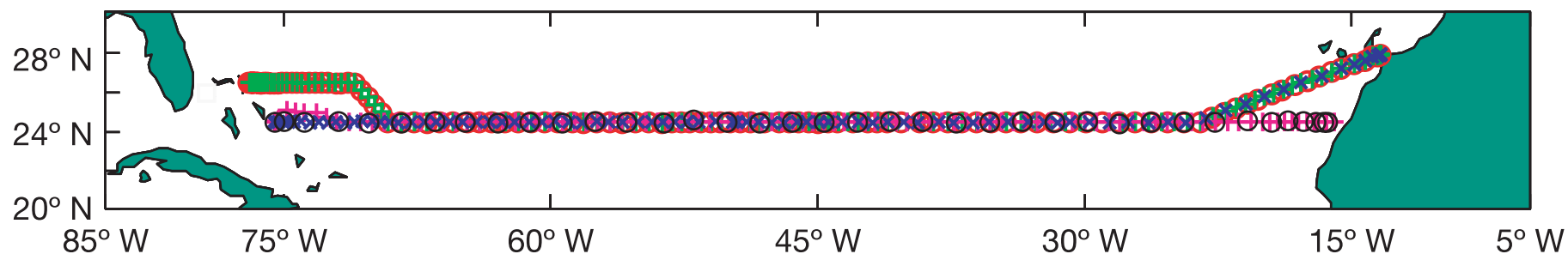


Figure 1 | Station positions for transatlantic hydrographic sections taken in 1957, 1981, 1992, 1998 and 2004. The 1957 and 1992 sections each went zonally along 24.58 N from the African coast to the Bahama Islands. Because of diplomatic clearance issues, the 1981, 1998 and 2004 sections angled southwestward from the African coast at about 28° N to join the 24.58 N section at about 23° W. The 1998 and 2004 sections angled northwestward at about 73° W to finish the section along 26.58 N.

Trying to estimate the warming effect of the Atlantic Meridional Overturning Circulation (AMOC)

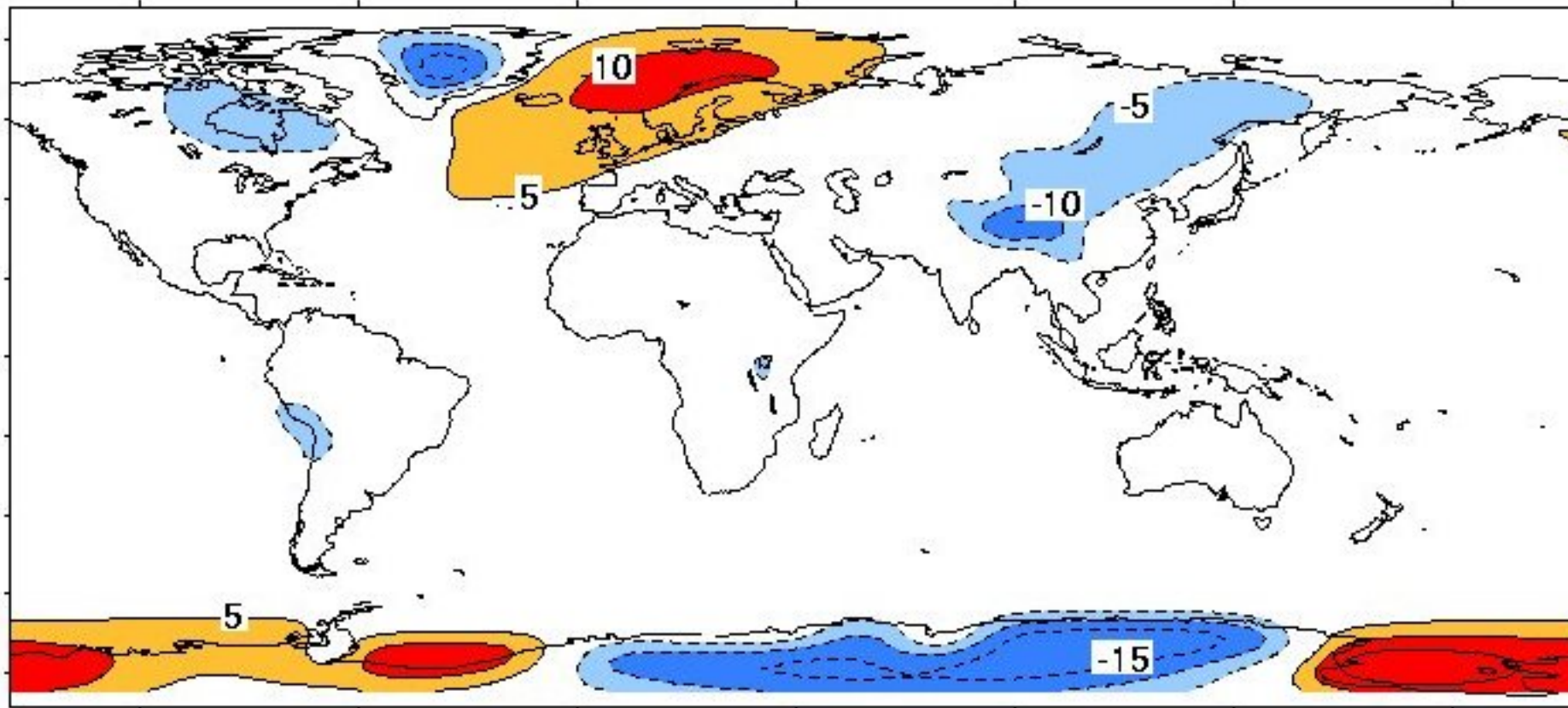


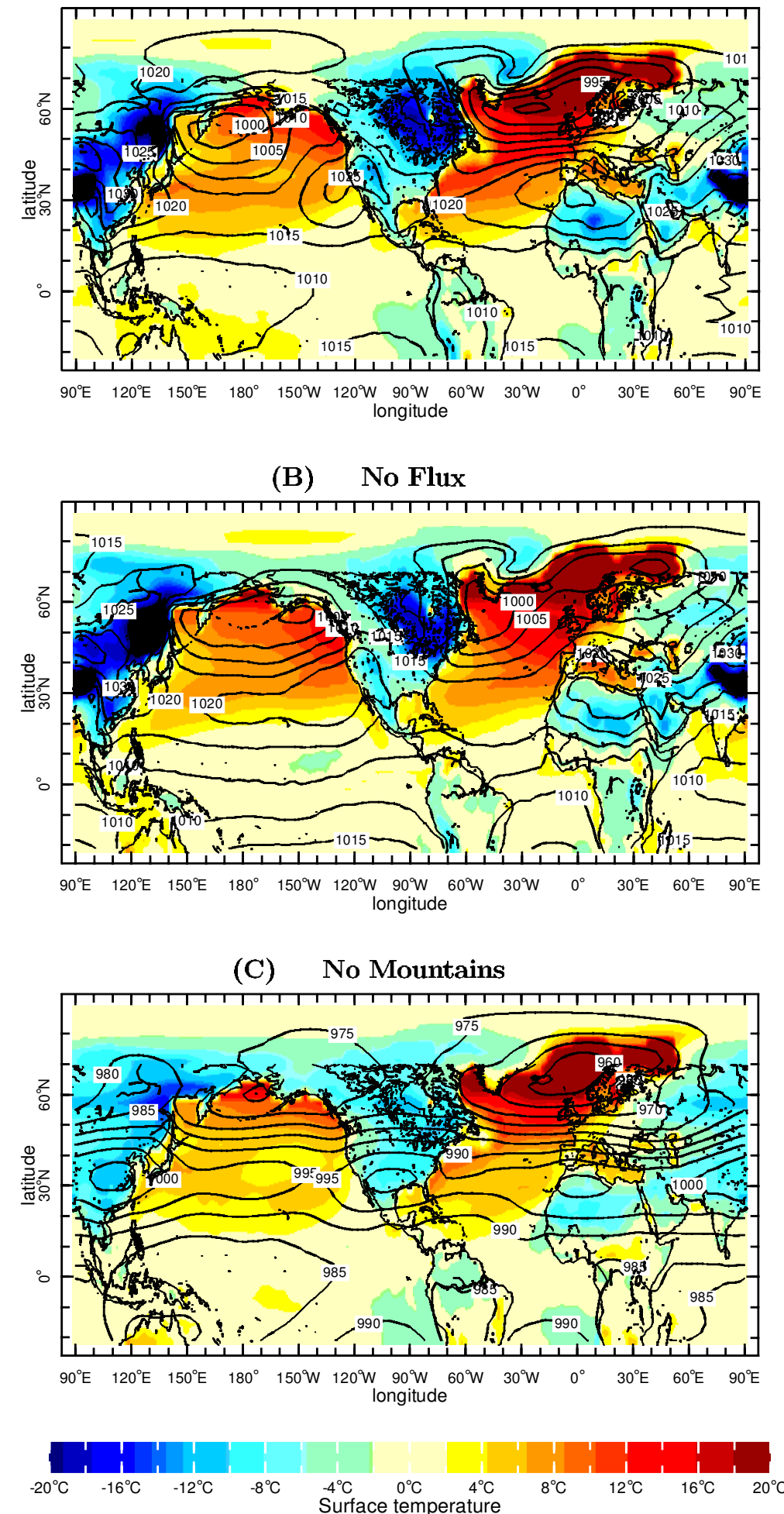
Figure 1. Deviation of the annual-mean surface air temperature from its zonal average, computed from the NCAR air temperature climatology. Anomalously cold areas are found over some continental regions, anomalously warm areas over ocean deep water formation regions.

[Whether this pattern should be attributed to the AMOC is debatable, see next slide.]

Is the Gulf Stream responsible for Europe's mild winters?

SEAGER, BATTISTI, YIN, GORDON, NAIK, CLEMENT & CANE, 2002

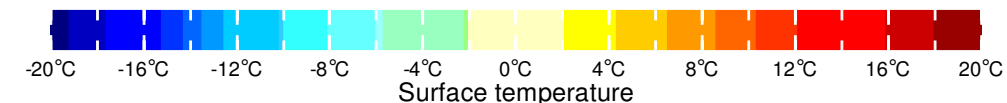
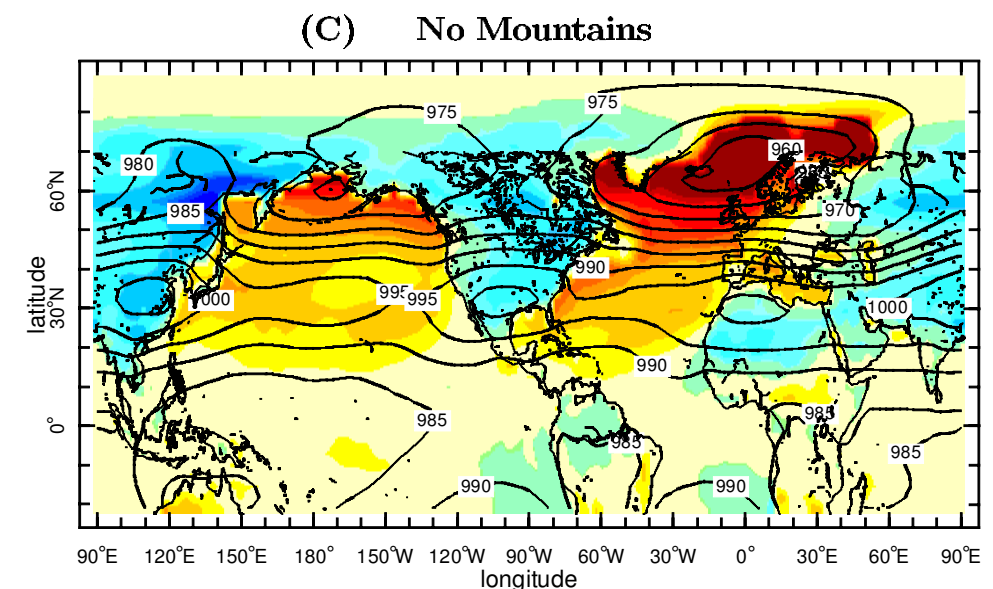
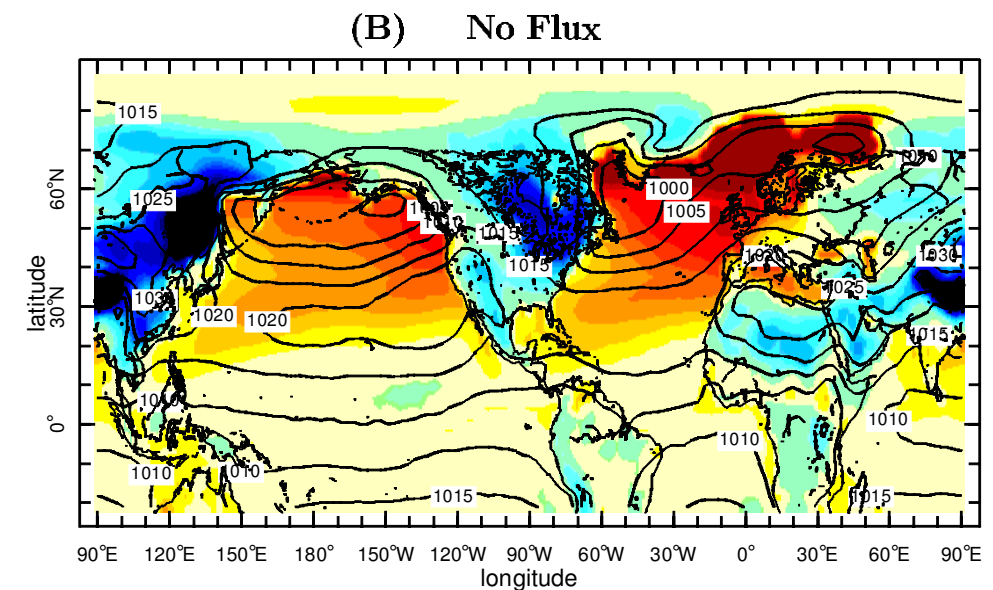
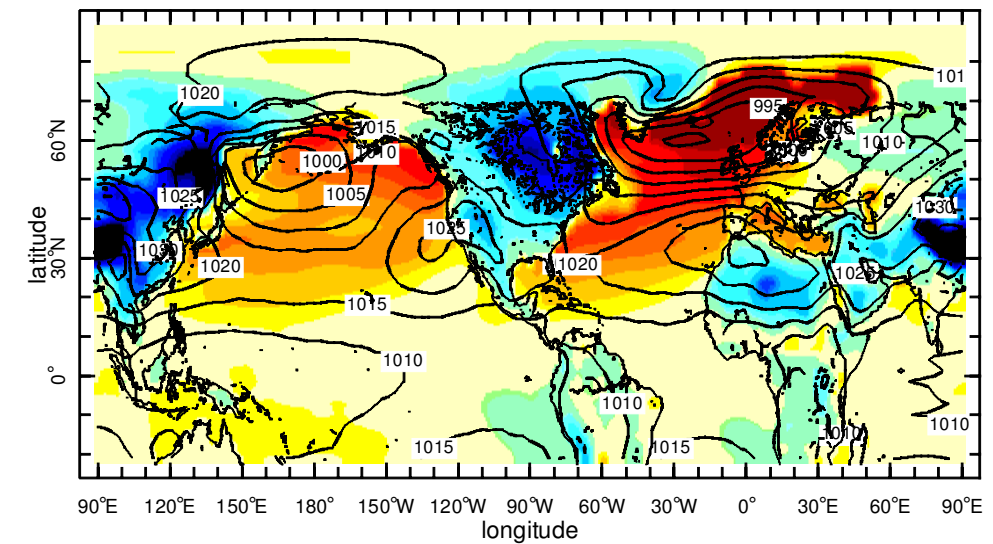
Figure 14. Sea-level pressure (mb) and zonal eddy surface temperature in degC (colours) for January for (a) the case with mountains and q-flux, (b) the case with mountains and the q-flux set to zero, and (c) the case without mountains but with the q-flux.



Is the Gulf Stream responsible for Europe's mild winters?

SEAGER, BATTISTI, YIN, GORDON, NAIK, CLEMENT & CANE, 2002

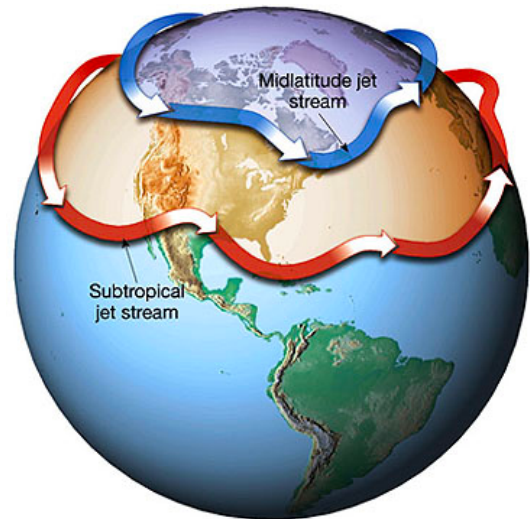
Figure 14. Sea-level pressure (mb) and zonal eddy surface temperature in degC (colours) for January for (a) the case with mountains and q-flux, (b) the case with mountains and the q-flux set to zero, and (c) the case without mountains but with the q-flux.



https://www.youtube.com/watch?v=huweohIh_Bw

➔ (some of) Europe's warmth relative to same latitude in North America is attributed to the position of the atmospheric jet stream, which is, in turn, affected by the Rocky mountains.

<https://www.constantinalexander.net/2013/02/ozone-depletion-trumps-greenhouse-gas-increase-in-jet-stream-shift.html>



Observing the Atlantic Meridional Overturning Circulation

RAPID: monitoring the Atlantic Meridional Overturning Circulation at 26.5°N

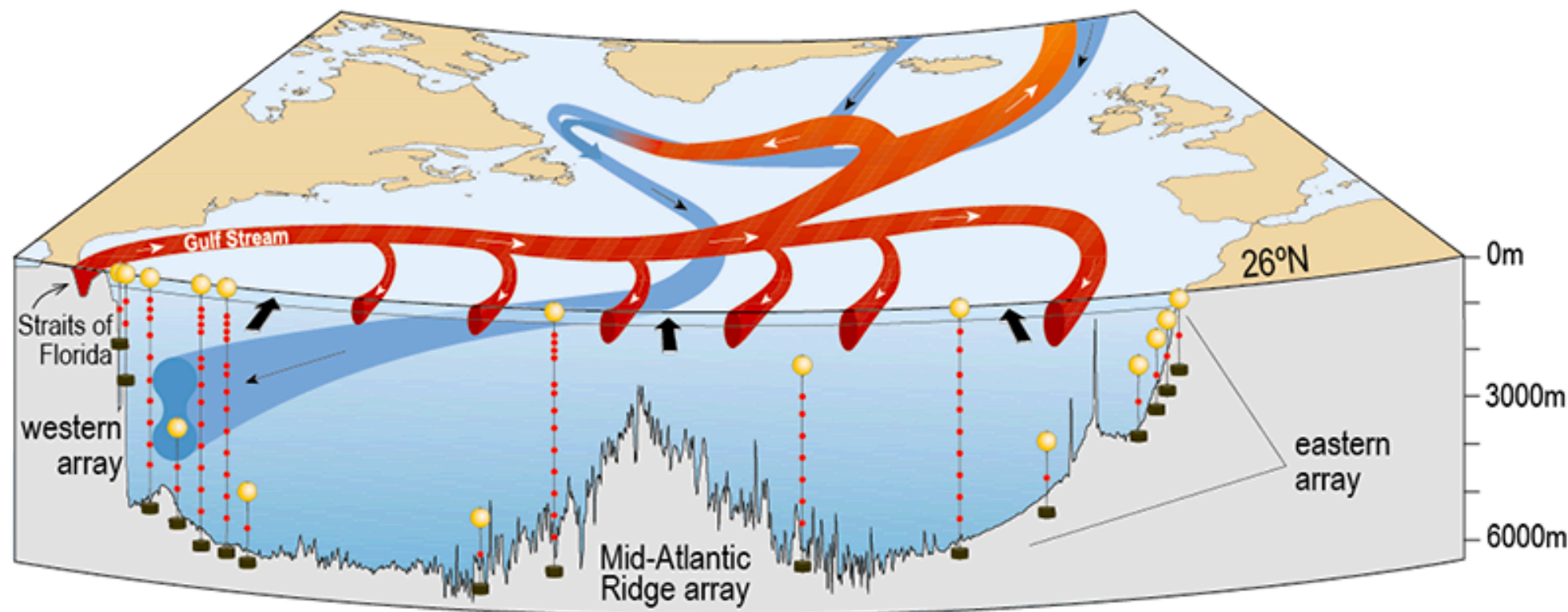
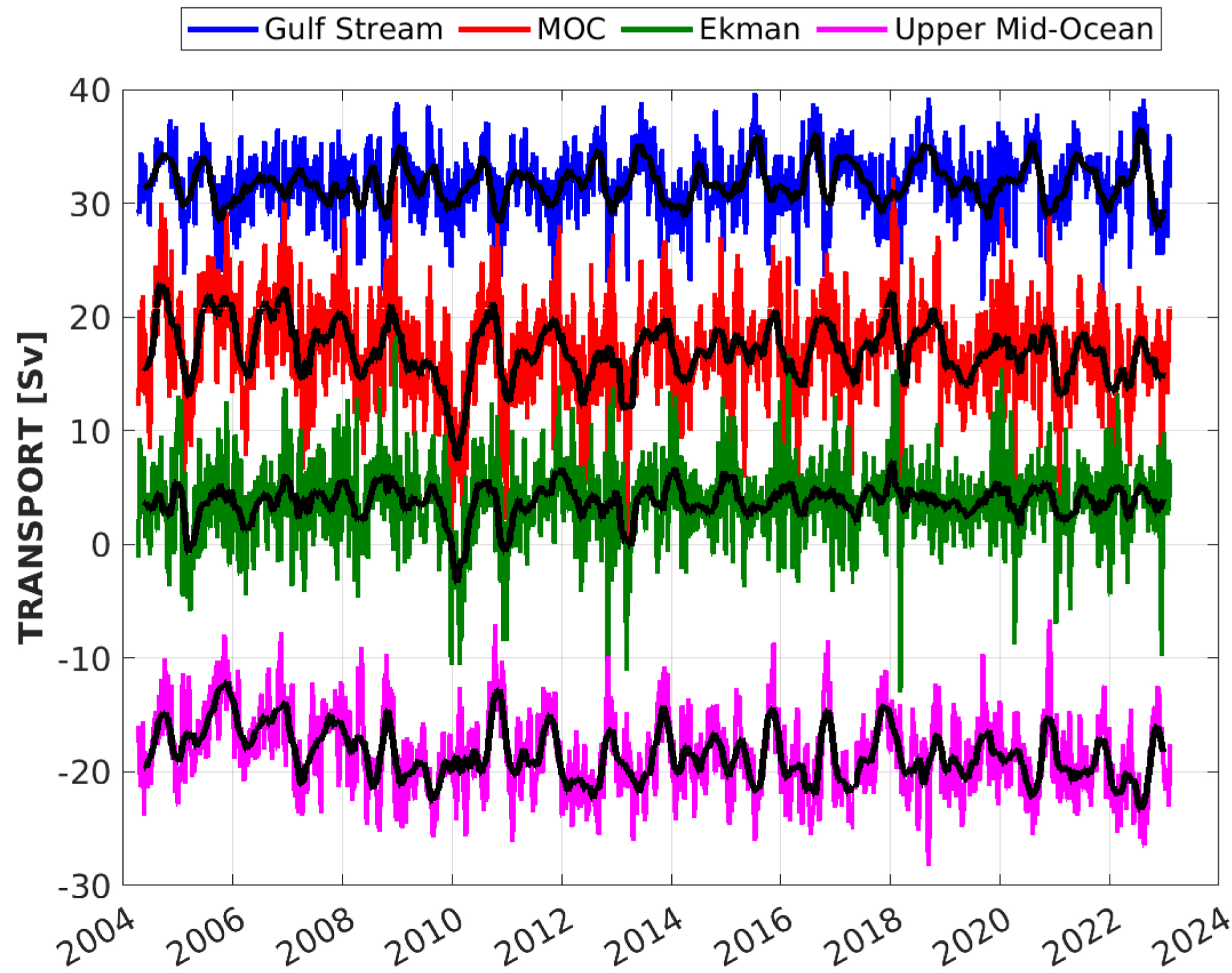


Figure 5. The North Atlantic overturning circulation with the location of the RAPID array moorings along 26°N. Modified from Church, 2007.

A view of the back deck of the RRS James Cook during the RAPID cruise in April 2014.



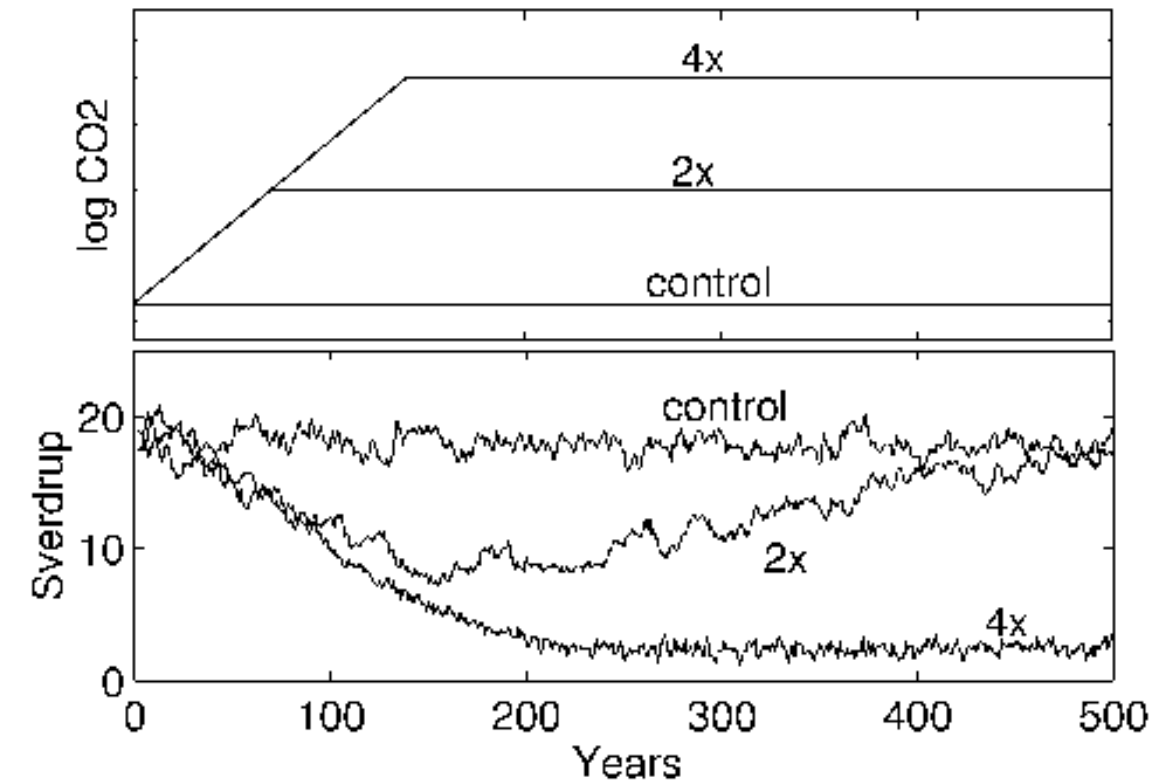
RAPID: monitoring the Atlantic Meridional Overturning Circulation at 26.5°N



The Atlantic Meridional Overturning Circulation Under a future climate change

Collapse of the Atlantic Meridional Overturning Circulation (AMOC) in a global warming scenario

Manabe and Stouffer 1993



Collapse of the Atlantic Meridional Overturning Circulation (AMOC) in a global warming scenario

Manabe and Stouffer 1993

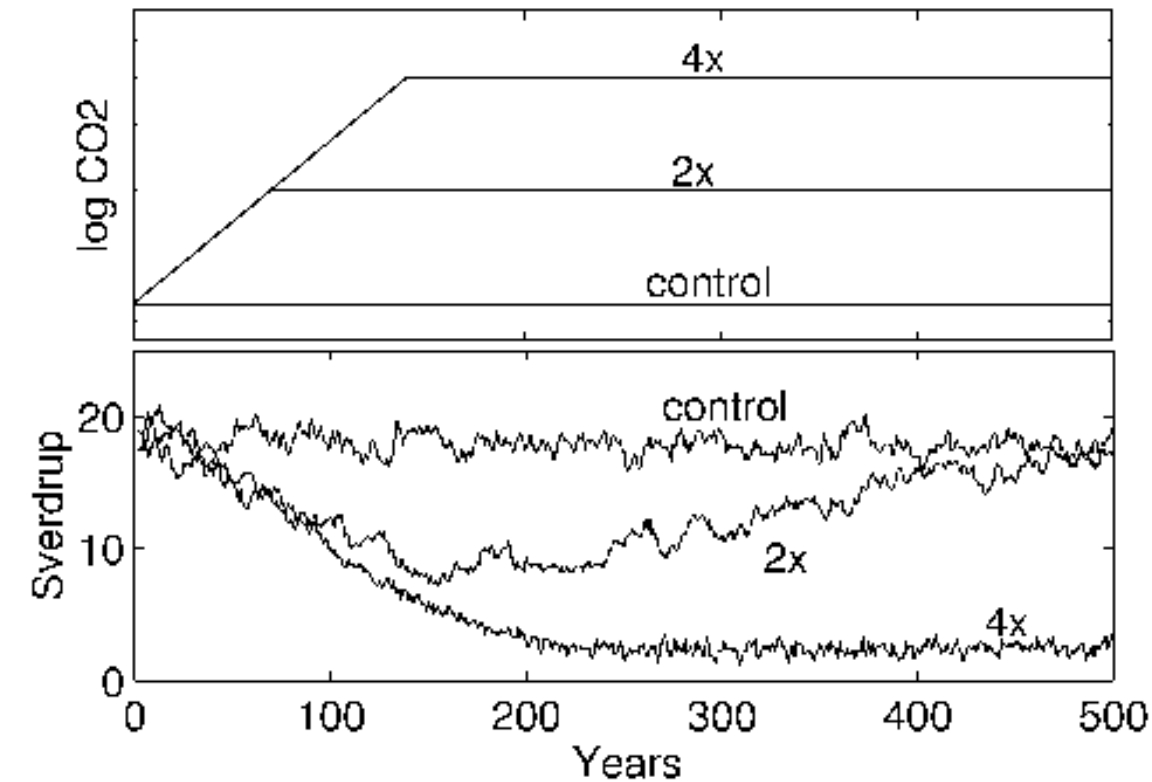
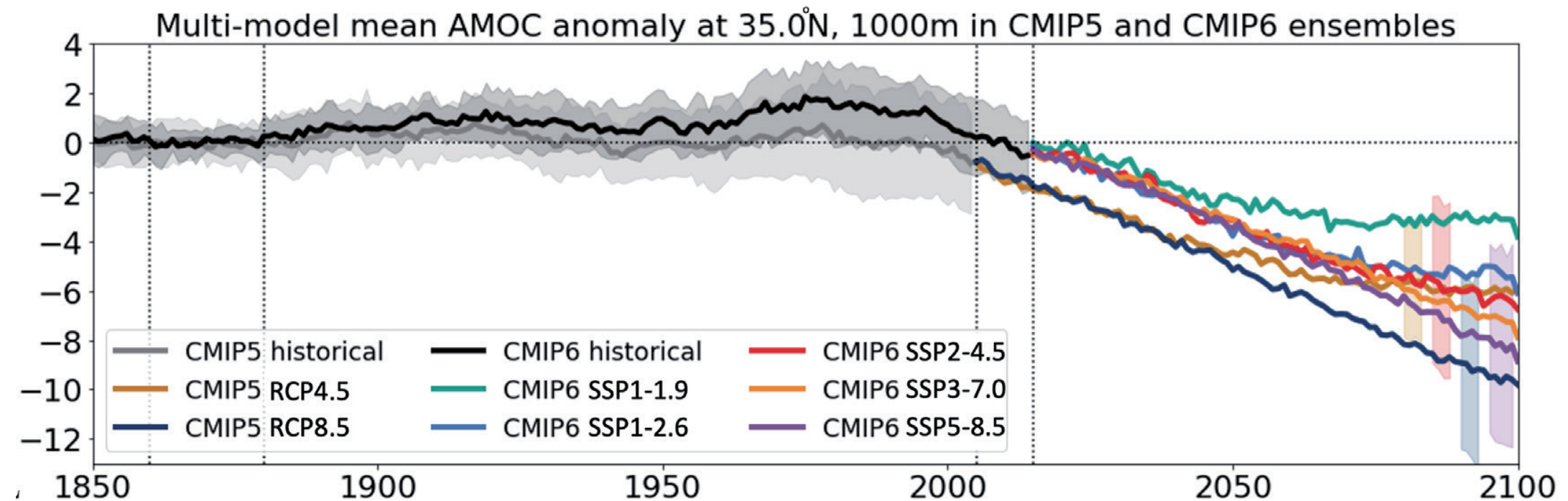


Figure 9.10 | Atlantic Meridional Overturning Circulation (AMOC) strength in simulations and sensitivity to resolution and forcing. Time series of AMOC from Coupled Model Inter-comparison Project Phase 5 & 6 (CMIP5 & CMIP6) based on (Menary et al., 2020b).

[IPCC AR6, 2022]



Collapse of the Atlantic Meridional Overturning Circulation (AMOC) in a global warming scenario

The Atlantic Meridional Overturning Circulation (AMOC) in the IPCC report

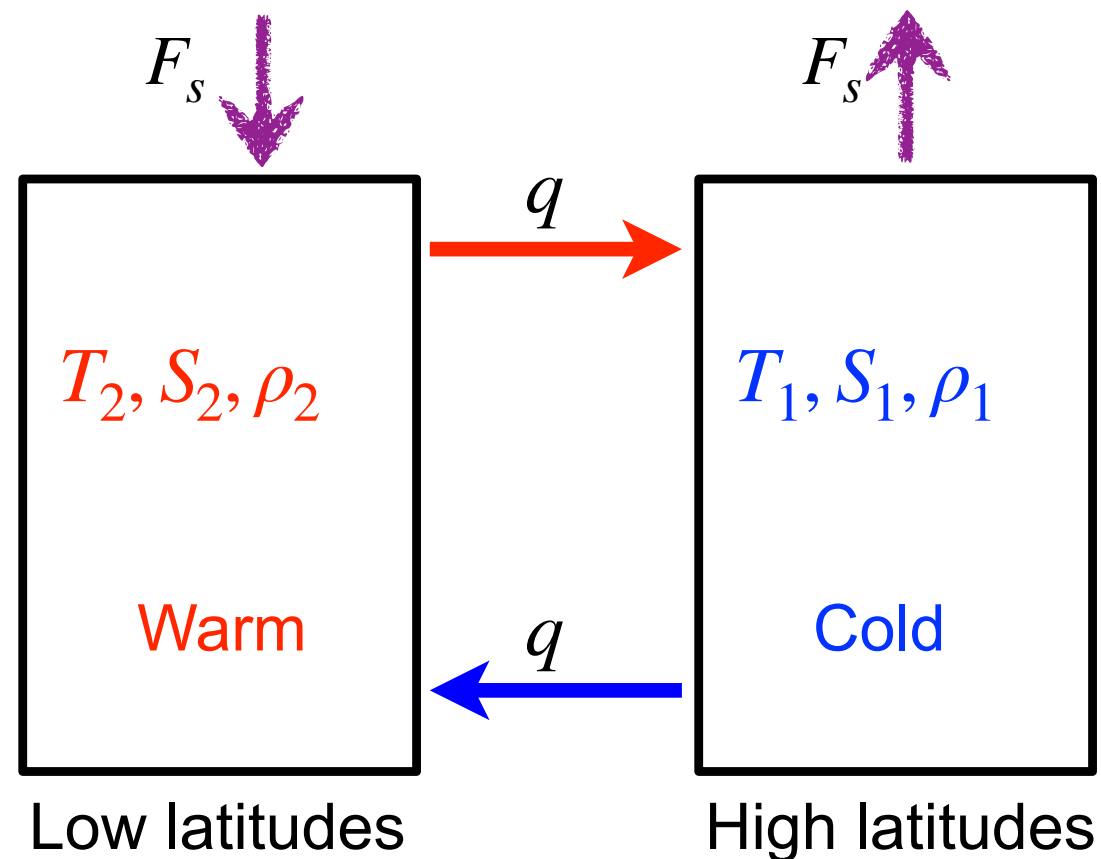
- “There is no observational evidence of a trend in the Atlantic Meridional Overturning Circulation (AMOC), based on the decade-long record of the complete AMOC and longer records of individual AMOC components. {3.6}”

The Atlantic Meridional Overturning Circulation (AMOC) in the IPCC report

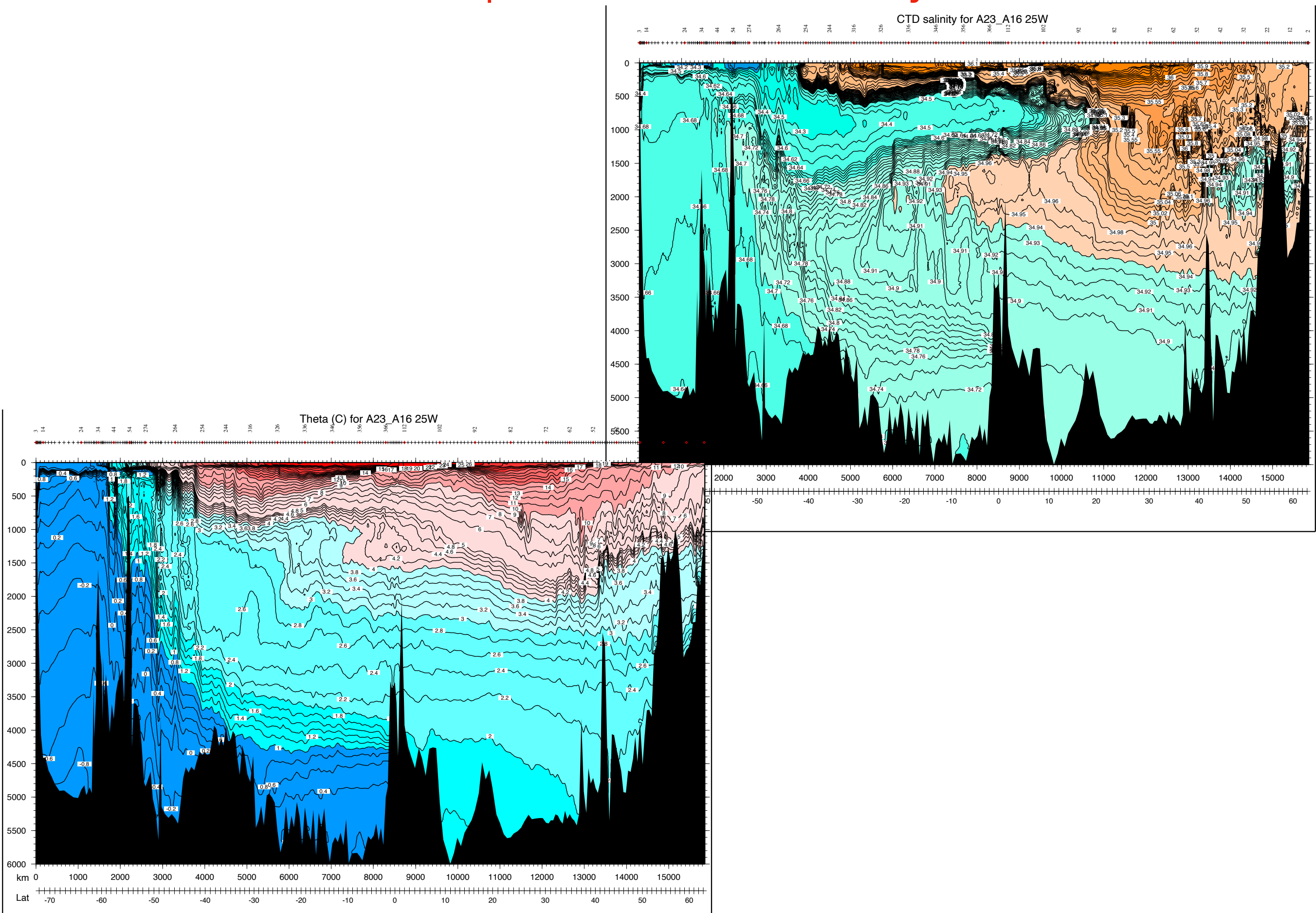
- “There is no observational evidence of a trend in the Atlantic Meridional Overturning Circulation (AMOC), based on the decade-long record of the complete AMOC and longer records of individual AMOC components. {3.6}”
- “It is very likely that the Atlantic Meridional Overturning Circulation (AMOC) will weaken over the 21st century. Best estimates and ranges for the reduction are 11% (1 to 24%) in RCP2.6 and 34% (12 to 54%) in RCP8.5. It is likely that there will be some decline in the AMOC by about 2050, but there may be some decades when the AMOC increases due to large natural internal variability. {11.3, 12.4}”

notes section 6.2:

The Stommel model (Marotzke's simplification),
understanding AMOC tipping points
(use next slides)



Atlantic temperature and salinity, WOCE



Multiple equilibria and hysteresis of the Atlantic Meridional Overturning Circulation (AMOC)

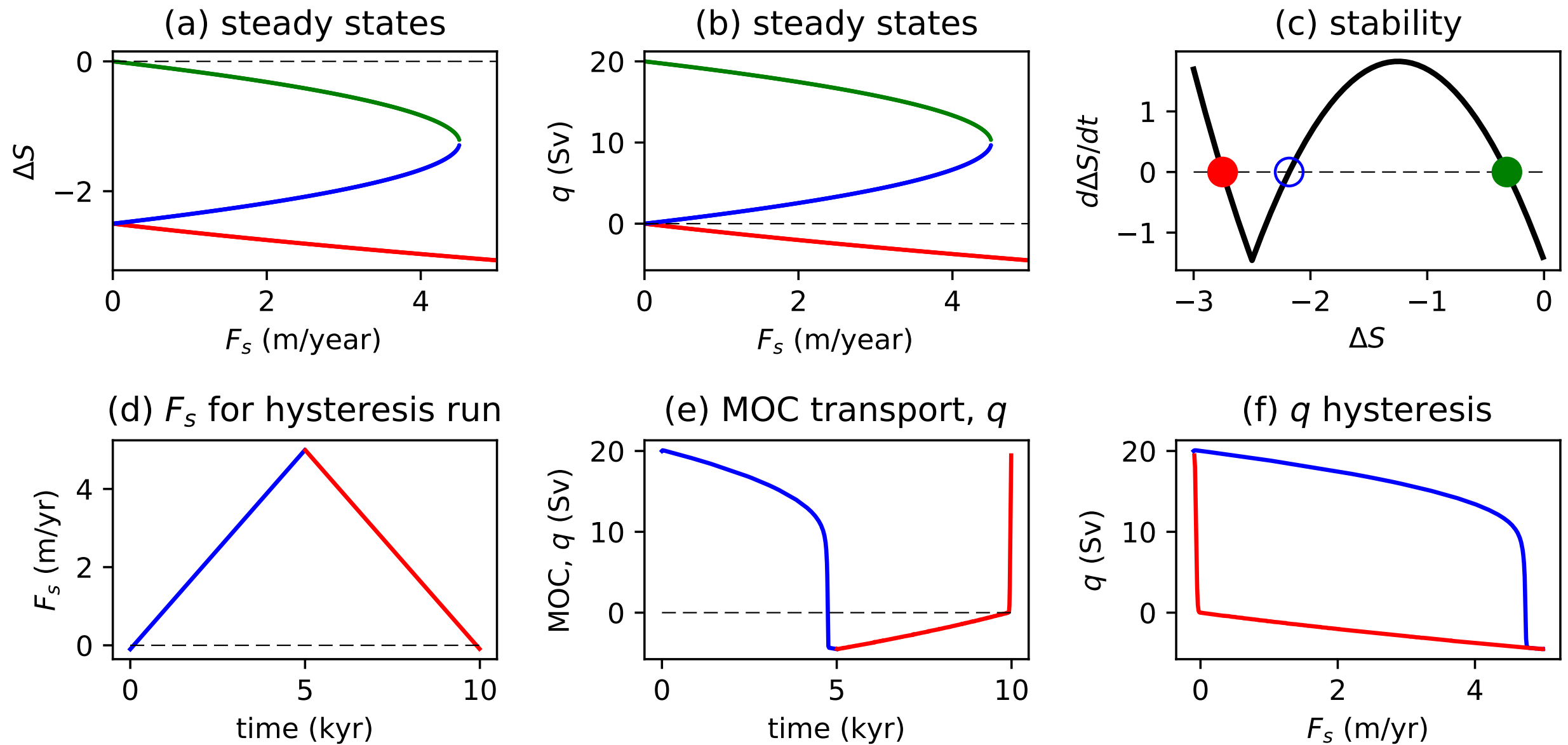
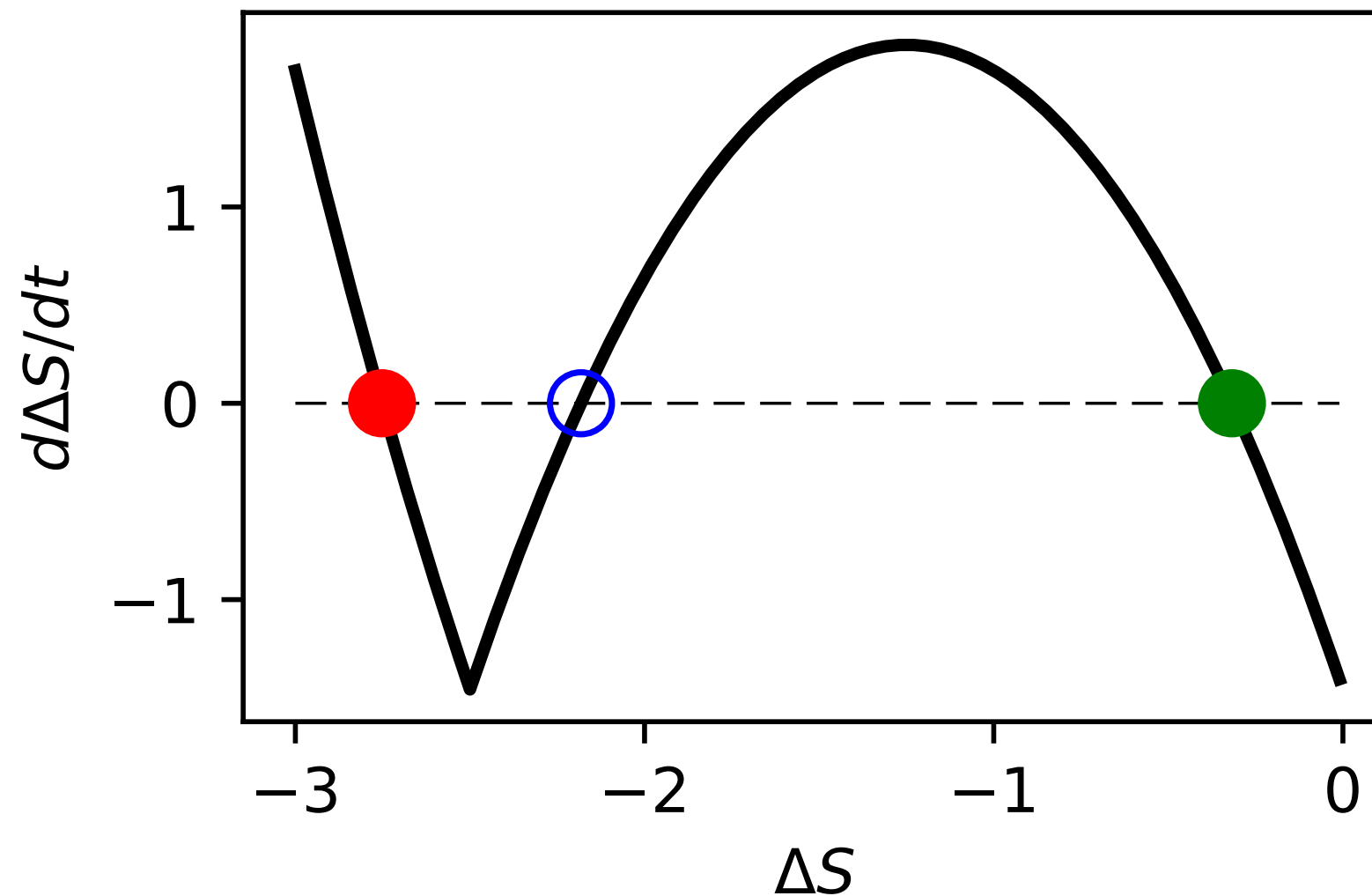


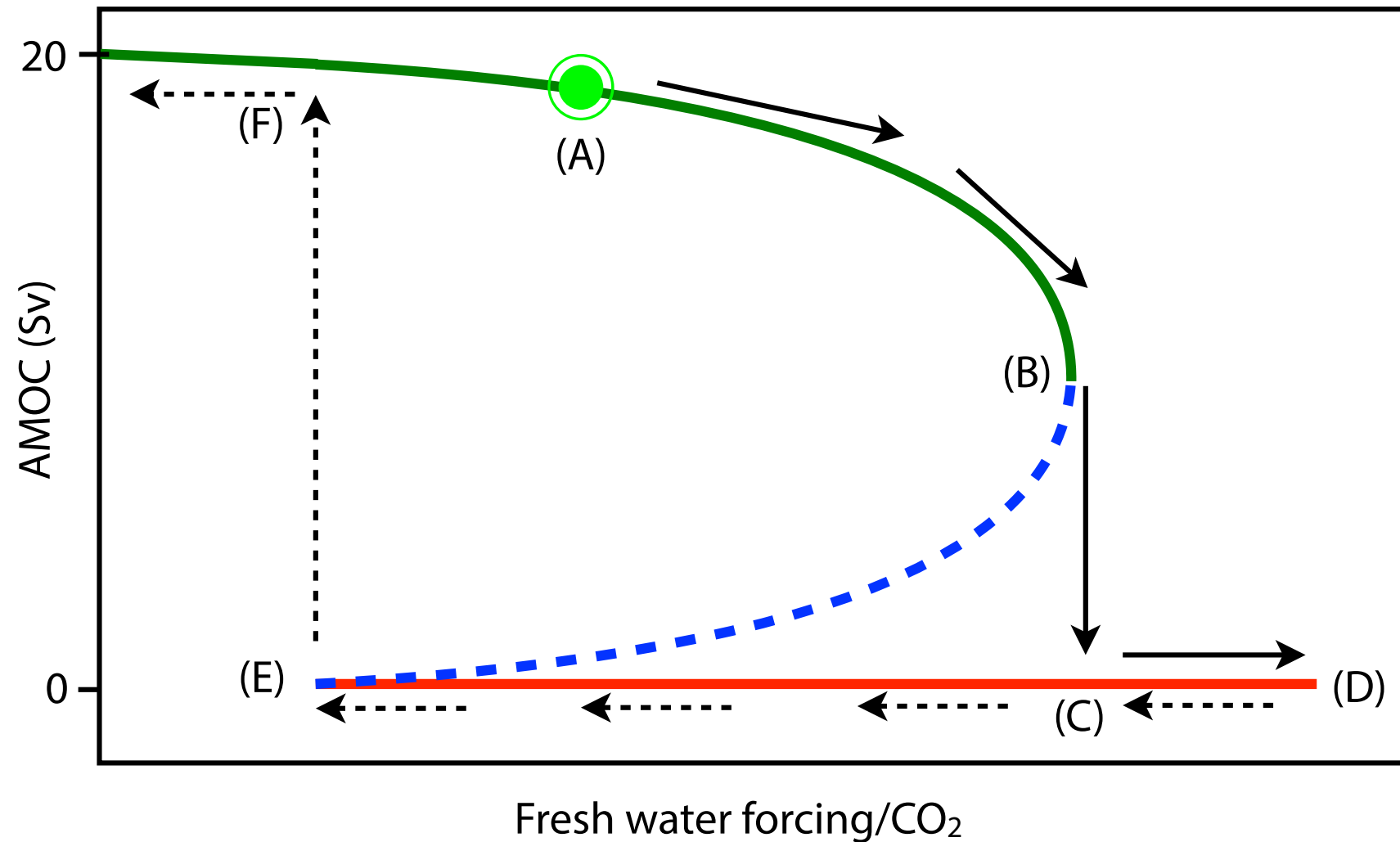
Figure 6.5: Solution of the 2-box Stommel model (Marotzke's simplification): (a, b) Steady states of salinity difference and MOC as a function of freshwater forcing. (c) Stability analysis. (d) Freshwater forcing for hysteresis run. (e, f) Hysteresis results.

Multiple equilibria and hysteresis of the Atlantic Meridional Overturning Circulation (AMOC)



Analyzing stability of a nonlinear dynamical system: Stommel box model (Marotzke's simplification) example

Multiple equilibria and hysteresis of the Atlantic Meridional Overturning Circulation (AMOC)



schematic of multiple equilibria and hysteresis (E.T., *Global Warming Science*, 2022)

Multiple equilibria and hysteresis of the Atlantic Meridional Overturning Circulation (AMOC) in full climate models

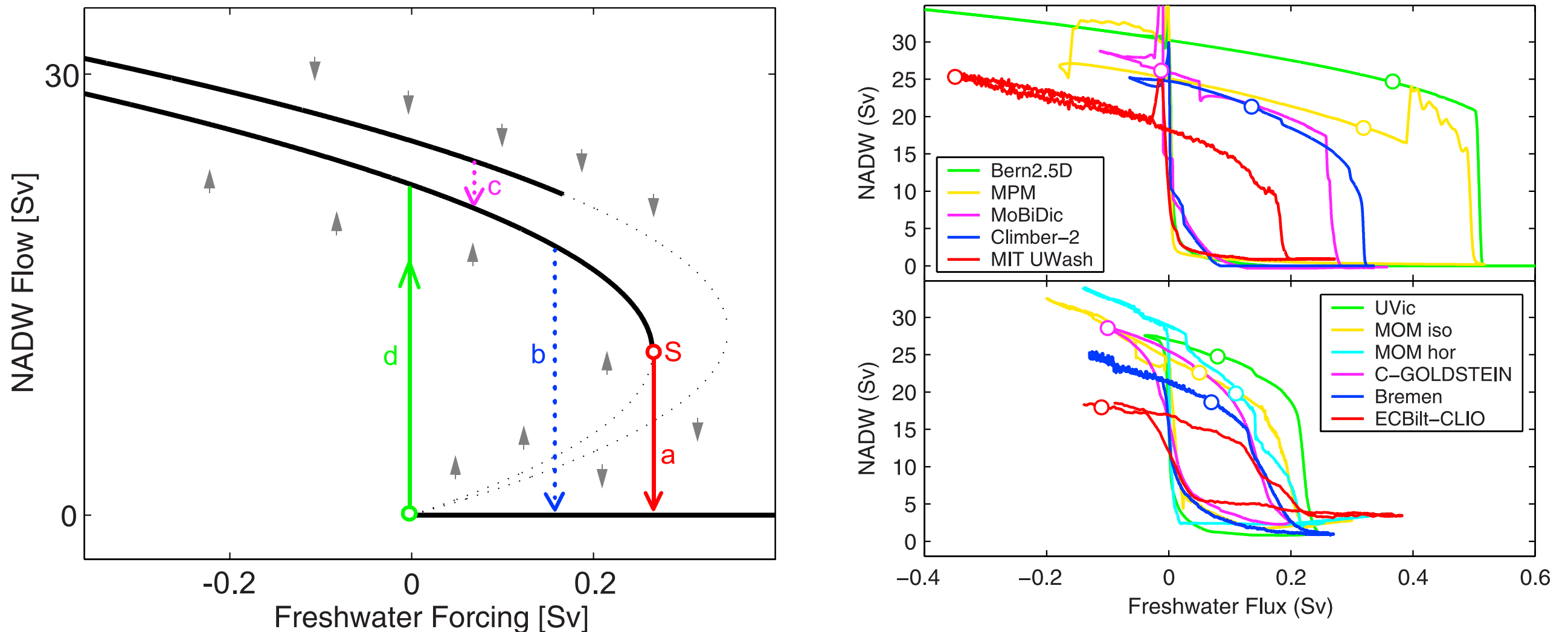


Figure 2. Hysteresis curves found in the model inter-comparison. The bottom panel shows coupled models with 3-D global ocean models, the top panel those with simplified ocean models (zonally averaged or, in case of the MIT_UWash model, rectangular basins). Curves were slightly smoothed to remove the effect of short-term variability. Circles show the present-day climate state of each model.

Consequences of collapse of Atlantic Meridional Overturning Circulation (AMOC)

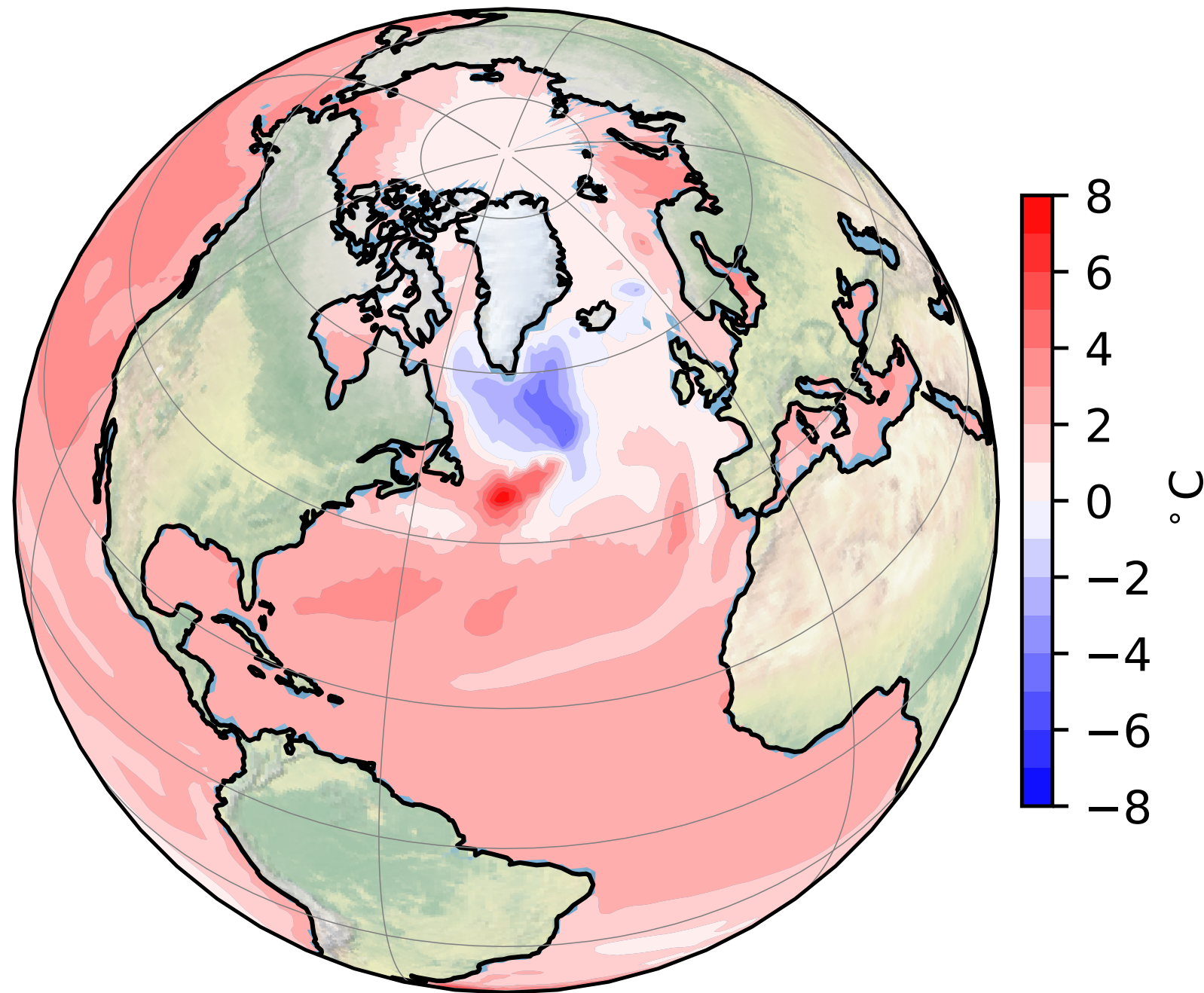


Figure 6.6: SST at 2100 minus that at 2006 in an RCP8.5 scenario.

AMOC tipping points, 2023

nature communications



Article

<https://doi.org/10.1038/s41467-023-39810-w>

Warning of a forthcoming collapse of the Atlantic meridional overturning circulation

Published: 25 July 2023

Peter Ditlevsen^{1,3} & Susanne Ditlevsen^{2,3}

AMOC is a major climate tipping element & a future collapse would have severe impacts... A recent weakening in circulation has been reported, but CMIP simulations suggest a full collapse is unlikely within the 21st century. Tipping to an undesired state is a growing concern. Predictions based on observations rely on early-warning signals: increase in variance (loss of resilience) & increased autocorrelation (critical slowing down), recently reported for AMOC. We provide statistical significance & data-driven estimators for the time of tipping: around mid-century...

The New York Times

Warming Could Push the Atlantic Past a 'Tipping Point' This Century

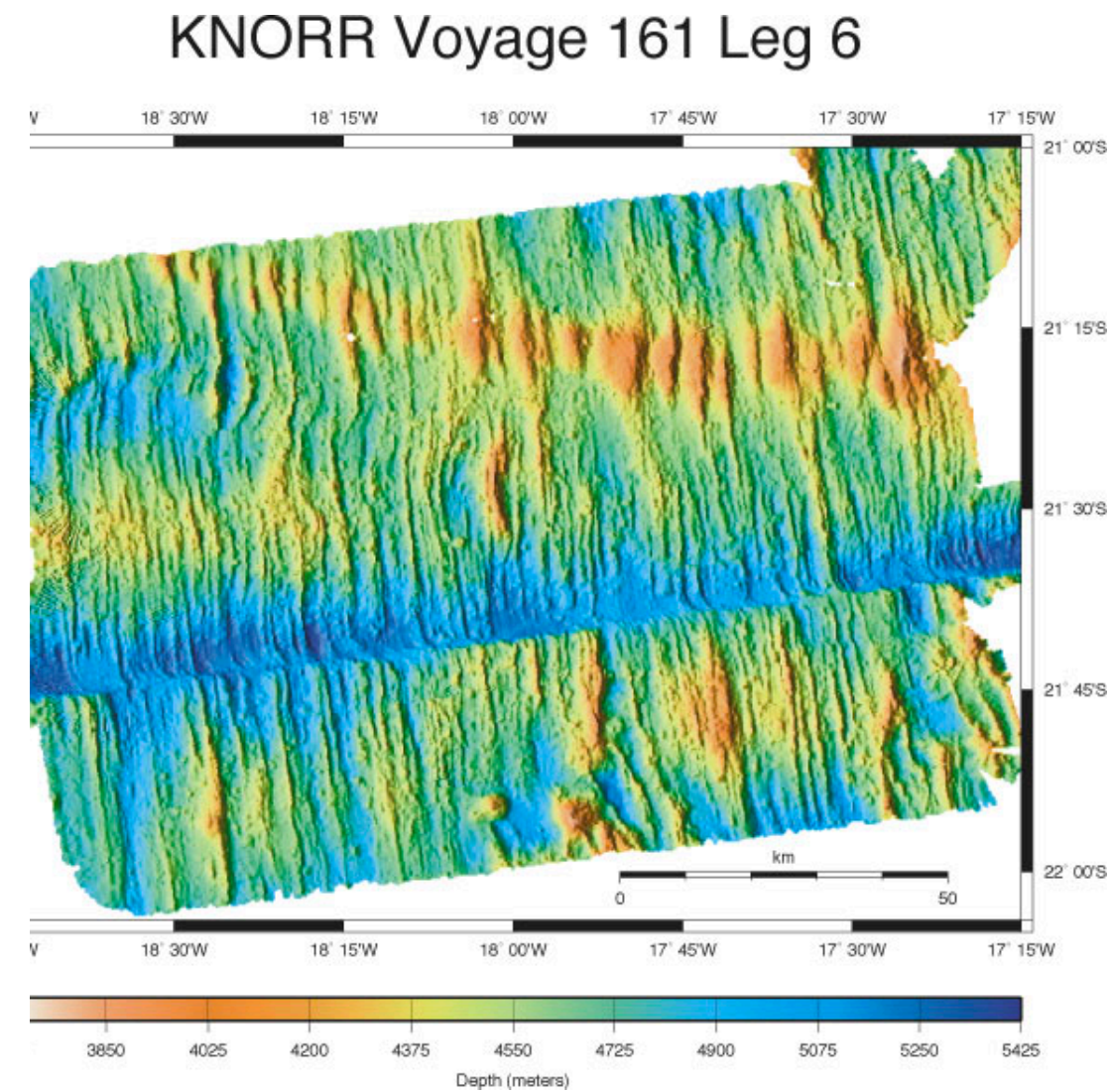
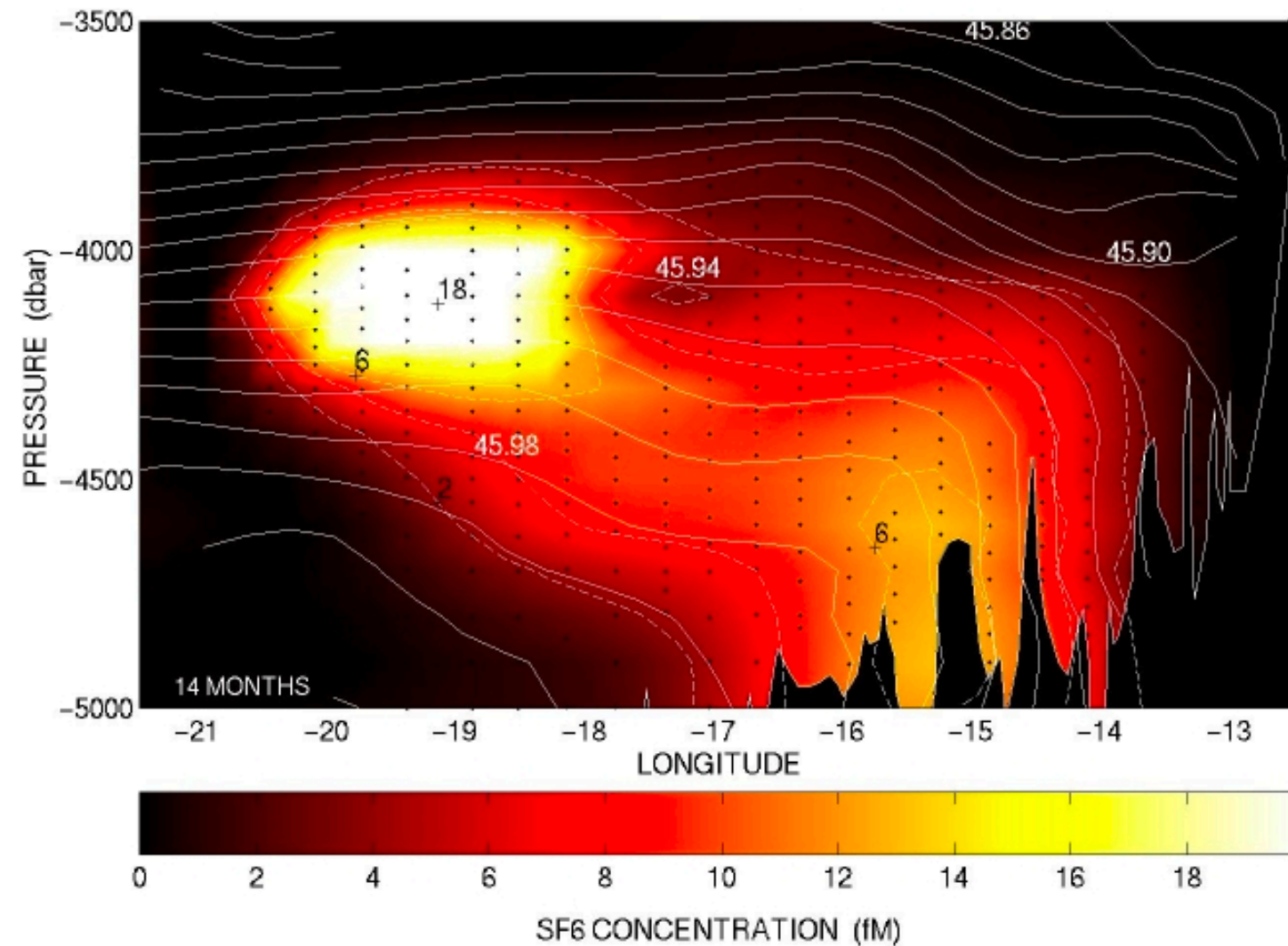
The system of ocean currents that regulates the climate for a swath of the planet could collapse sooner than expected, a new analysis found.

July 25.

graduate level

THC scaling from Vallis showing that the AMOC amplitude depends on small-scale ocean vertical (diapycnal) turbulent mixing

Ocean diapycnal mixing & rough topography: Brazil basin tracer release experiment



tracer concentration & σ_4 from valley where tracer was released obtained in 1997, 14 months after release. dots show sample locations, blue bar labelled 'INJ' shows the location and size of the initial patch. The valley is enclosed by ridges to the north and south whose depths are roughly where the white density contours bend sharply down.

Figure 2. SeaBeam box survey. The shift in the bathymetry on the southern edge of the valley is real, and not an artifact. The tracer was released over this valley at 21.7 S, 18.4 W. The current meter mooring was in the valley to the east of this point at 21.6 S, 17.8 W.

Ocean diapycnal mixing and tides

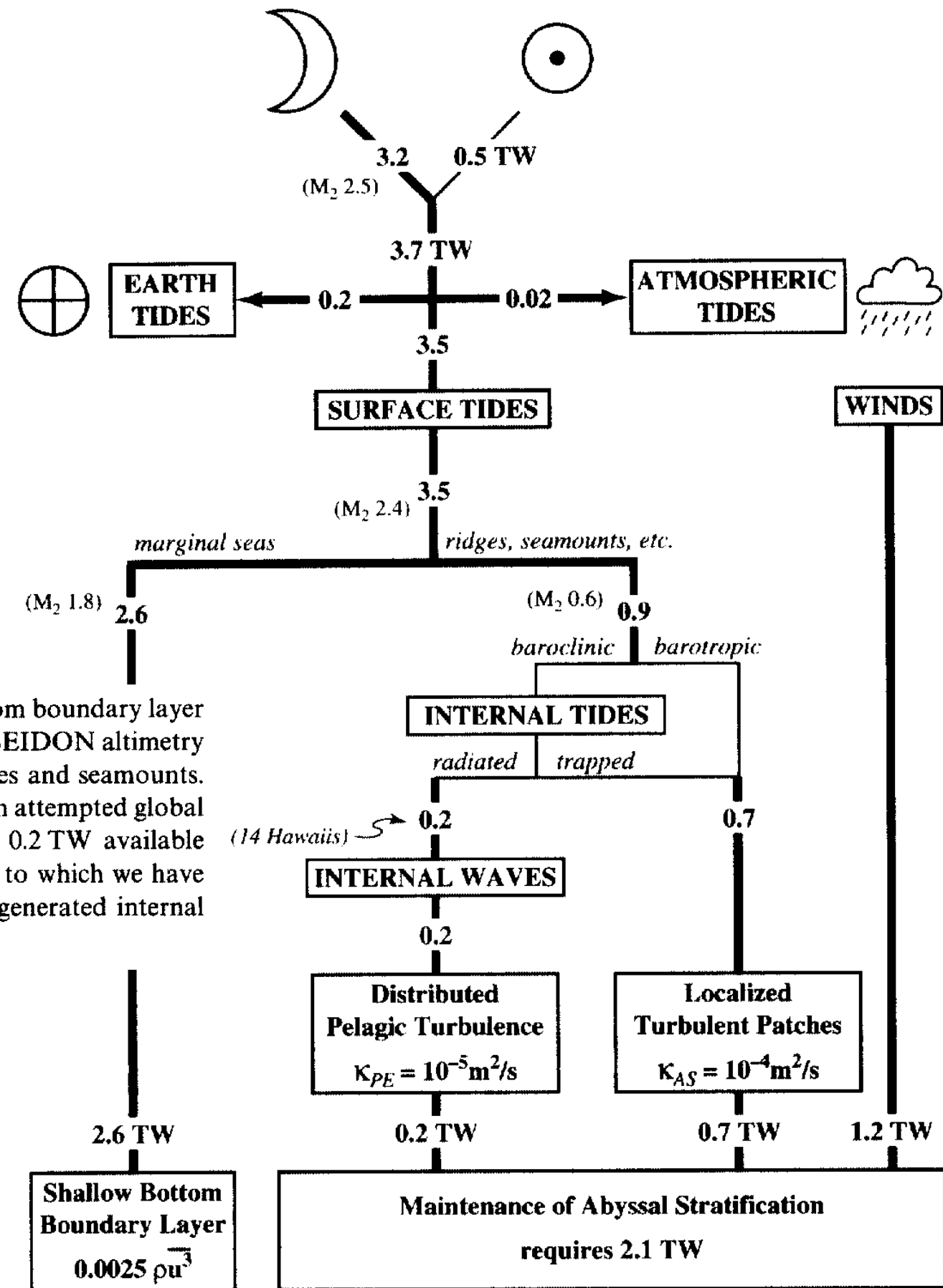


Fig. 4. An impressionistic budget of tidal energy flux. The traditional sink is in the bottom boundary layer (BBL) of marginal seas. Preliminary results from Egbert (1997) based on TOPEX/-POSEIDON altimetry suggest that 0.9 TW (including 0.6 TW of M_2 energy) are scattered at open ocean ridges and seamounts. Light lines represent speculation with no observational support. “14 Hawaiiis” refers to an attempted global extrapolation of surface to internal tide scattering measured at Hawaii, resulting in 0.2 TW available for internal wave generation. The wind energy input is estimated from Wunsch (1998), to which we have added 0.2 TW to balance the energy budget. This extra energy is identified as wind-generated internal waves — radiating into the abyss and contributing to mixing processes.

The Adiabatic AMOC alternative

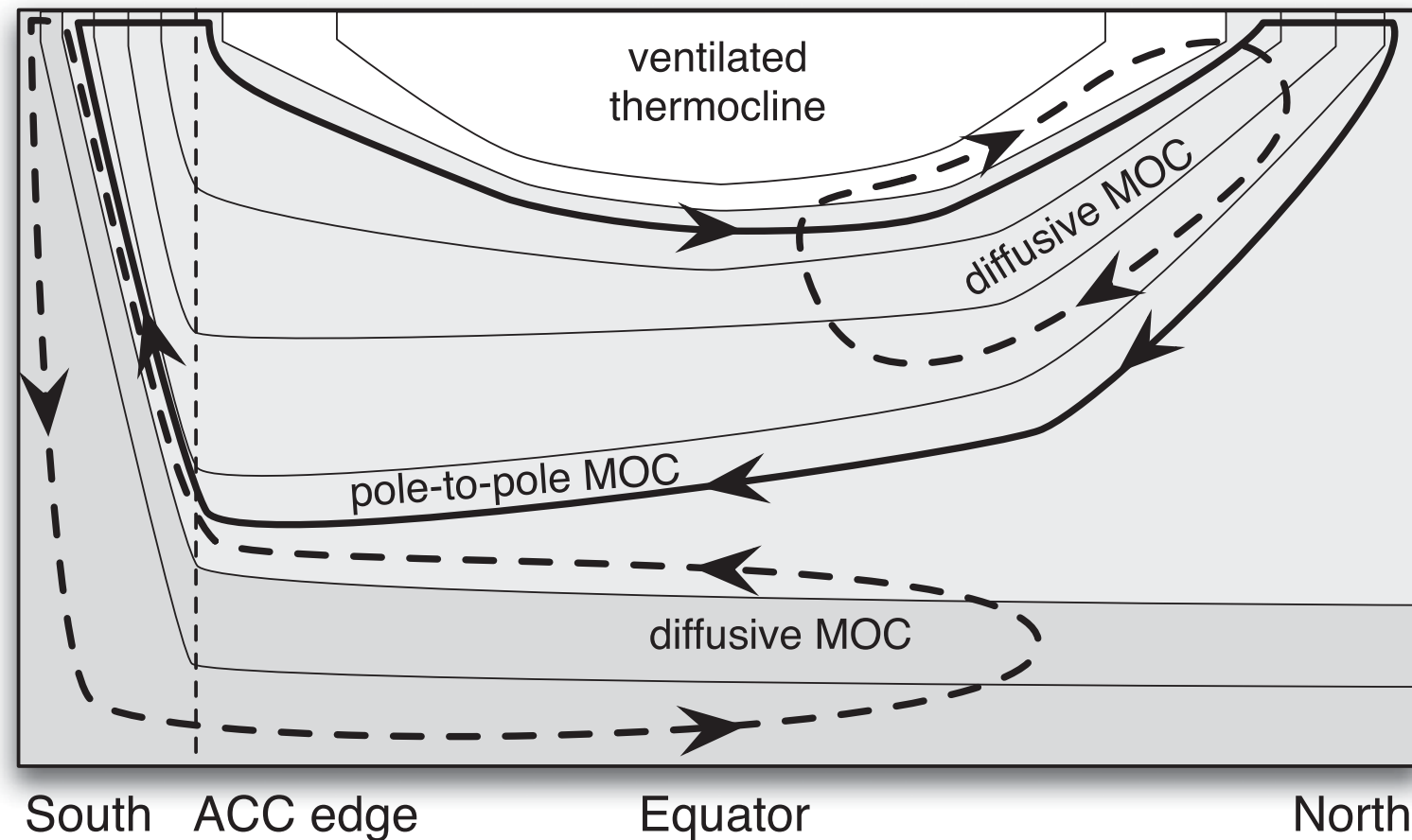


FIG. 1. A sketch of the present-day ROC as represented by the residual flow. A pole-to-pole cell (thick solid line) with sinking in high latitudes in the North Atlantic and upwelling in the ACC region coexists with weaker diffusive cells characterized by high-latitude sinking in each hemisphere and upwelling mostly confined to the same hemisphere (thick dashed lines). The thin solid lines show isopycnals. The isopycnals in the ventilated thermocline region do not outcrop in the ACC region. The isopycnals in the heavily shaded region outcrop in the channel but not in the North Atlantic. The group of three intermediate isopycnals outcrop both in the ACC and the North Atlantic, and it is along these surfaces that the pole-to-pole ROC can exist with diapycnal diffusion confined to the mixed layer. The total ROC is the combination of the pole-to-pole cell and the two diffusive cells.

The Adiabatic AMOC alternative

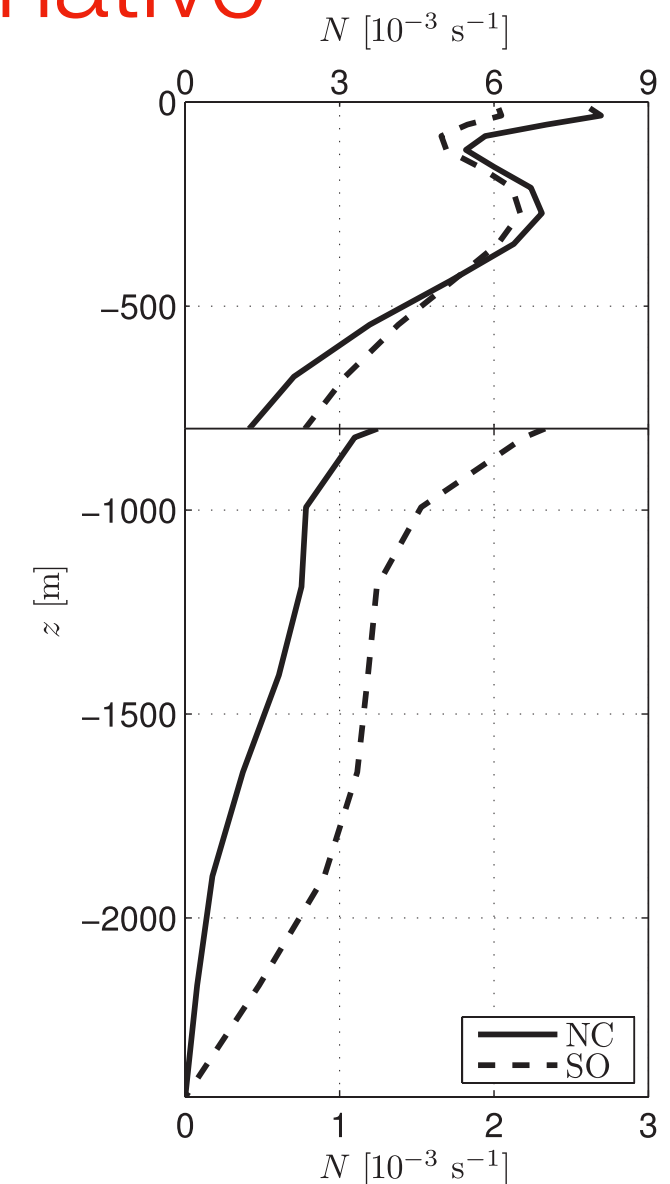
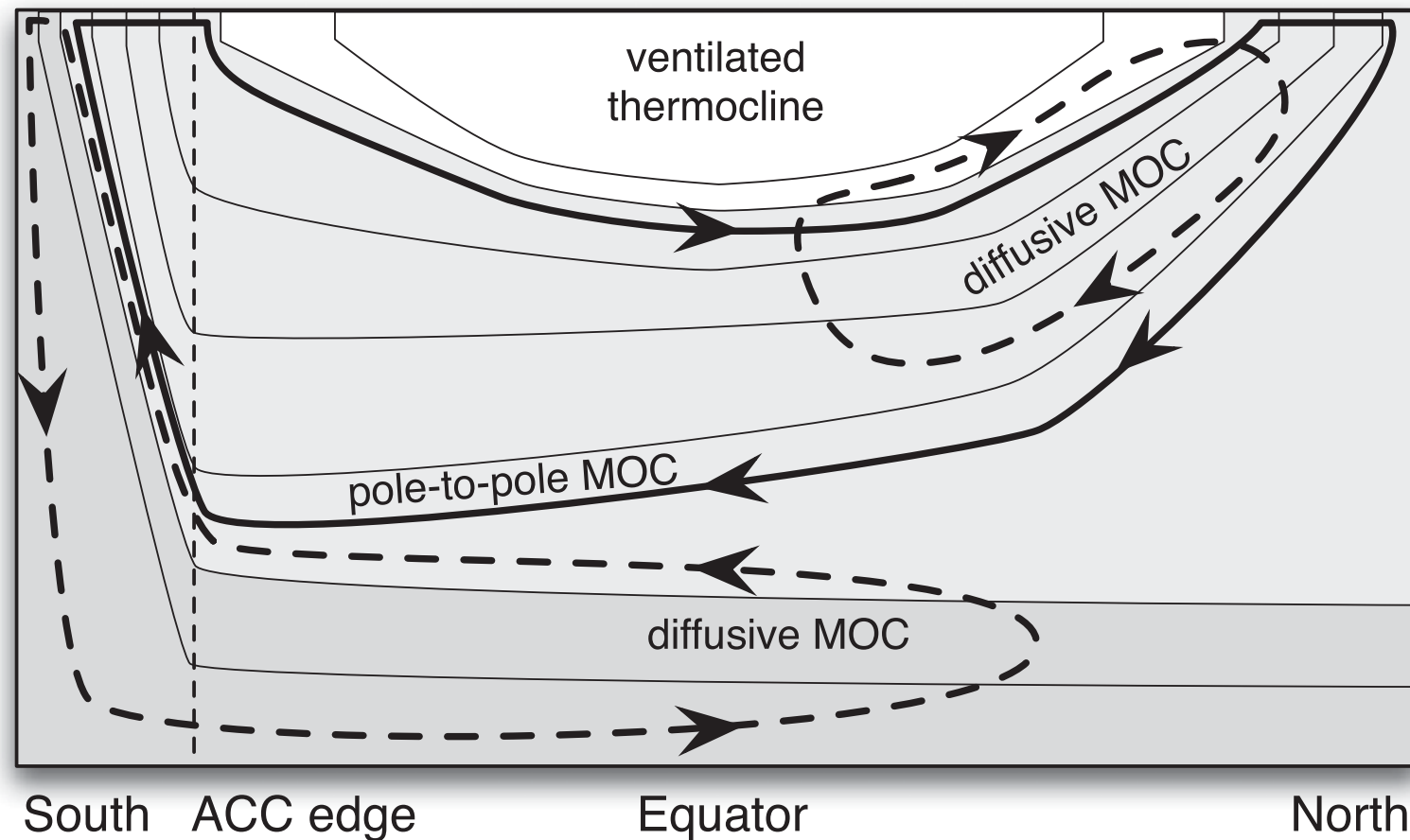


FIG. 6. Profiles of time-averaged buoyancy frequency N in the southern subtropical gyre 600 km from the western boundary for the NC (solid) and SO (dashed) experiments. The scale of the abscissa has been expanded by a factor of 3 below 800 m to show detail in the abyss. The profile is averaged over time and a 60 km \times 60 km horizontal area.

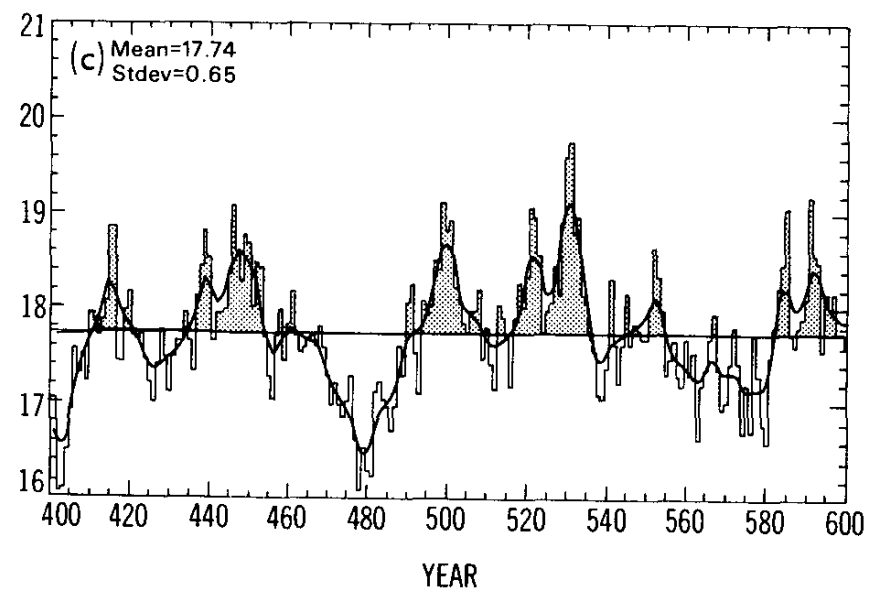
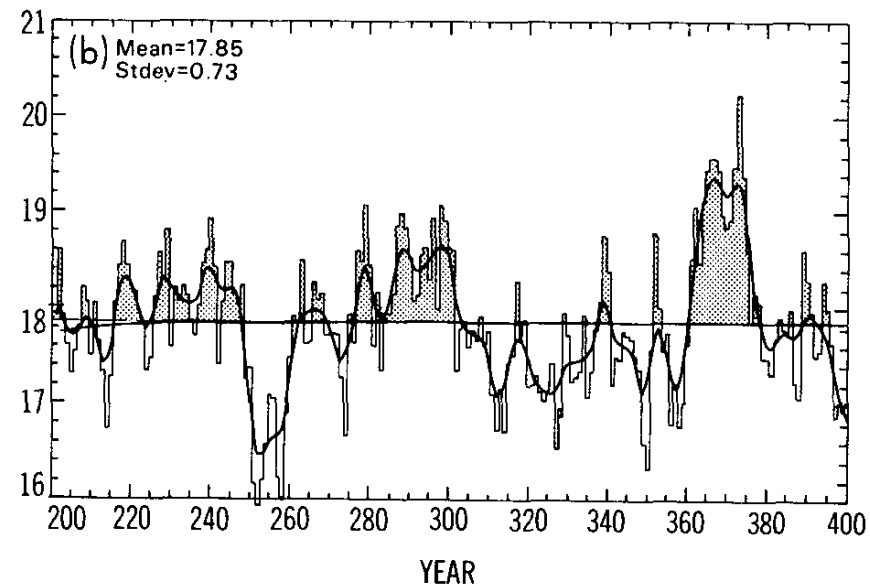
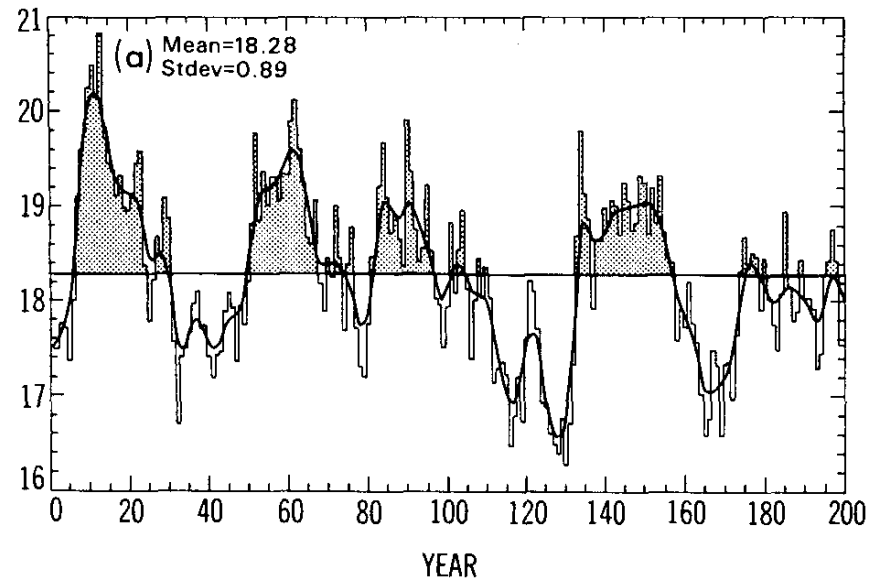
Wolfe and Cessi 2010

FIG. 1. A sketch of the present-day ROC as represented by the residual flow. A pole-to-pole cell (thick solid line) with sinking in high latitudes in the North Atlantic and upwelling in the ACC region coexists with weaker diffusive cells characterized by high-latitude sinking in each hemisphere and upwelling mostly confined to the same hemisphere (thick dashed lines). The thin solid lines show isopycnals. The isopycnals in the ventilated thermocline region do not outcrop in the ACC region. The isopycnals in the heavily shaded region outcrop in the channel but not in the North Atlantic. The group of three intermediate isopycnals outcrop both in the ACC and the North Atlantic, and it is along these surfaces that the pole-to-pole ROC can exist with diapycnal diffusion confined to the mixed layer. The total ROC is the combination of the pole-to-pole cell and the two diffusive cells.

Wolfe and Cessi 2011

graduate level

AMOC variability



A winter scene in Europe's Little Ice Age, 14th Century
Pieter Breugel the Elder.

In-class workshop

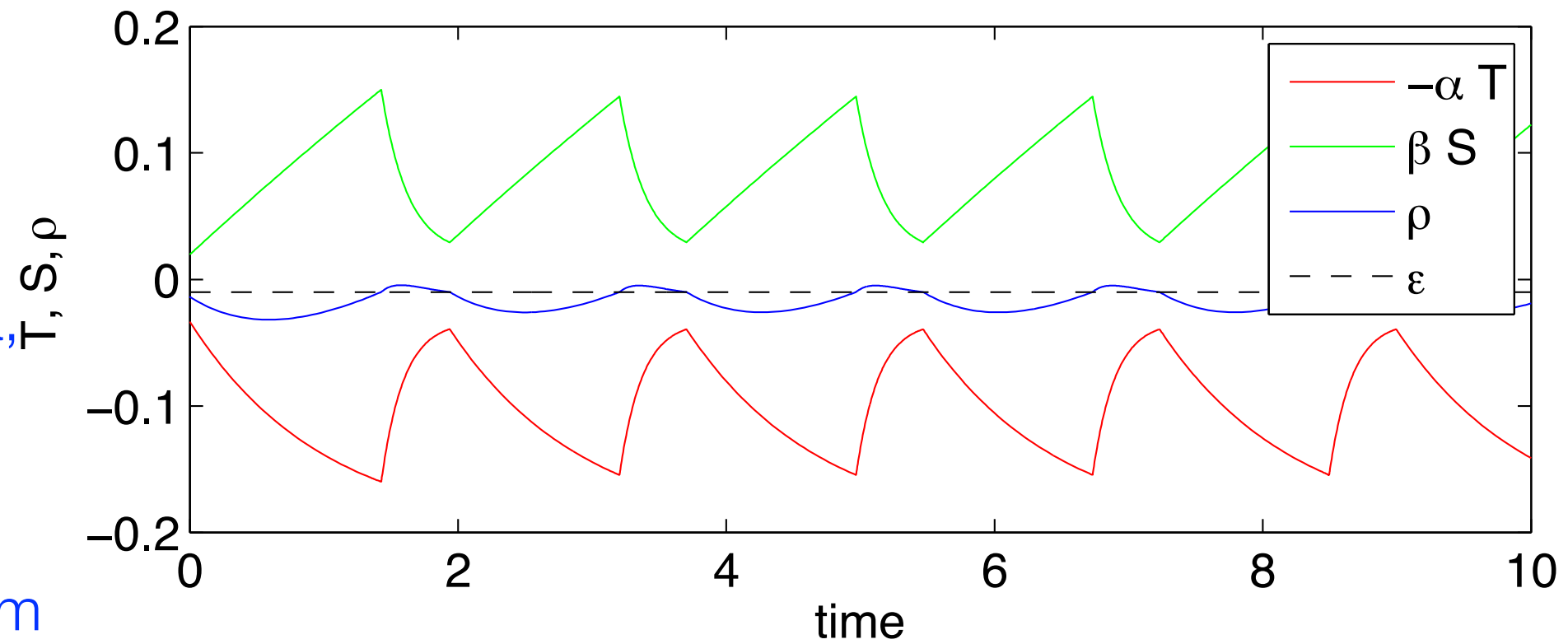
Find T and S for the convective state of Welander's flip-flop model
(present model using Dijkstra, 2000, section 6.2.3)

AMOC: self-sustained convective variability

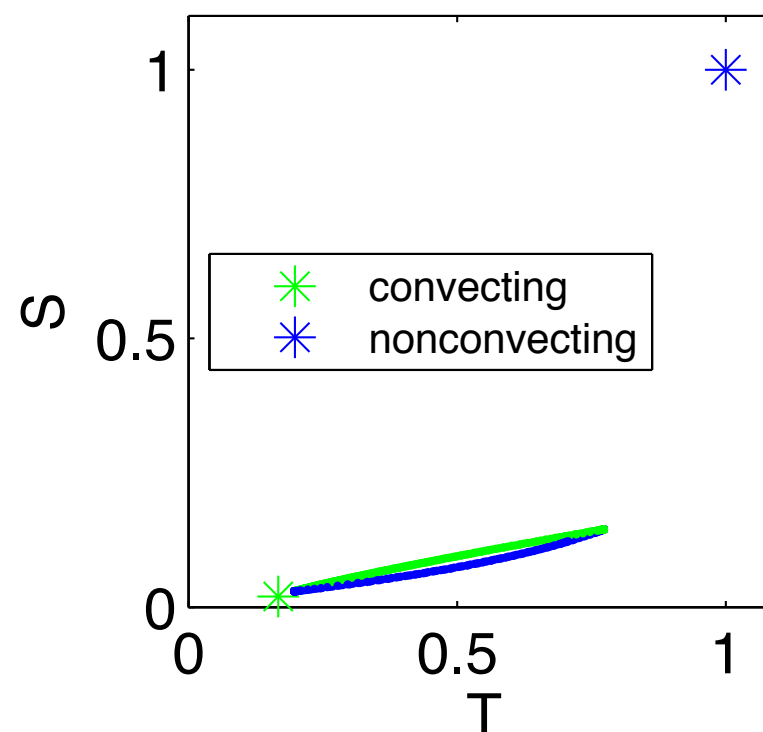
Notes:

1. Flip-flop oscillations (Welander 1982; Dijkstra, 2000, section 6.2.3);
2. Figure here: results of Welander1982_flip_flop.m
3. Relaxation oscillations, Strogatz (1994) example 7.5.1 pp. 212–213.

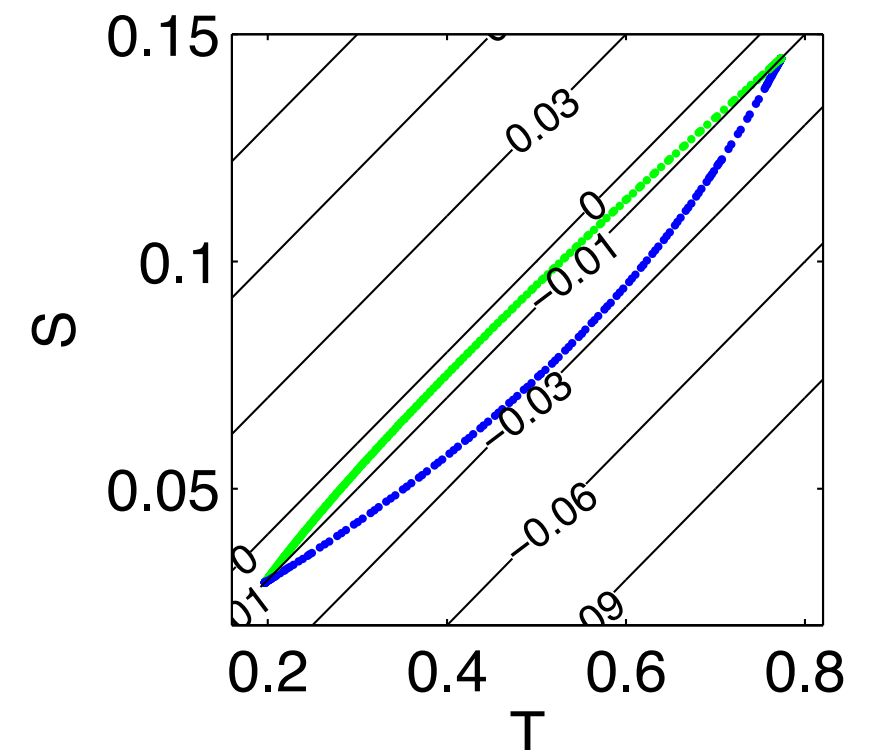
Welandar flip-flop oscillations



phase space

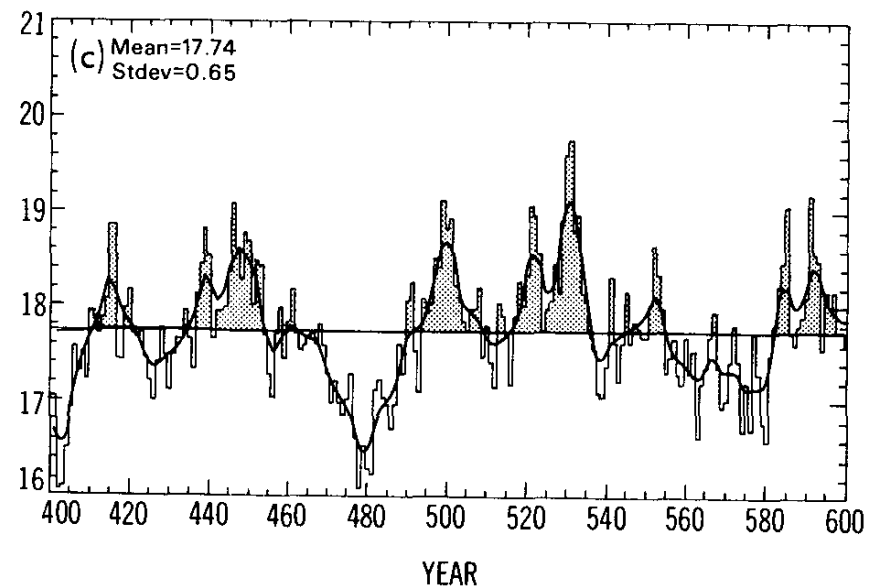
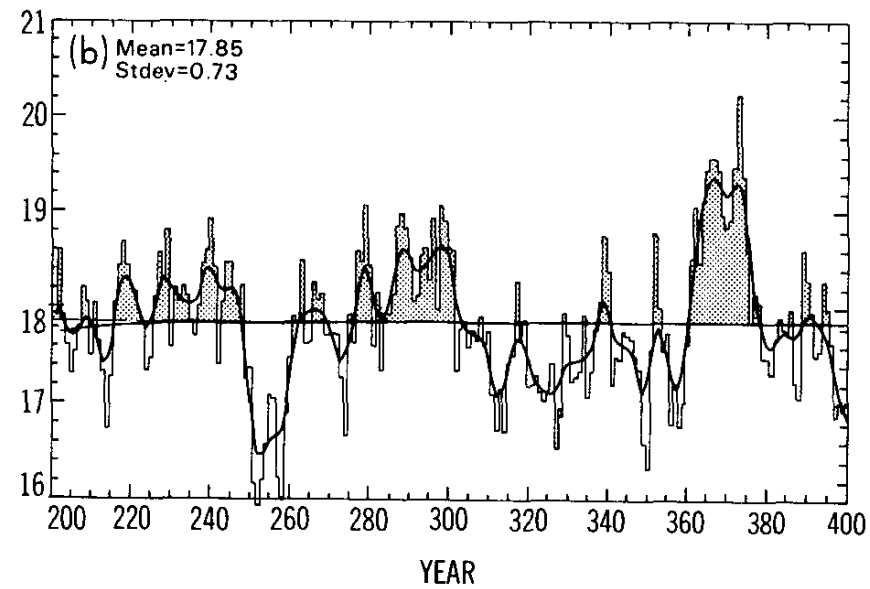
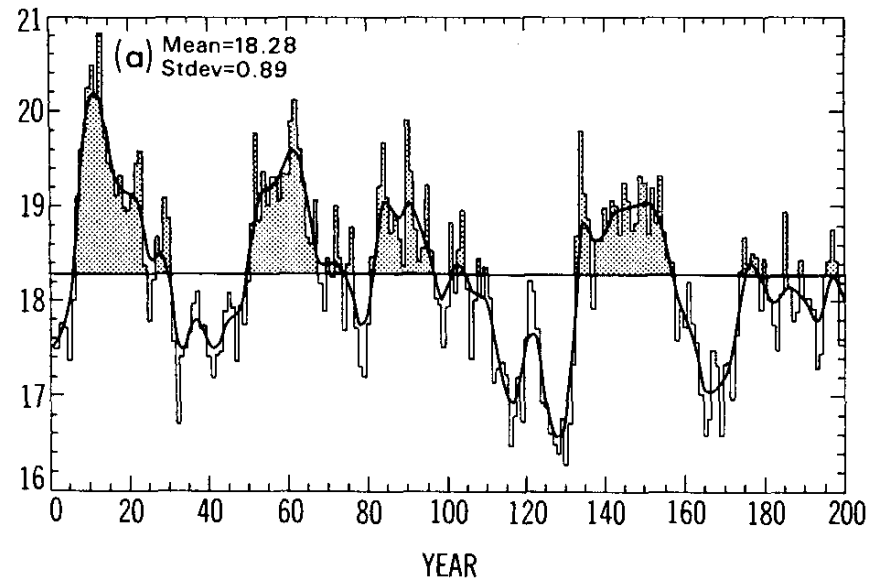


zoom-in & ρ contours



graduate level

AMOC: stochastic variability in a GCM

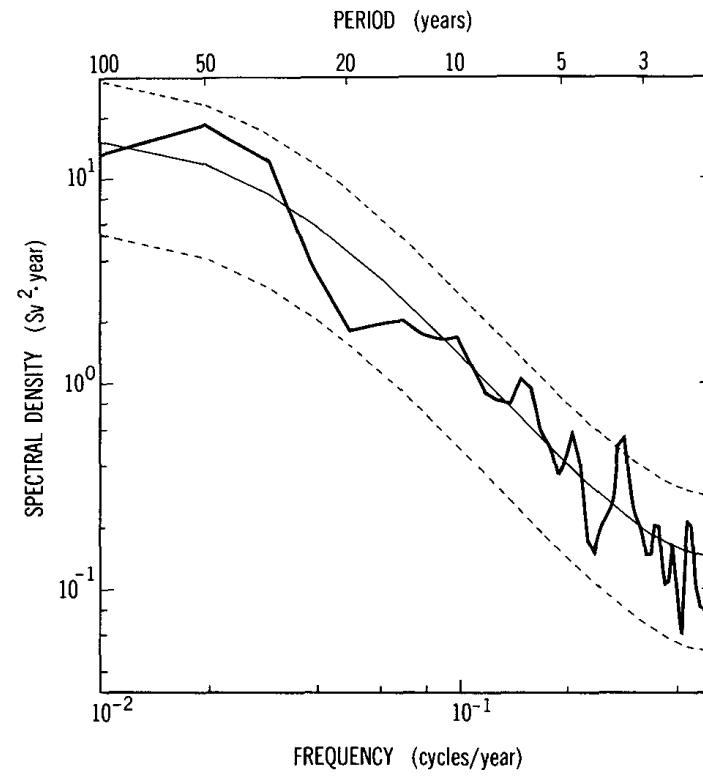
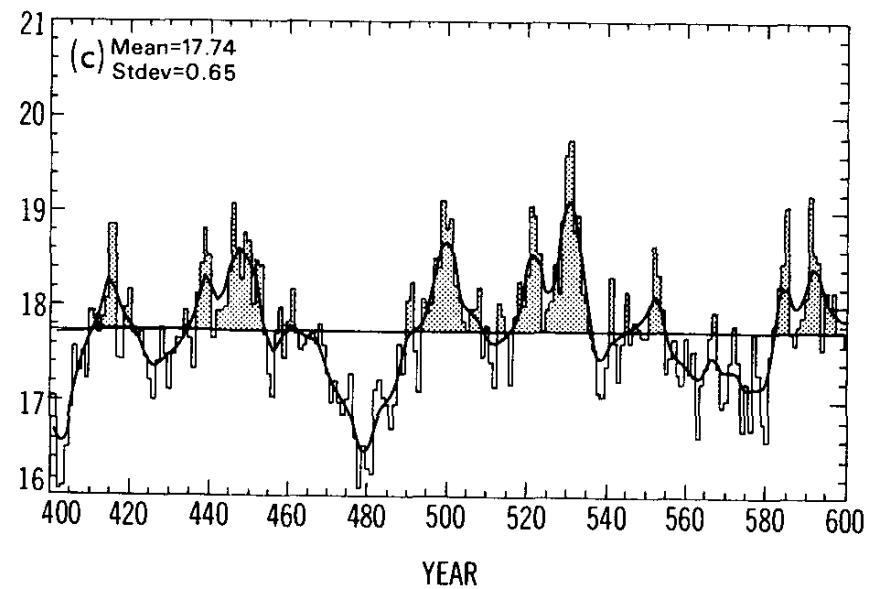
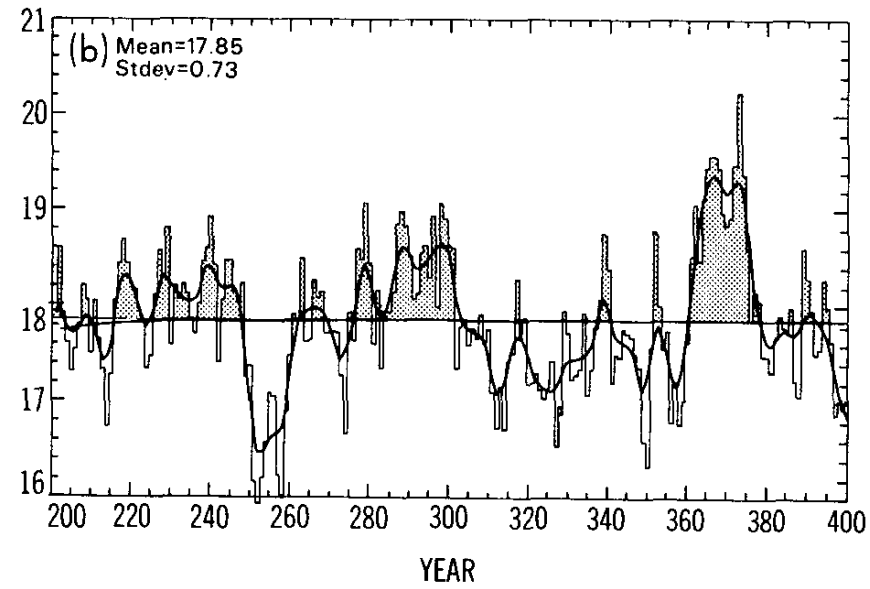
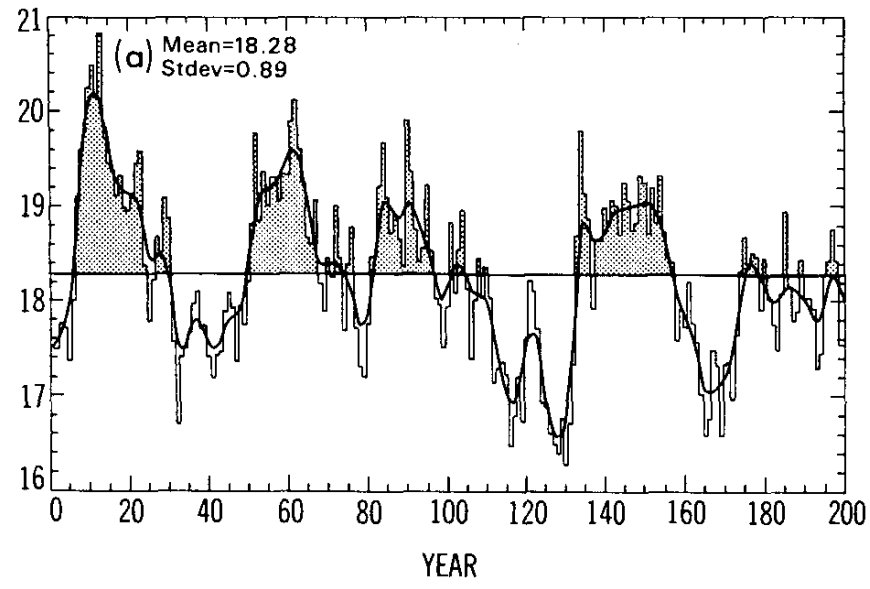


Delworth, Manabe and Stouffer 1993

Proposed mechanism: feedback between SST and wind...

graduate level

AMOC: stochastic variability in a GCM

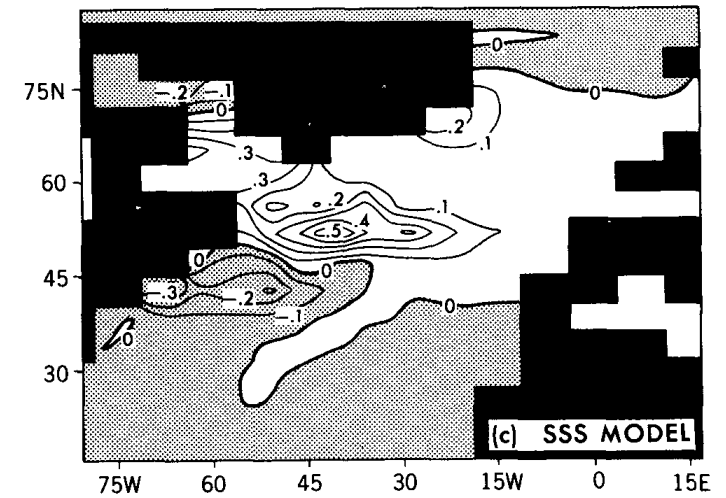
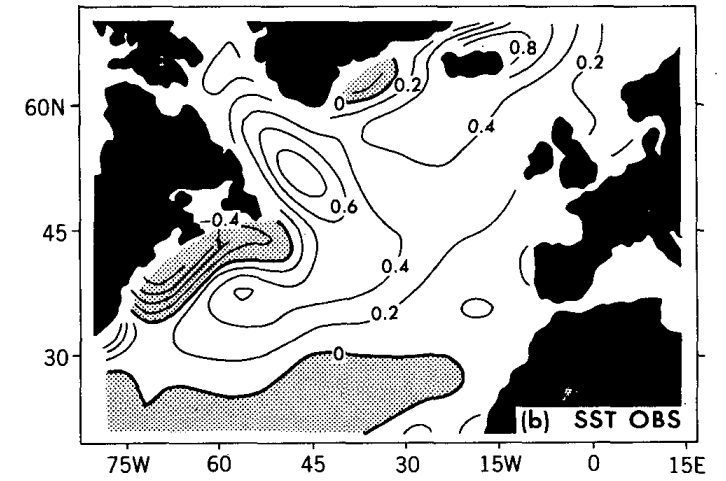
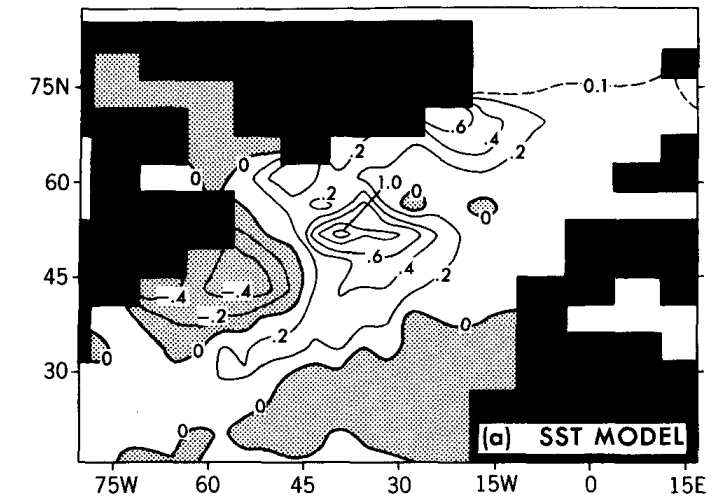
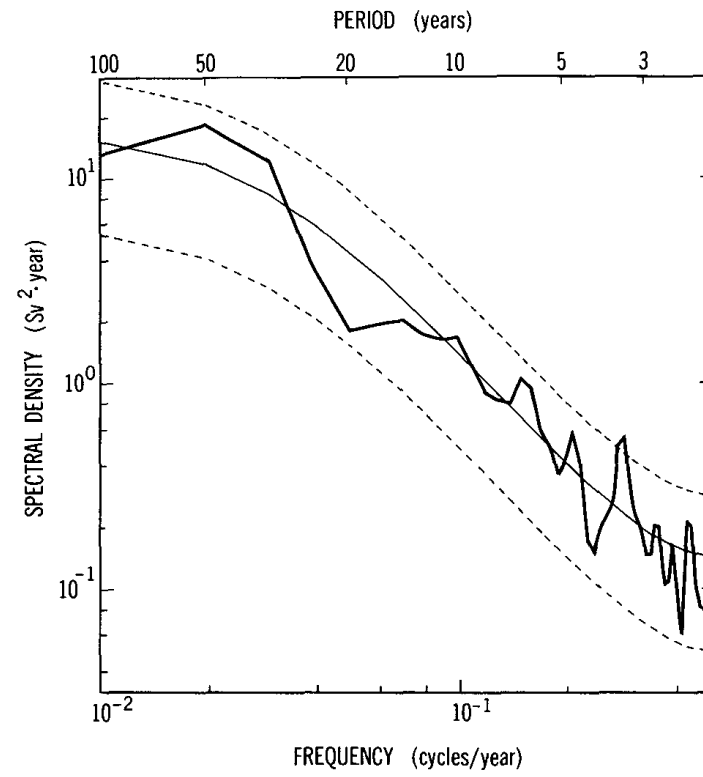
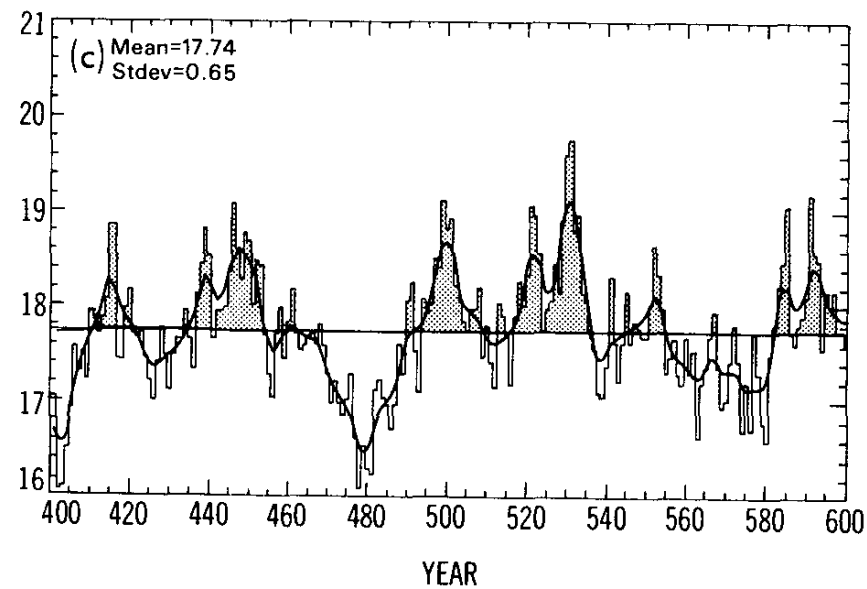
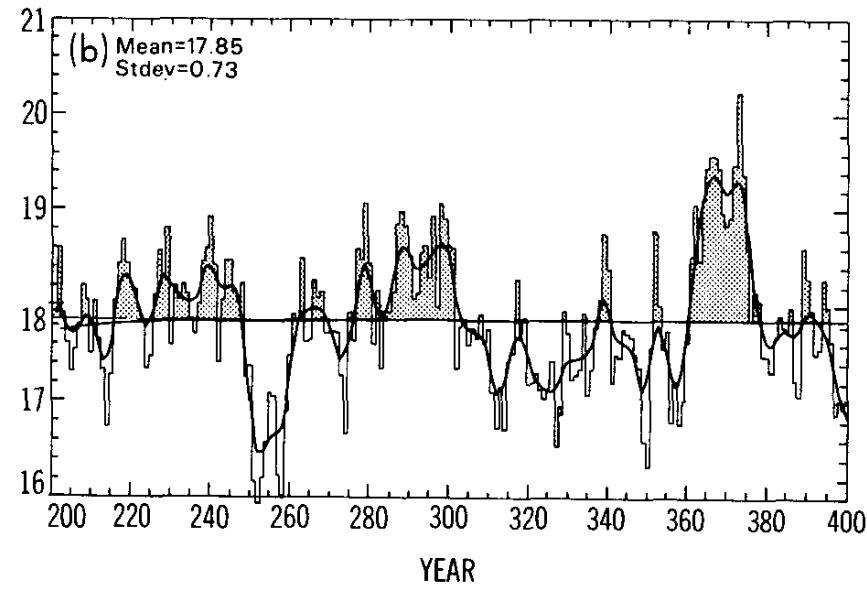
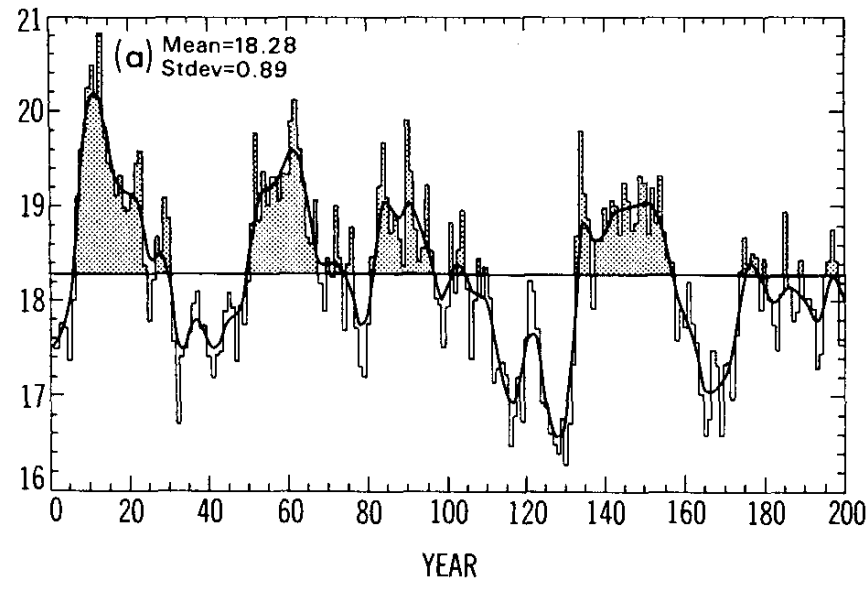


Delworth, Manabe and Stouffer 1993

Proposed mechanism: feedback between SST and wind...

graduate level

AMOC: stochastic variability in a GCM

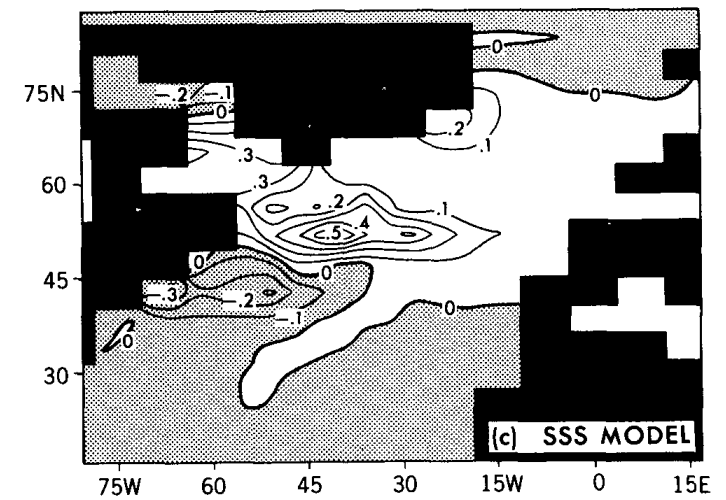
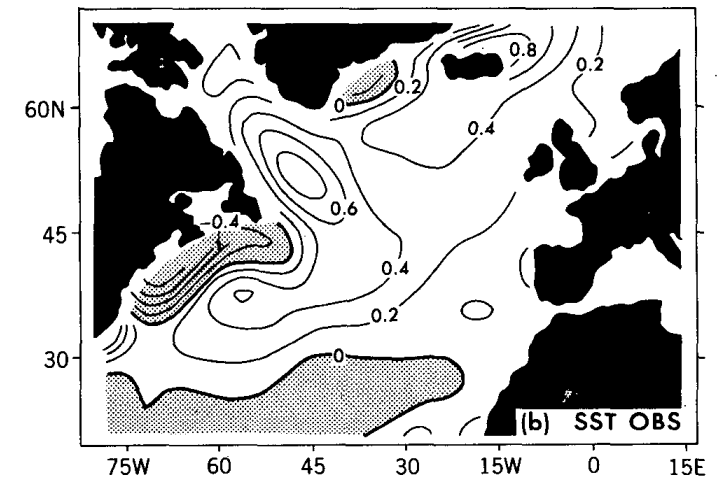
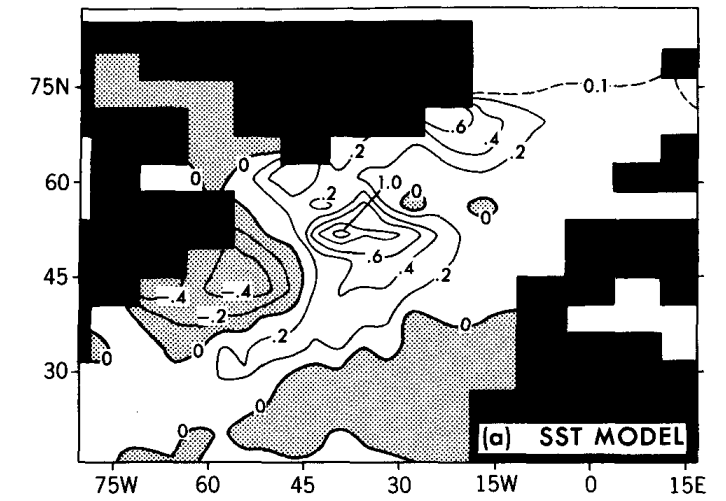
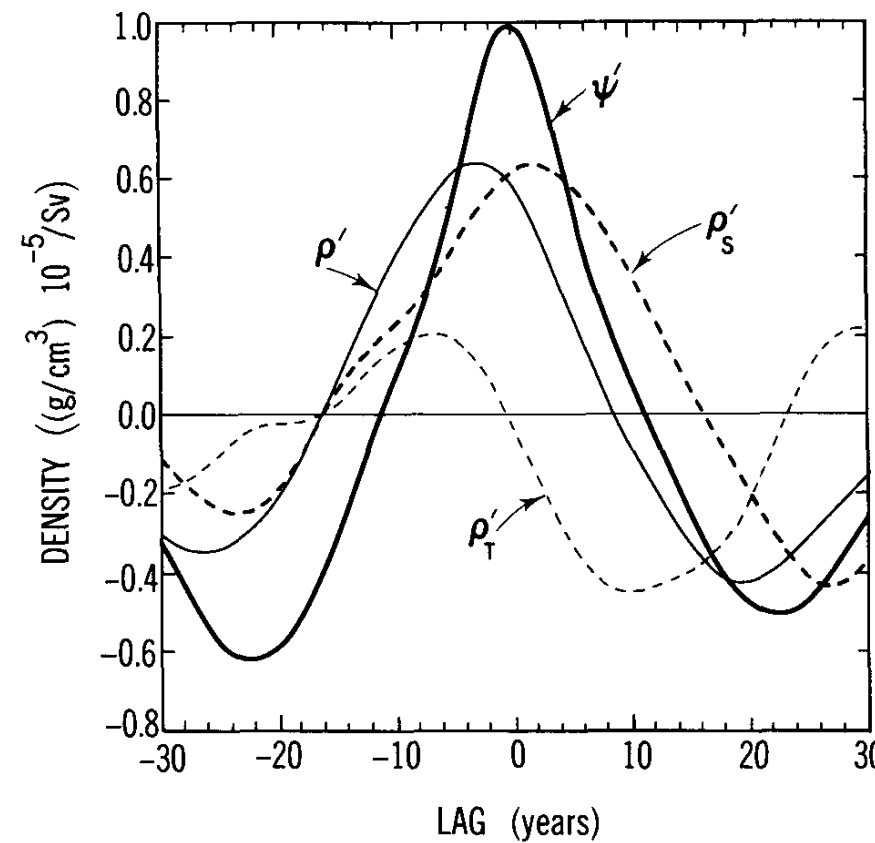
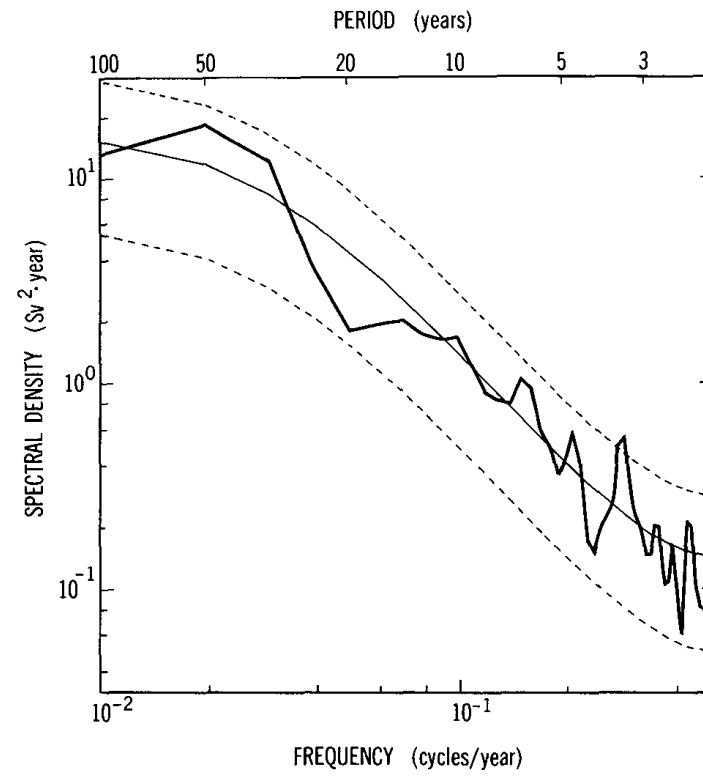
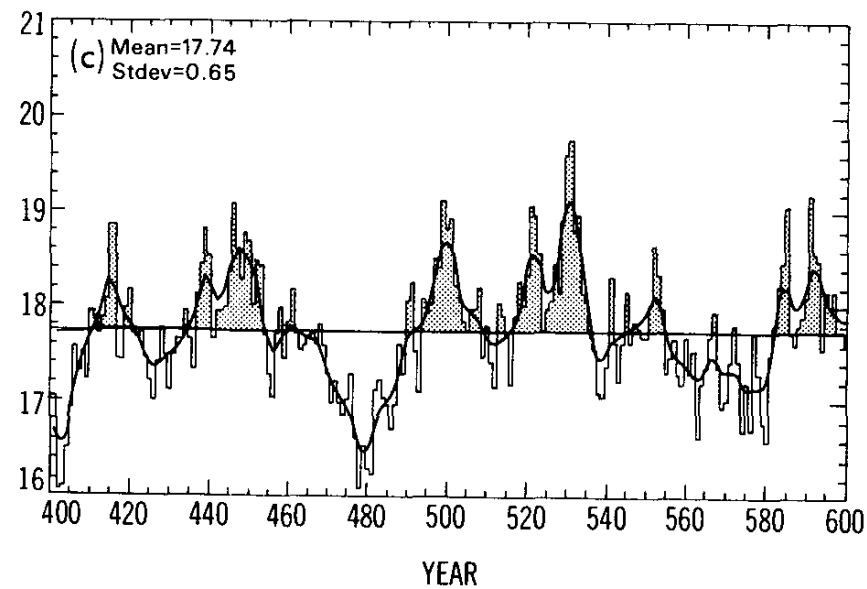
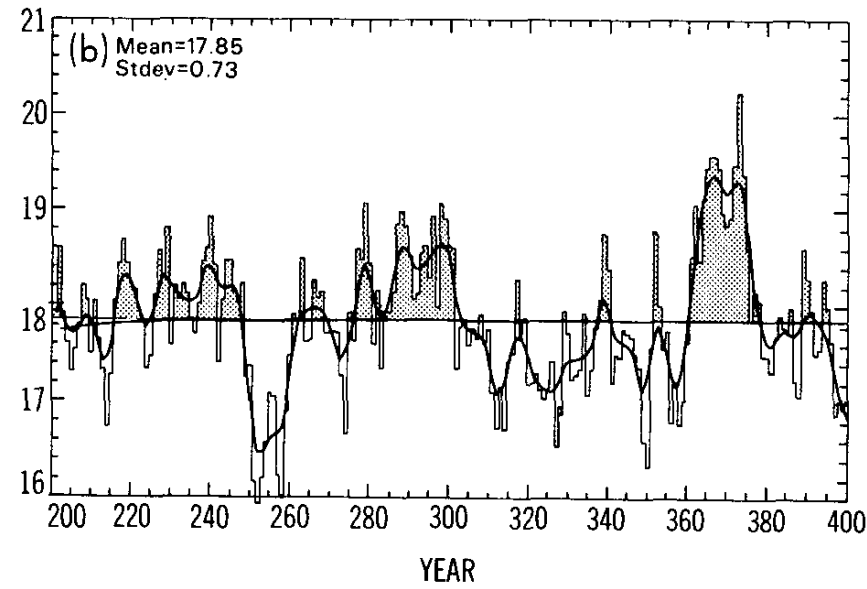
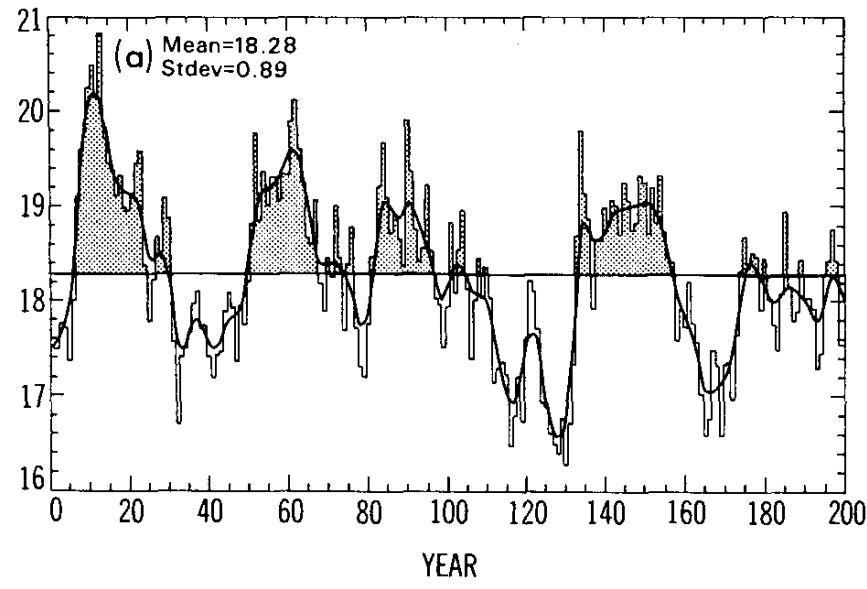


Delworth, Manabe and Stouffer 1993

graduate level

Proposed mechanism: feedback between SST and wind...

AMOC: stochastic variability in a GCM



Delworth, Manabe and Stouffer 1993

graduate level

Proposed mechanism: feedback between SST and wind...

AMOC: stochastic variability in a GCM

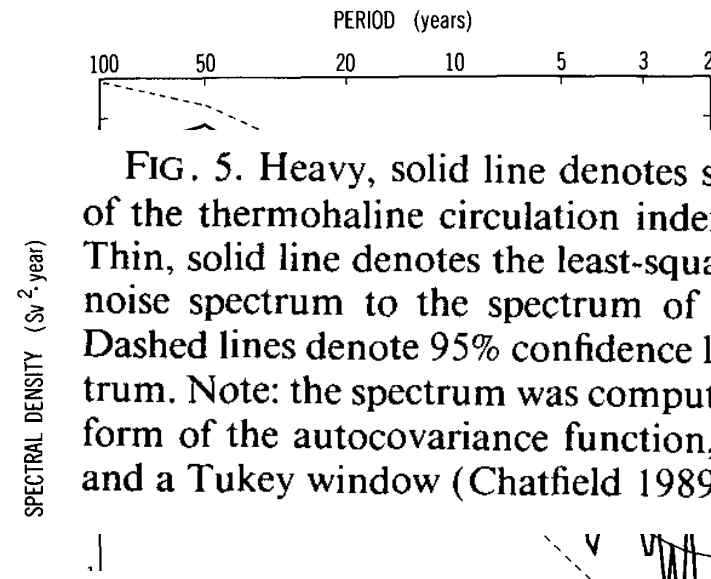
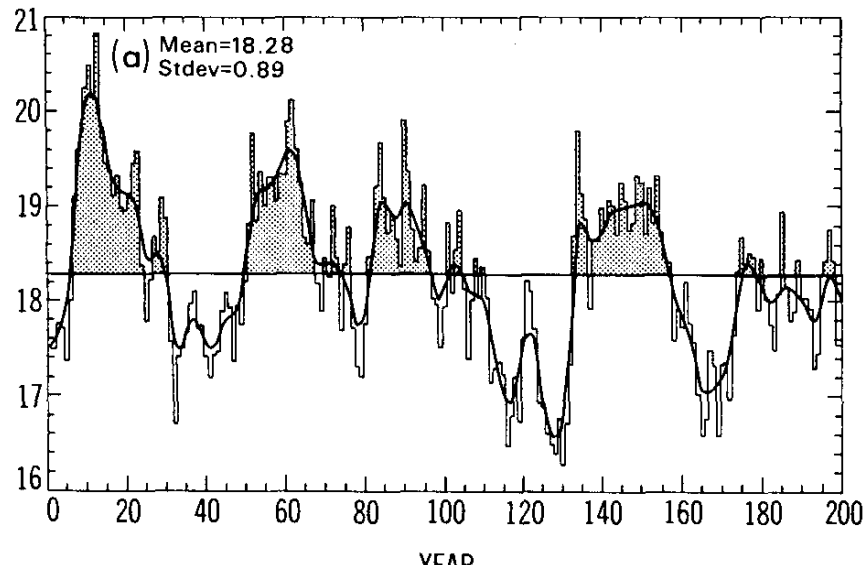


FIG. 5. Heavy, solid line denotes spectrum of the first 200 years of the thermohaline circulation index time series shown in Fig. 4. Thin, solid line denotes the least-squares best fit of a theoretical red noise spectrum to the spectrum of the thermohaline circulation. Dashed lines denote 95% confidence limits about the red noise spectrum. Note: the spectrum was computed by taking the Fourier transform of the autocovariance function, using a maximum of 50 lags and a Tukey window (Chatfield 1989, chapter 7).

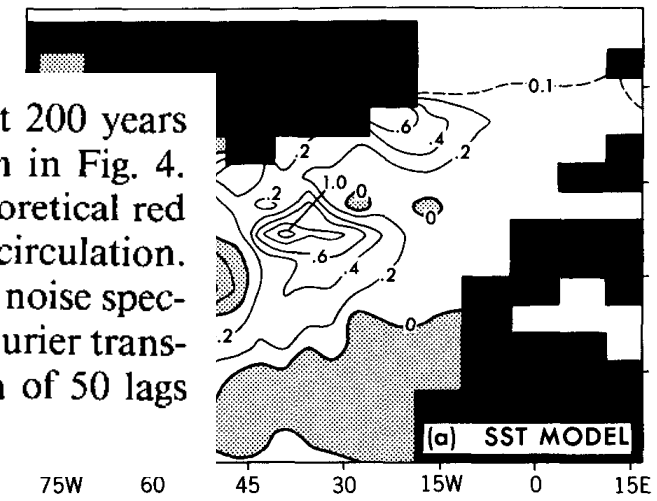


FIG. 6. (a) Differences in annual-mean model sea surface temperature between four decades with anomalously large THC index values and four decades with anomalously small THC index values. Units are degrees Celsius. Values less than zero are stippled. (b) Differences in observed sea surface temperature between the periods 1950-1964 (warm period) and 1970-1984 (cold period). Units are degrees Celsius. Values less than zero are stippled (adapted from Kushnir 1993). (c) Differences in annual-mean model sea surface salinity, computed in the same manner as (a). Units are practical salinity units.

FIG. 4. Time series of the annual-mean intensity of the index of the meridional overturning in the North Atlantic. Units are Sverdrups ($10^6 \text{ m}^3 \text{ s}^{-1}$). Heavy, solid line is a smoothed time series computed by applying a 13-point binomial filter to the annual-mean data (approximately a 10-year low-pass filter). (a) Years 1-200, (b) years 201-400, (c) years 401-600.

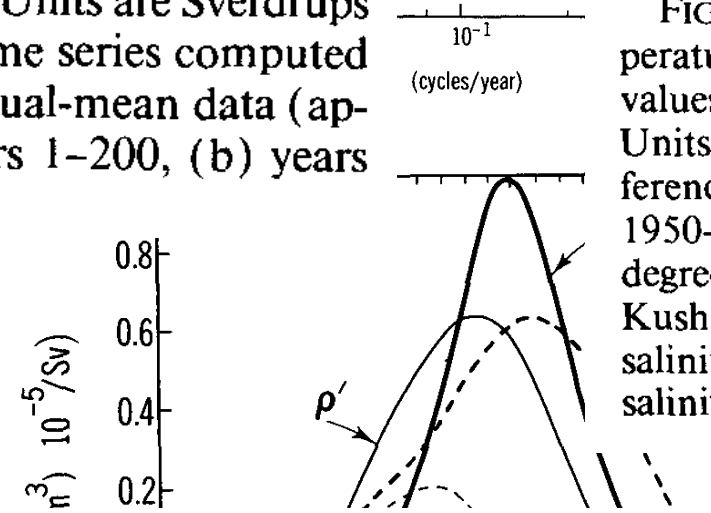
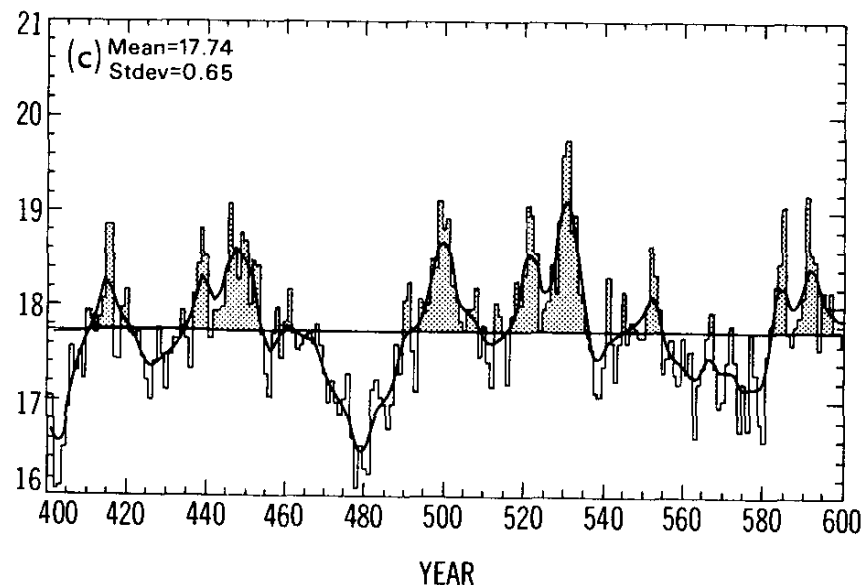
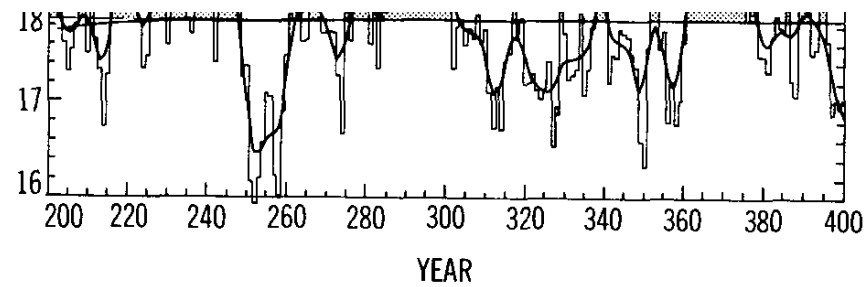
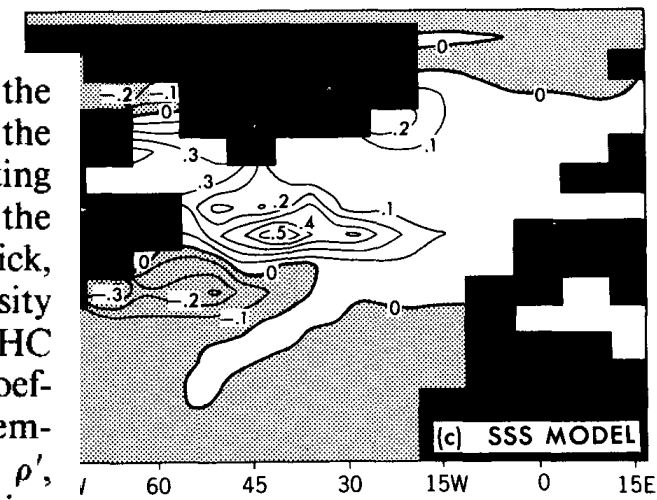


FIG. 8. Regression coefficients between various quantities and the time series of the THC index. The heavy, solid line (ψ') denotes the regression coefficients of the THC index with itself (thus representing a "typical" fluctuation). The thin, solid line (ρ') represents the regression coefficients between density and the THC index. The thick, dashed line (ρ'_S) denotes the regression coefficients for the density changes attributable solely to changes in salinity versus the THC index, while the thin, dashed line (ρ'_T) represents the regression coefficients for the density changes attributable solely to changes in temperature versus the THC index. The regression coefficients for ρ' , ρ'_S , and ρ'_T were averaged vertically and horizontally over the sinking region.



Stouffer, Manabe and Stouffer 1993

Proposed mechanism: feedback between SST and wind...

graduate level

AMOC: The advective feedback

Start with a perturbation corresponding to an enhanced salinity at the higher latitudes (e.g., box 2)

- ➔ Higher density there
- ➔ Stronger transport due to large meridional density gradient
- ➔ Enhanced advection/transport of salt from lower latitudes (box 1)
- ➔ Warmer temperature of advected water rapidly dissipated by cooling to the high-latitude atmosphere
- ➔ Left with a net additional salt perturbation to higher latitudes
- ➔ positive feedback

Oscillation itself is driven by the advection of salinity anomalies around the meridional plane.

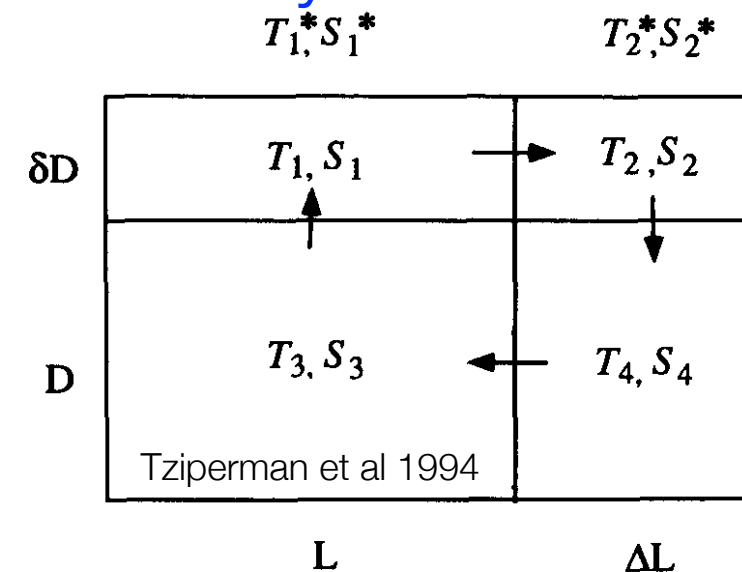


FIG. 3. Schematic plot of the box model geometry.

AMOC: stochastic variability, stability regimes of box model

Analysis:

- Write the conservation equations

$$\rho = -\alpha(T - T_0) + \beta(S - S_0)$$

$$v = [(\rho_4 - \rho_3) + \delta(\rho_2 - \rho_1)]/b$$

$$\delta \frac{\partial T_1}{\partial t} = v\delta(T_3 - T_1) + \delta(T_1^* - T_1)$$

$$\delta \Delta \frac{\partial T_2}{\partial t} = v\delta(T_1 - T_2) + \delta(T_2^* - T_2)$$

$$\frac{\partial T_3}{\partial t} = v\delta(T_4 - T_3)$$

$$\Delta \frac{\partial T_4}{\partial t} = v\delta(T_2 - T_4)$$

$$\delta \frac{\partial S_1}{\partial t} = v\delta(S_3 - S_1) + F_s^1$$

$$\delta \Delta \frac{\partial S_2}{\partial t} = v\delta(S_1 - S_2) + F_s^2$$

$$\frac{\partial S_3}{\partial t} = v\delta(S_4 - S_3)$$

$$\Delta \frac{\partial S_4}{\partial t} = v\delta(S_2 - S_4)$$

- Calculate the steady state $\bar{T}_i, \bar{S}_i, \bar{v}$

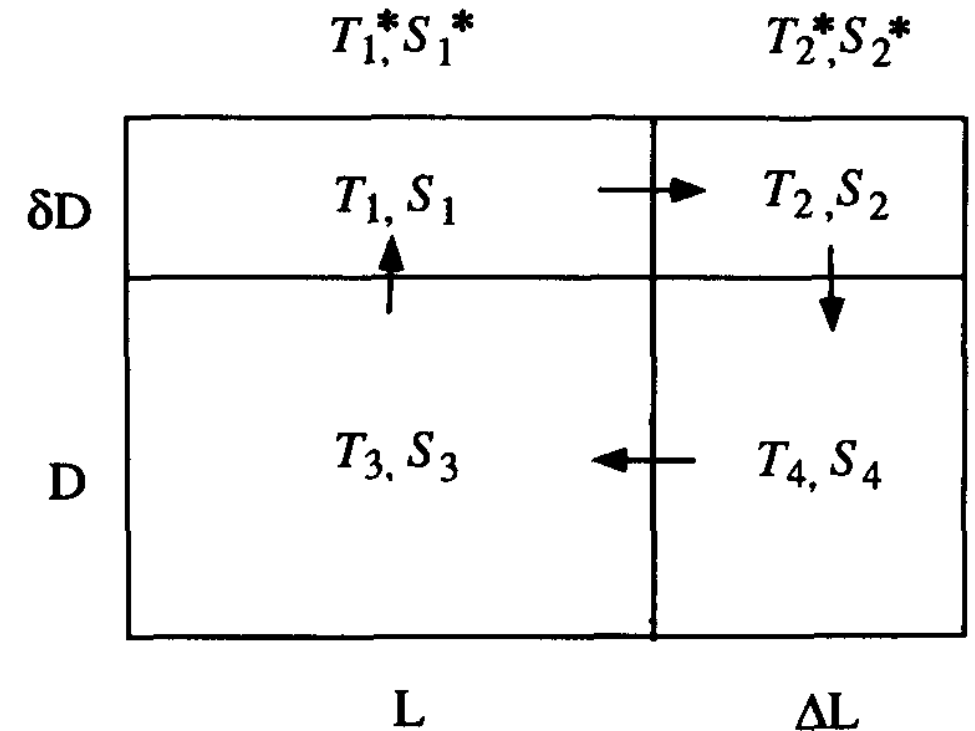


FIG. 3. Schematic plot of the box model geometry.

Tziperman et al 1994

- Linearize:

$$\delta \frac{\partial T'_1}{\partial t} = v'\delta(\bar{T}_3 - \bar{T}_1) + \bar{v}\delta(T'_3 - T'_1) - \delta T'_1$$

$$\delta \frac{\partial S'_1}{\partial t} = v'\delta(\bar{S}_3 - \bar{S}_1) + \bar{v}\delta(S'_3 - S'_1)$$

- Let $\mathbf{x}(t) = (T'_1, T'_2, T'_3, T'_4, S'_1, S'_2, S'_3, S'_4)$

- Linearized equations in matrix form $\frac{d\mathbf{x}}{dt} = A\mathbf{x}$

- Calculate eigenvalues/vectors of A , $\lambda_i, \hat{\mathbf{e}}_i$

- Deduce stability properties from real & imaginary parts of λ_i

AMOC: stochastic variability, stability regimes of box model

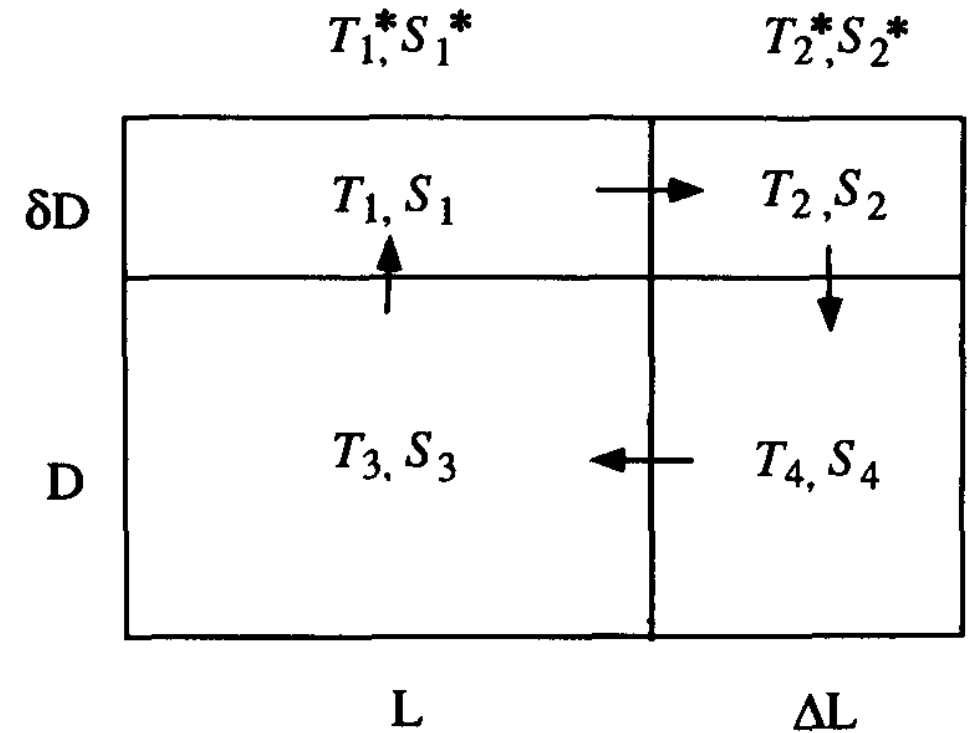
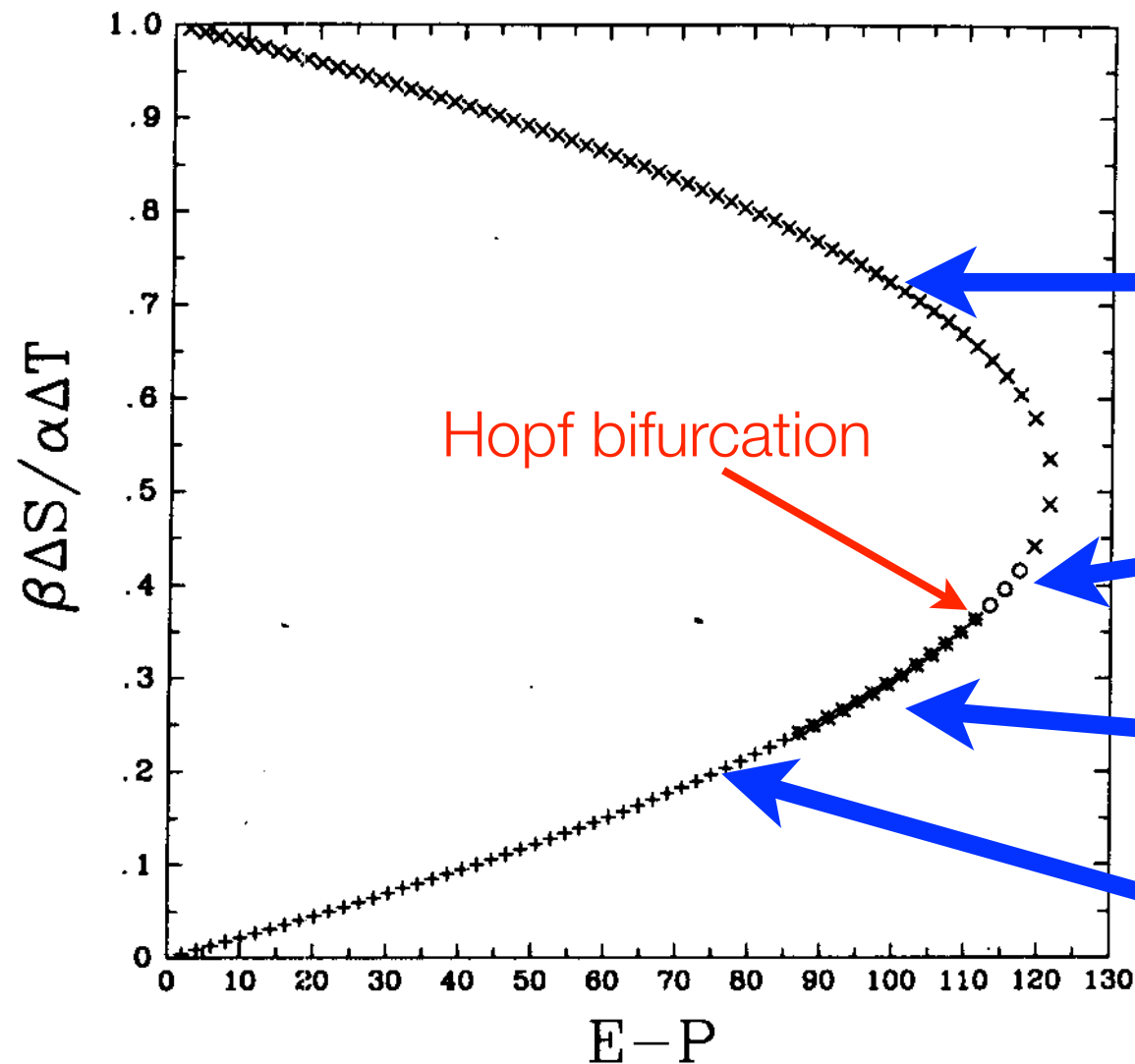


FIG. 3. Schematic plot of the box model geometry.

(a) Stability regimes under mixed b.c.



exponentially stable

oscillatory stable

oscillatory unstable

exponentially unstable

AMOC: stochastic variability, stability regimes of box model

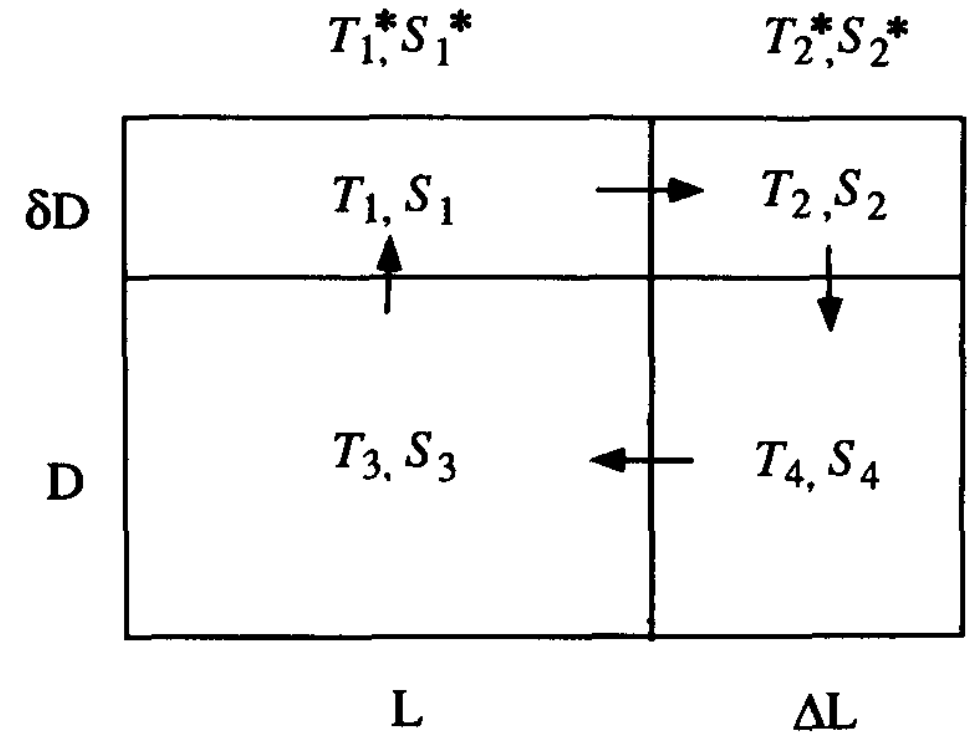
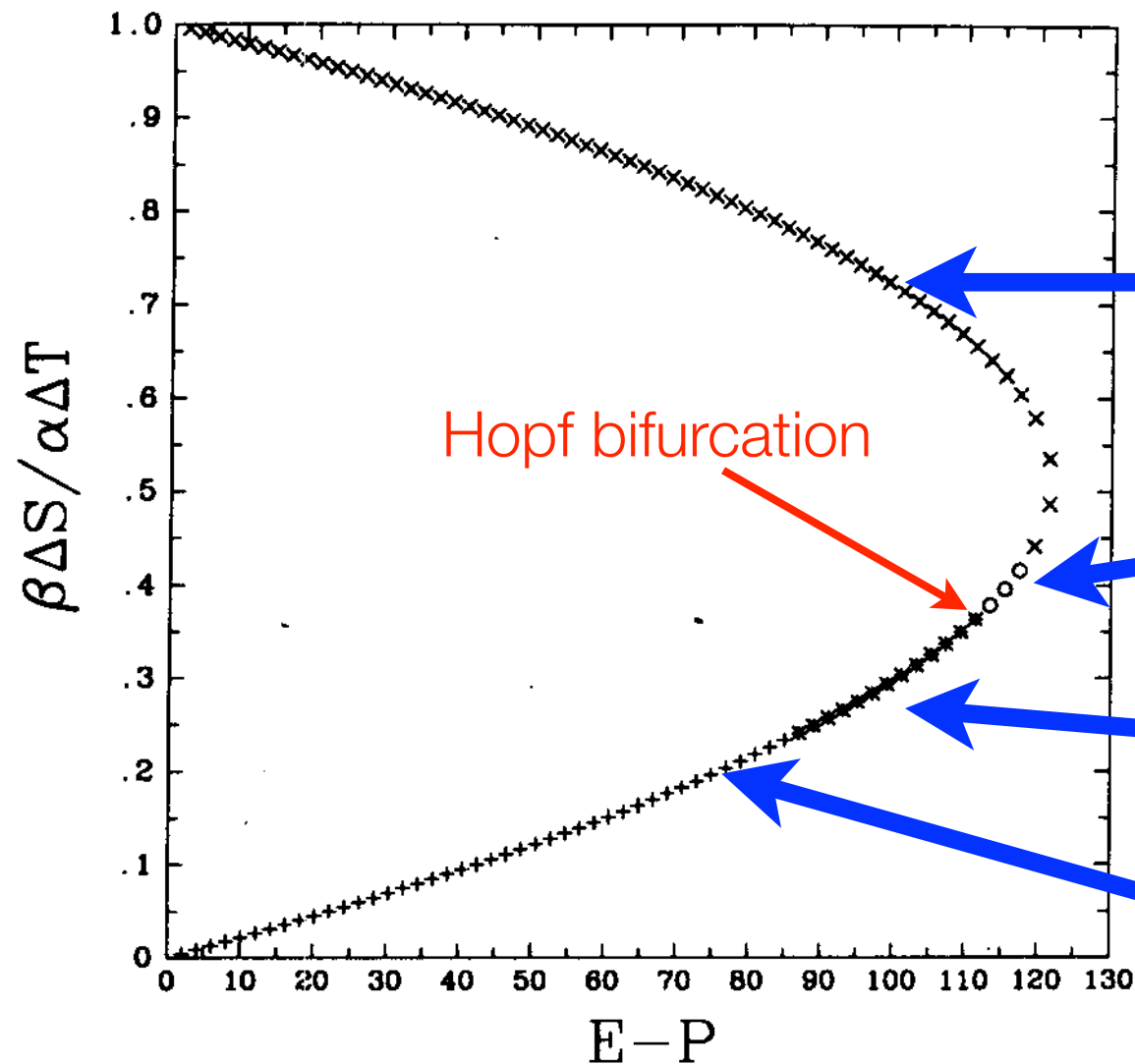


FIG. 3. Schematic plot of the box model geometry.

(a) Stability regimes under mixed b.c.



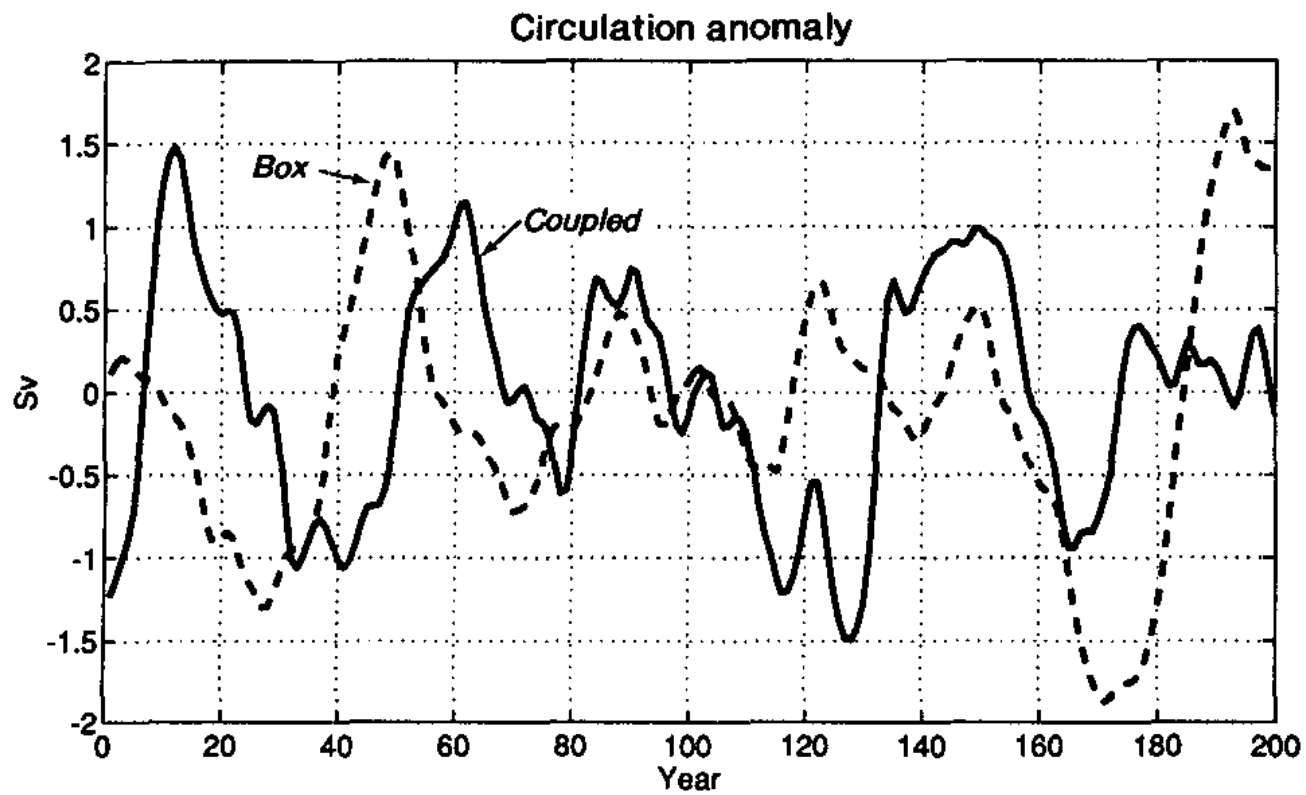
exponentially stable

oscillatory stable

oscillatory unstable

exponentially unstable

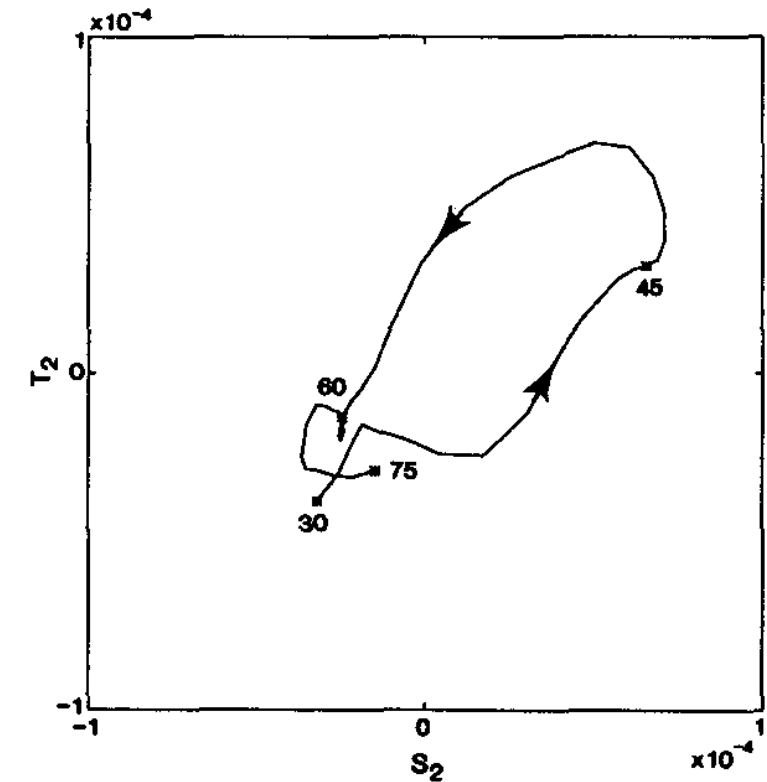
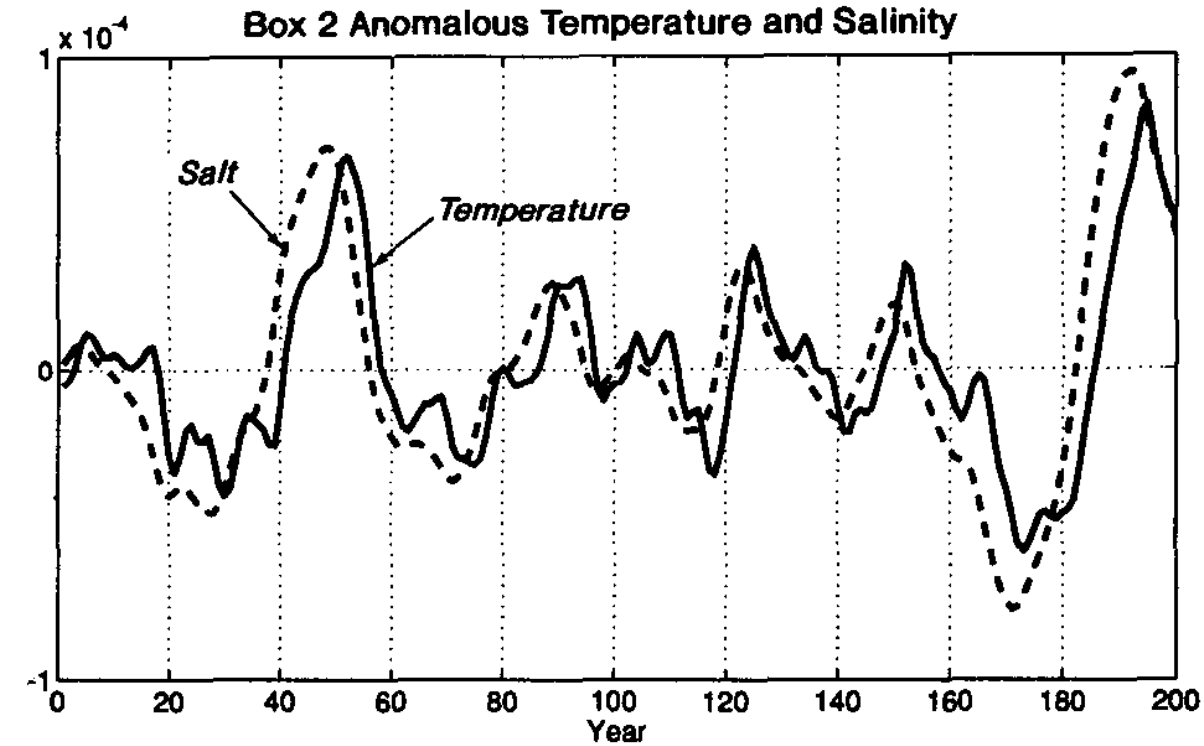
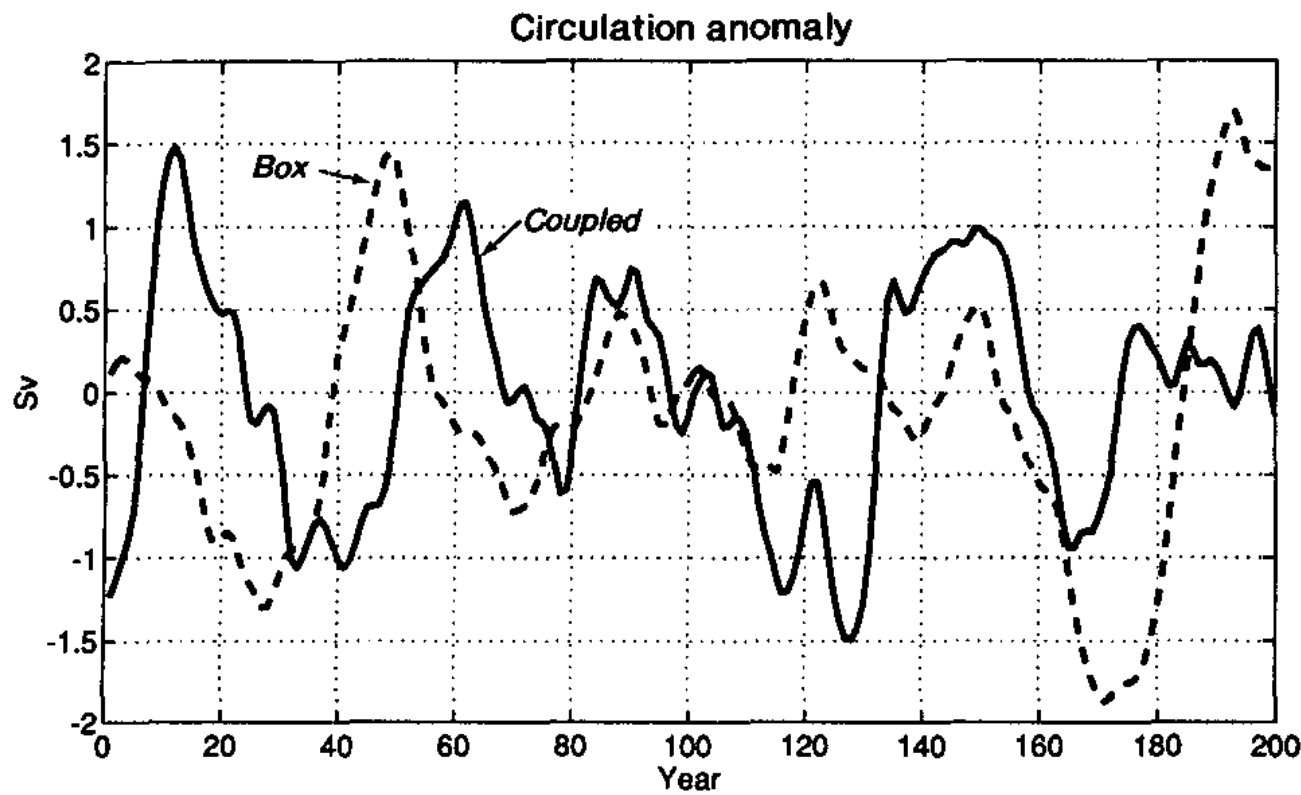
AMOC: stochastic excitation of damped oscillatory mode



Griffies & Tziperman 1995

Stochastic forcing of a damped oscillatory mode fits GCM results graduate level

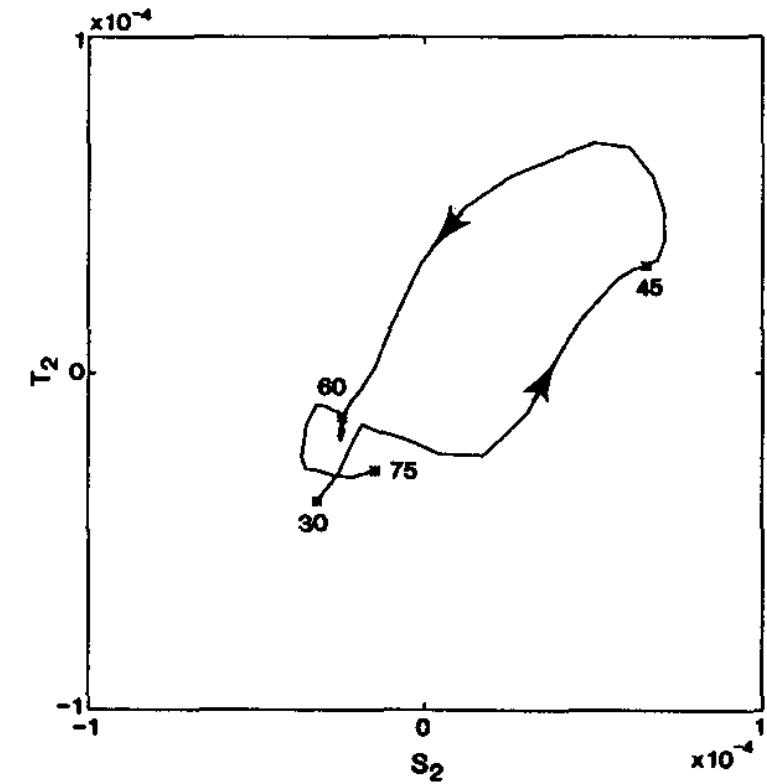
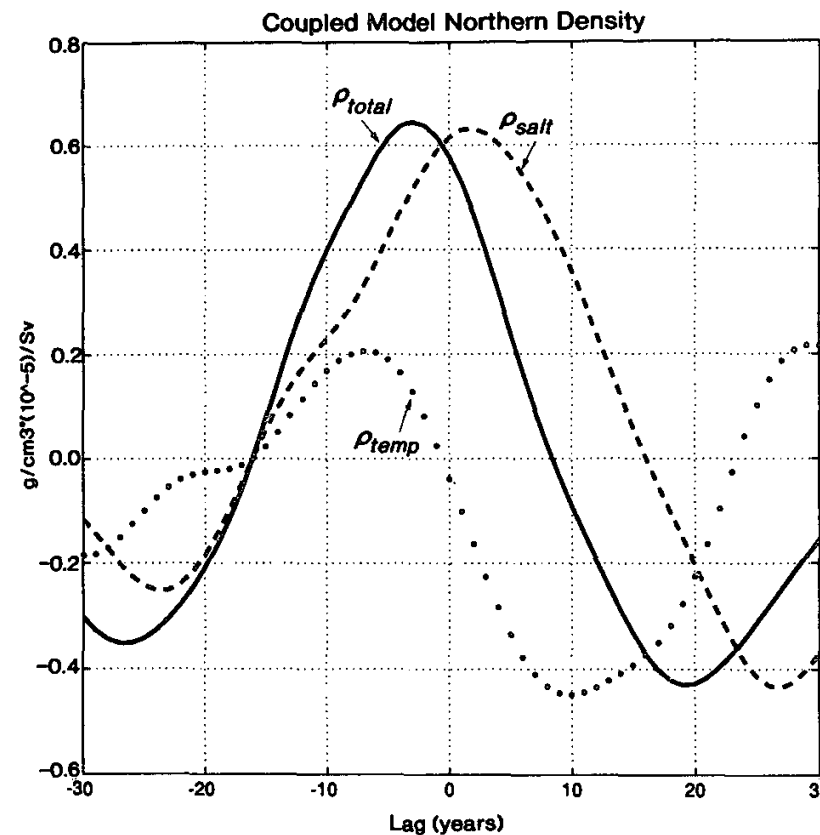
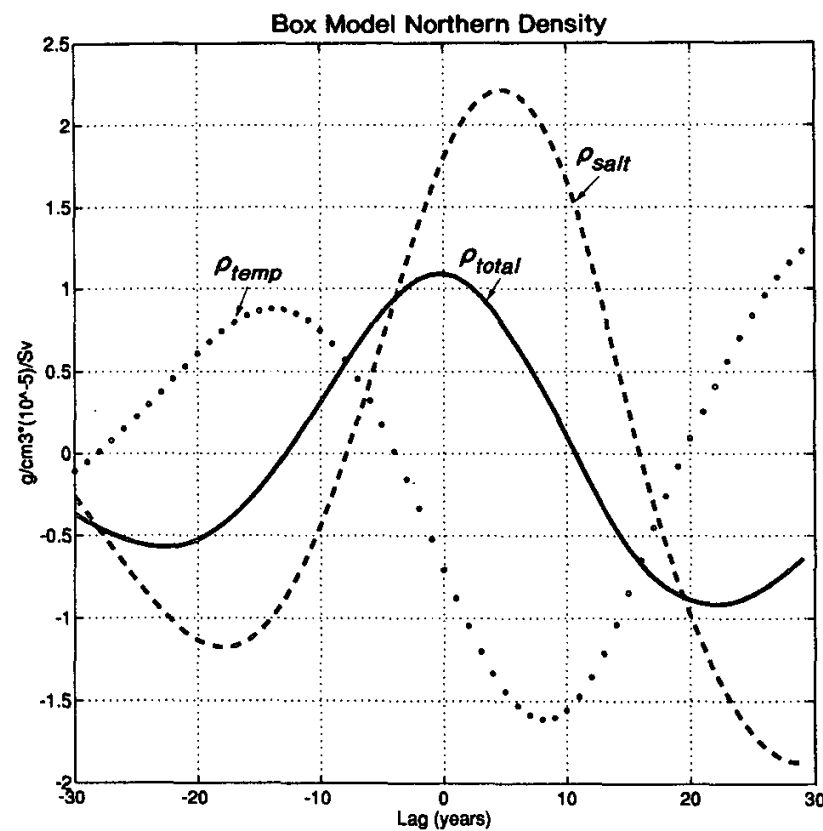
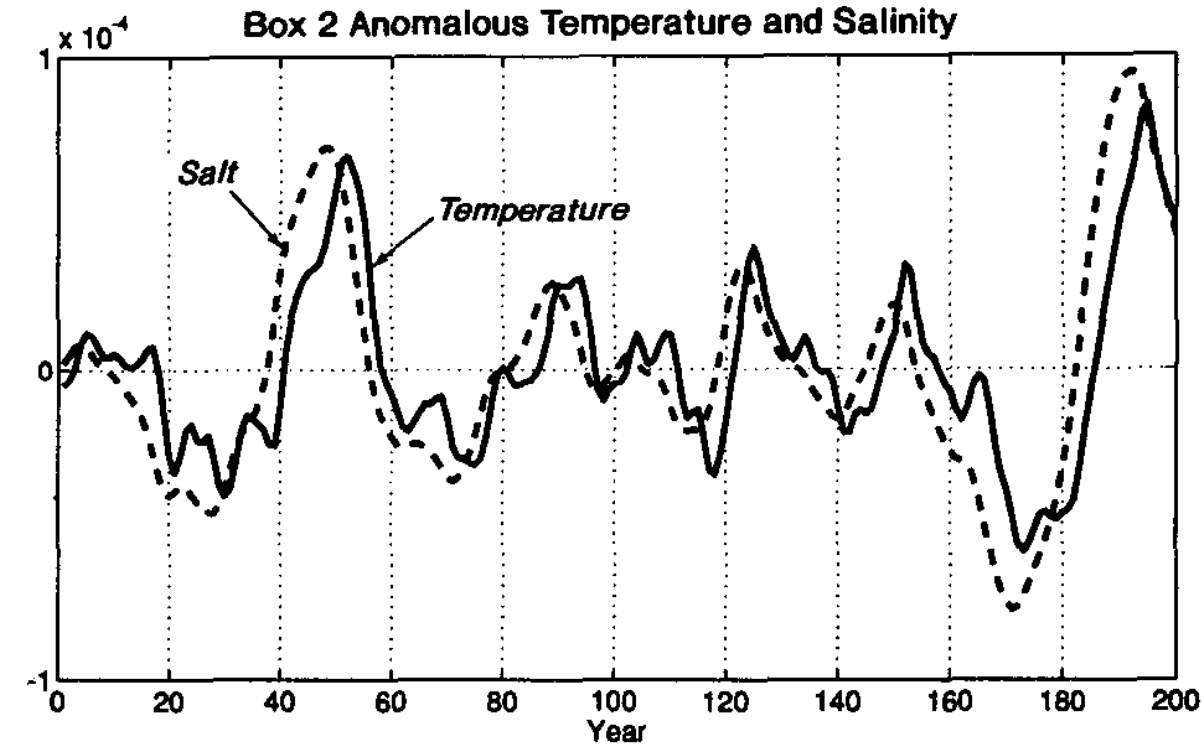
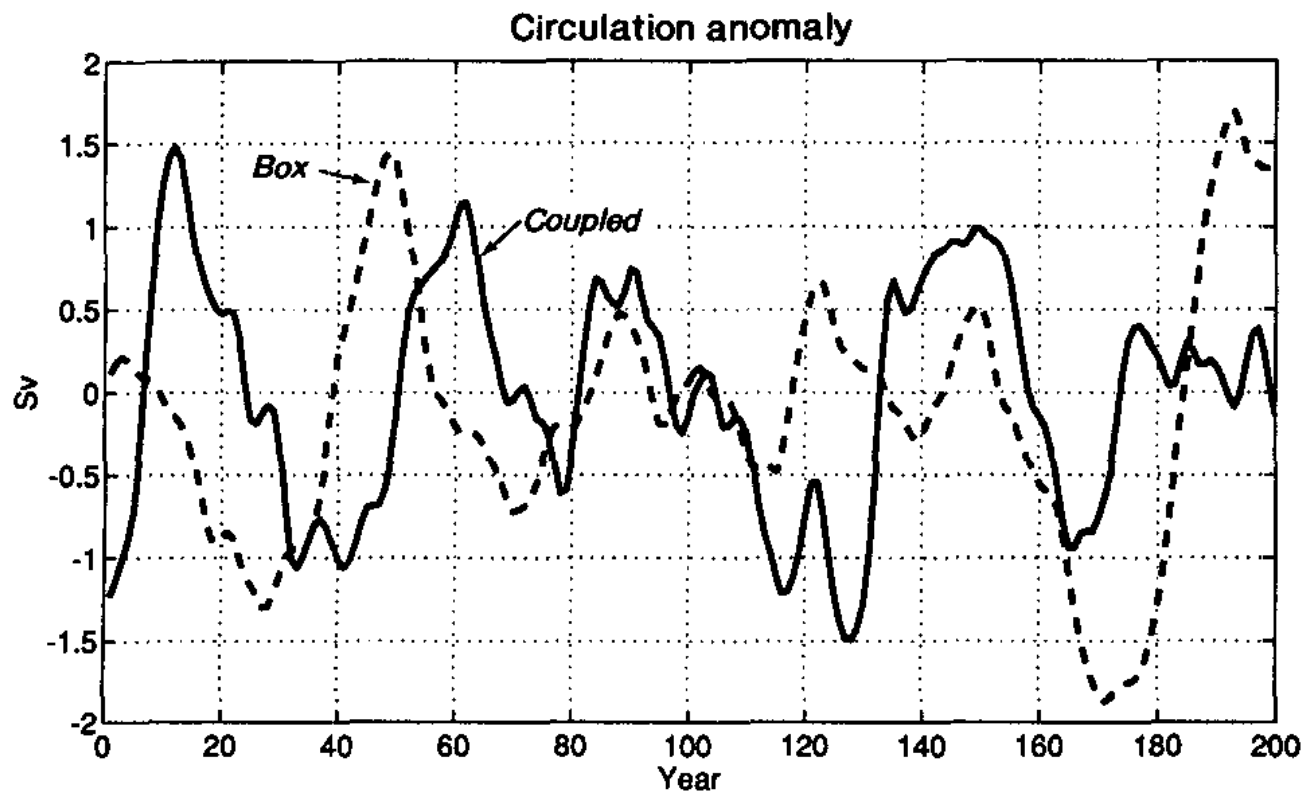
AMOC: stochastic excitation of damped oscillatory mode



Griffies & Tziperman 1995

Stochastic forcing of a damped oscillatory mode fits GCM results graduate level

AMOC: stochastic excitation of damped oscillatory mode



Griffies & Tziperman 1995

Regression of NA temperature, salinity, density, with AMOC

Stochastic forcing of a damped oscillatory mode fits GCM results graduate level

AMOC: stochastic excitation of damped oscillatory mode

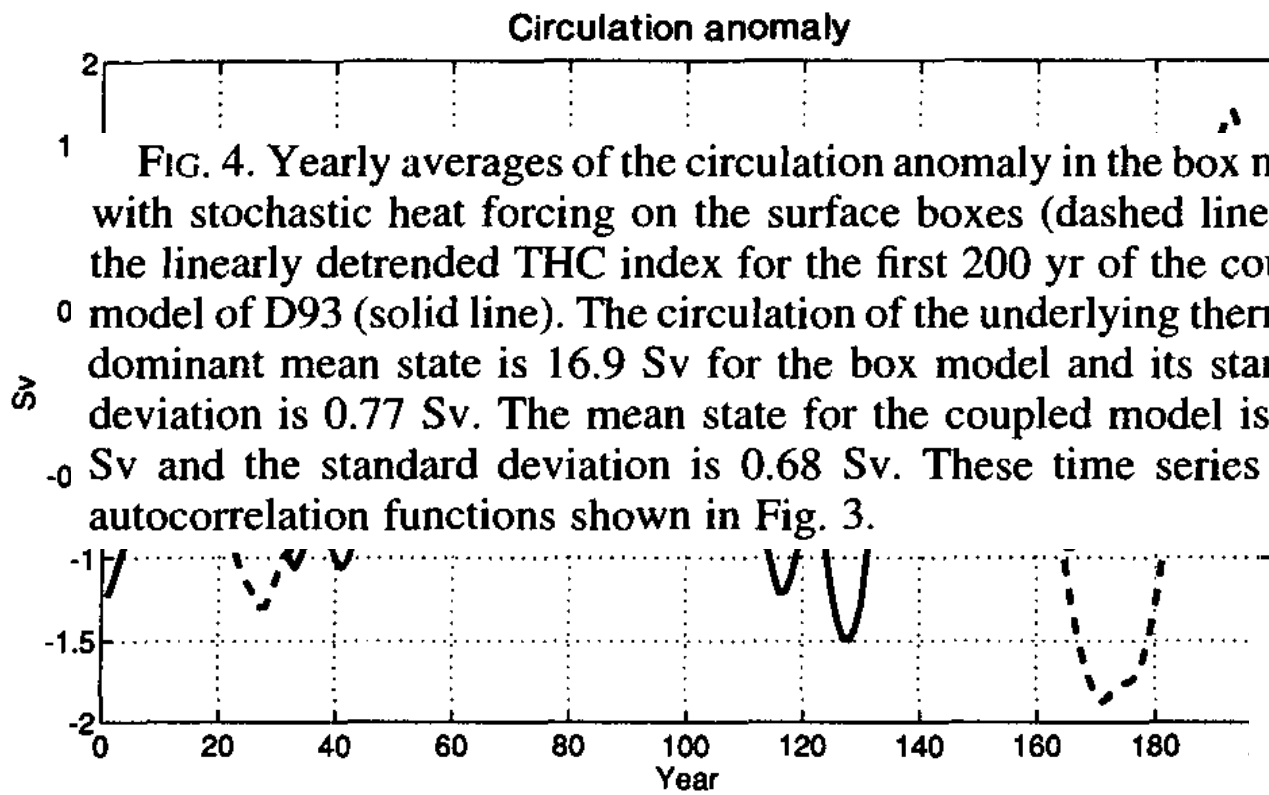


FIG. 4. Yearly averages of the circulation anomaly in the box model with stochastic heat forcing on the surface boxes (dashed line) and the linearly detrended THC index for the first 200 yr of the coupled model of D93 (solid line). The circulation of the underlying thermally dominant mean state is 16.9 Sv for the box model and its standard deviation is 0.77 Sv. The mean state for the coupled model is 18.3 Sv and the standard deviation is 0.68 Sv. These time series have autocorrelation functions shown in Fig. 3.

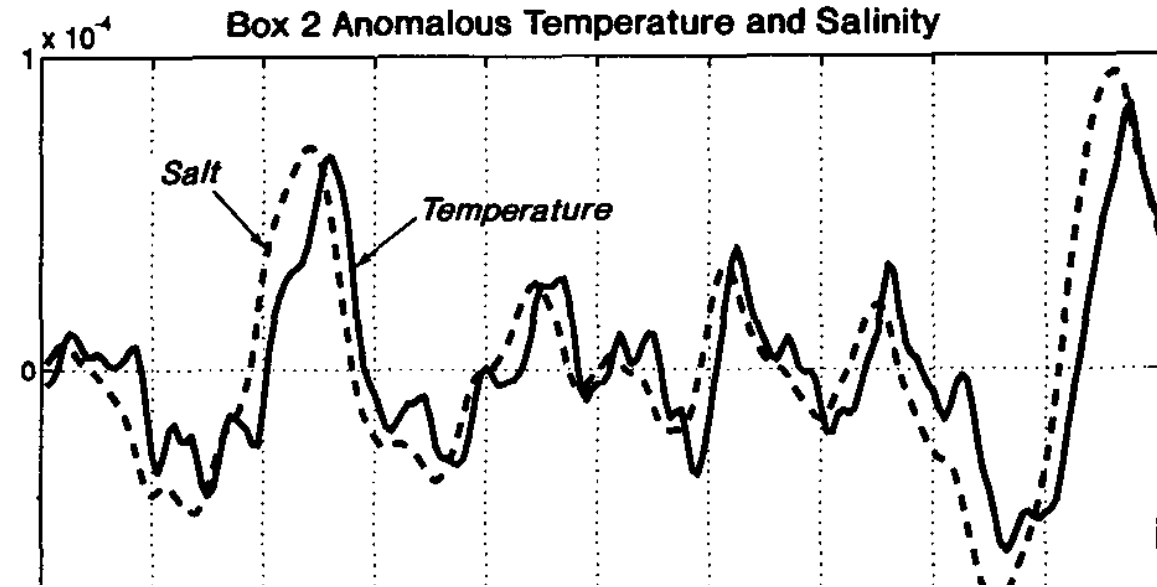


FIG. 5. (a) Dimensionless temperature anomaly $\alpha T_2'$ (solid line) and salinity anomaly $\beta S_2'$ (dashed line) for the northern surface box (box 2) in the box model with surface stochastic forcing. Note the phase relation (salt leads temperature) indicative of the oscillating mode shown in Fig. 2. (b) The $(\beta S_2', \alpha T_2')$ plane for years 30–70 of (a) with selected years indicated. The trajectory is in the counterclockwise direction since salt leads temperature.

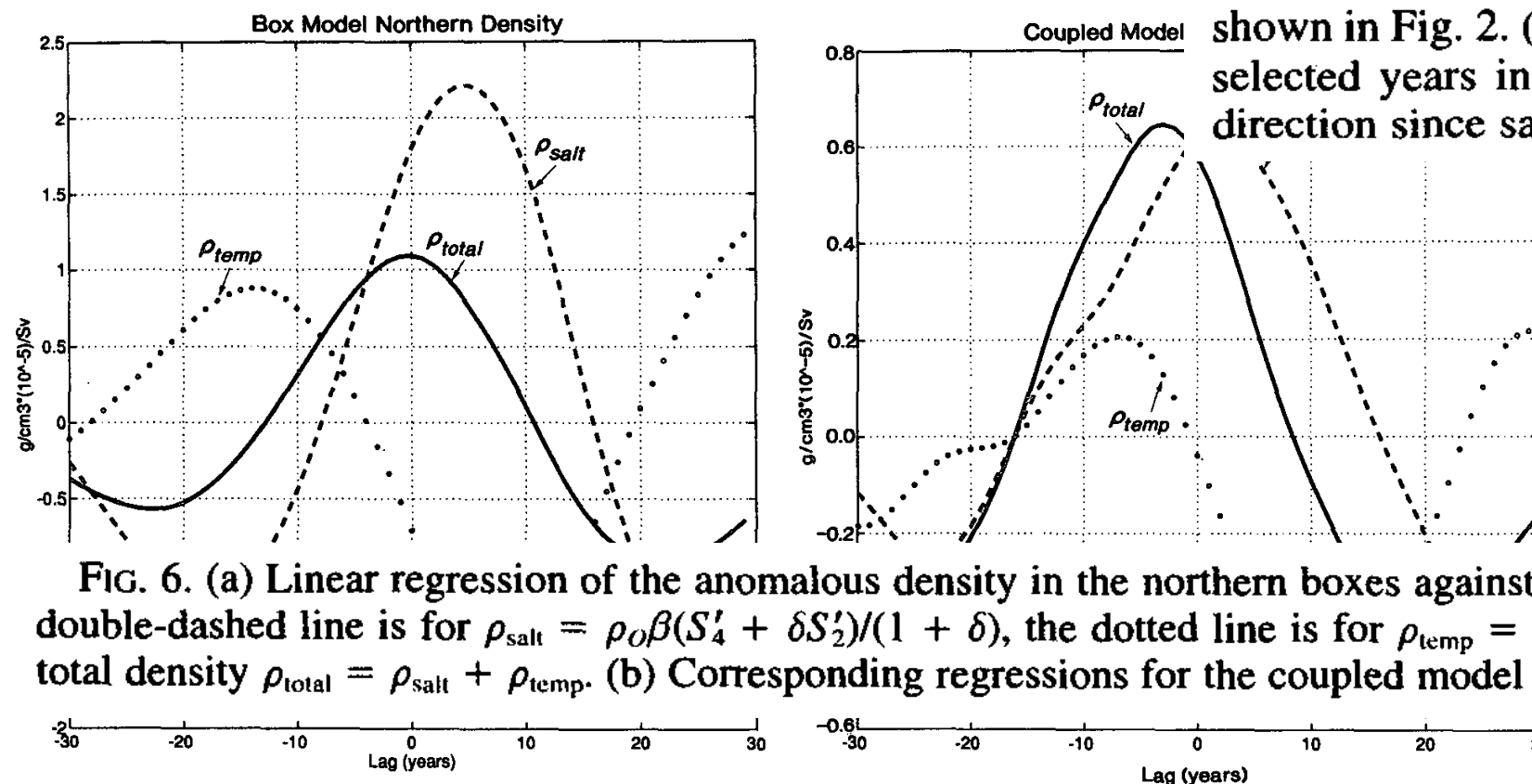
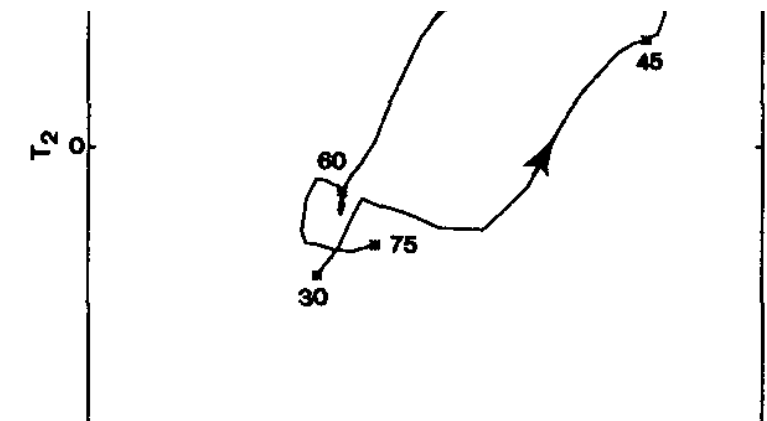


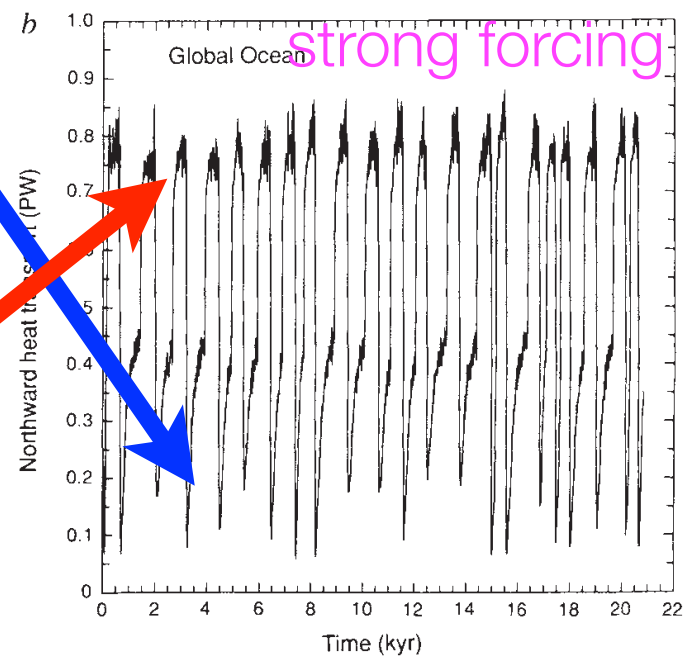
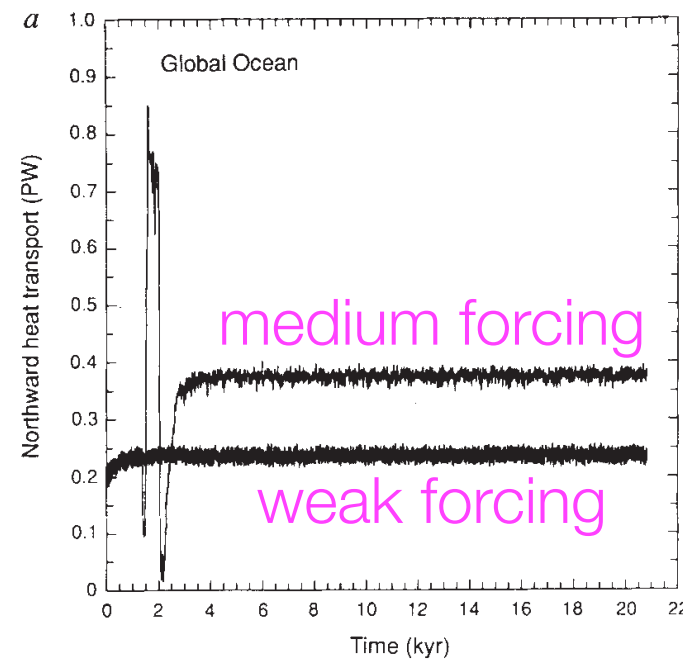
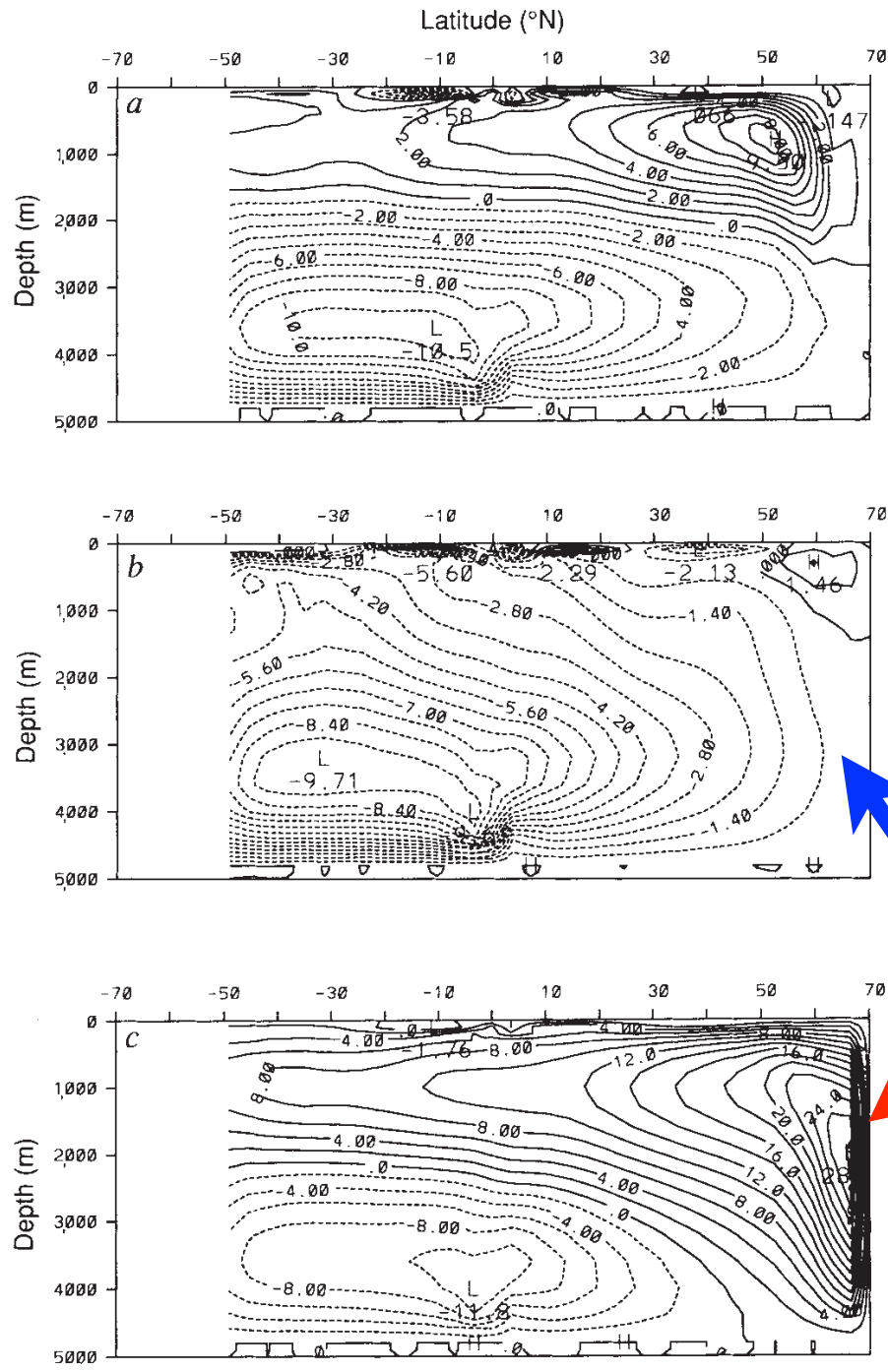
FIG. 6. (a) Linear regression of the anomalous density in the northern boxes against the filtered anomalous thermohaline circulation. The double-dashed line is for $\rho_{\text{salt}} = \rho_0 \beta (S_4' + \delta S_2') / (1 + \delta)$, the dotted line is for $\rho_{\text{temp}} = -\rho_0 \alpha (T_4' + \delta T_2') / (1 + \delta)$, and the solid line is for the total density $\rho_{\text{total}} = \rho_{\text{salt}} + \rho_{\text{temp}}$. (b) Corresponding regressions for the coupled model (Fig. 8 of D93).



Regression of NA temperature, salinity, density, with AMOC

Stochastic forcing of a damped oscillatory mode fits GCM results graduate level

AMOC: stochastic forcing of jumps between steady states



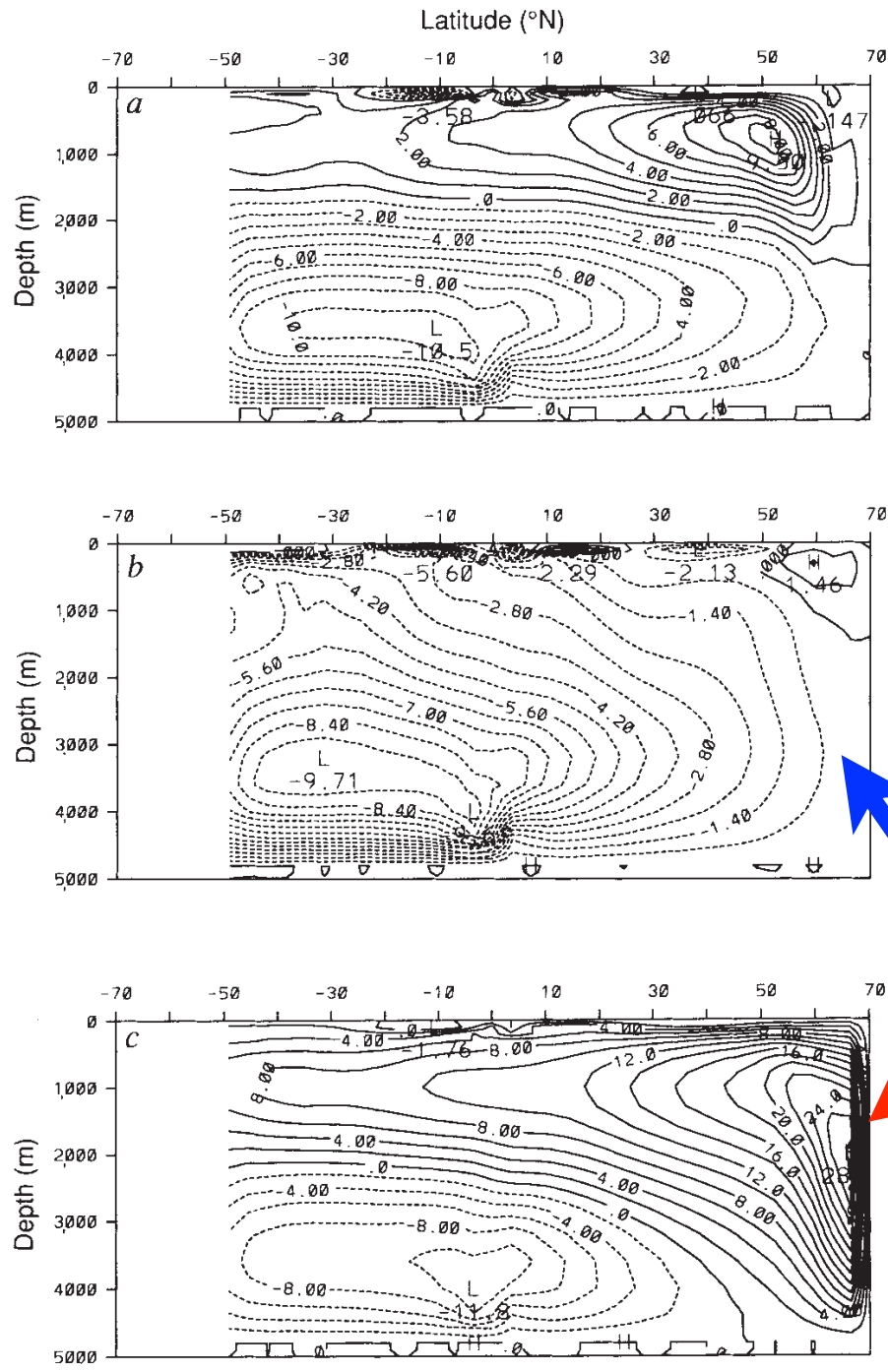
GCM

Weaver and Hughes 1994, Cessi 1994

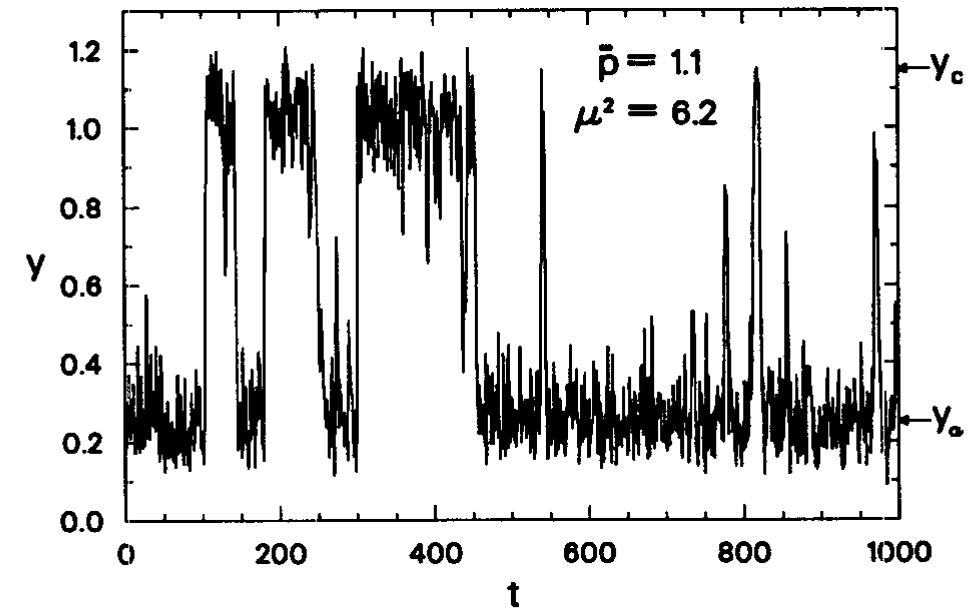
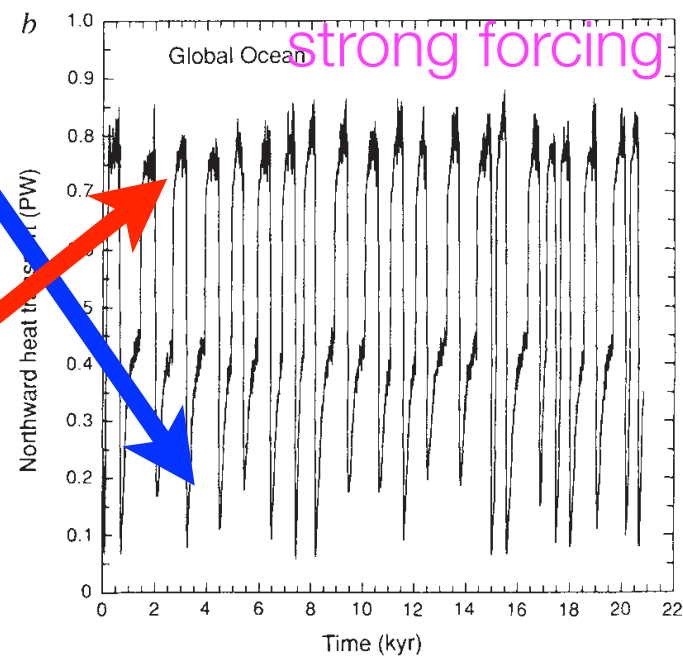
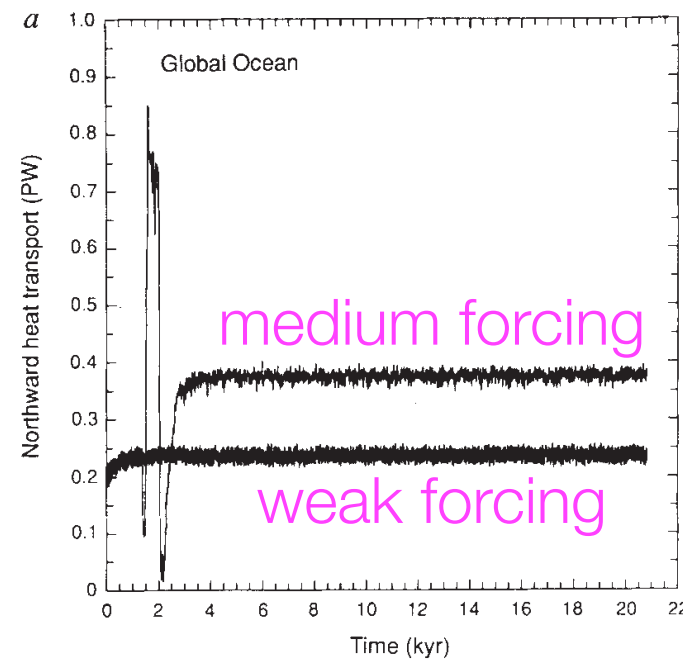
Strong stochastic forcing of Stommel model and of GCM

graduate level

AMOC: stochastic forcing of jumps between steady states



GCM



Stommel model

Weaver and Hughes 1994, Cessi 1994

Strong stochastic forcing of Stommel model and of GCM

graduate level

AMOC: stochastic forcing of jumps between steady states

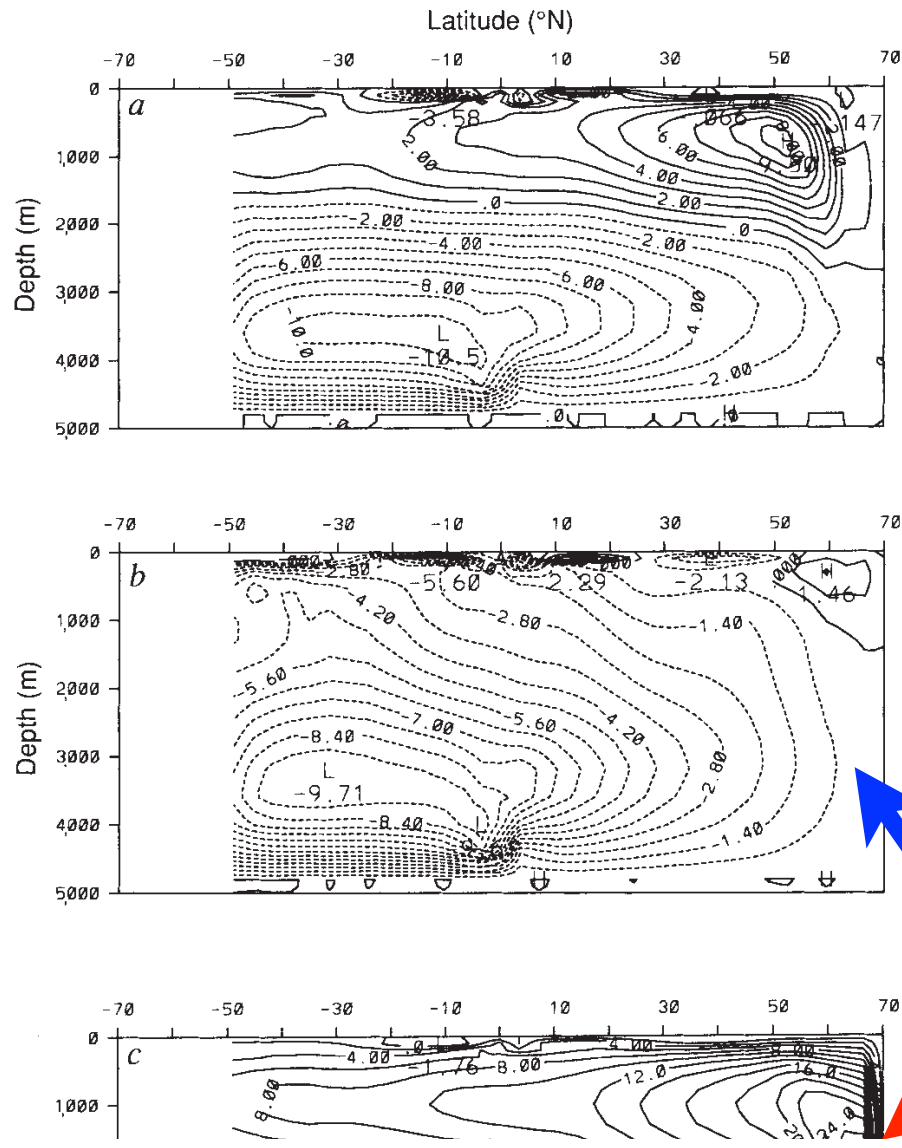


FIG. 2 The Atlantic Ocean meridional overturning streamfunction in Sv (1 Sv is $10^6 \text{ m}^3 \text{ s}^{-1}$) for the three equilibria. *a*, The normal 'present-day' conveyor. *b*, The weak 'colder' conveyor. *c*, The strong 'warmer' conveyor. The x-axis is the latitude with positive and negative values indicating °N and °S, respectively. Positive and negative contours indicate clockwise and counterclockwise circulations, respectively, with H and L indicating local maxima and minima, respectively.

FIG. 4 The global ocean poleward heat transport at 28° N over the 20,800 yr of integration. *a*, The weak stochastic experiment (standard deviation, s.d. = 16 mm per month, lower curve) and the medium stochastic experiment (s.d. = 32 mm per month, upper curve). *b*, The strong stochastic experiment (s.d. = 48 mm per month).

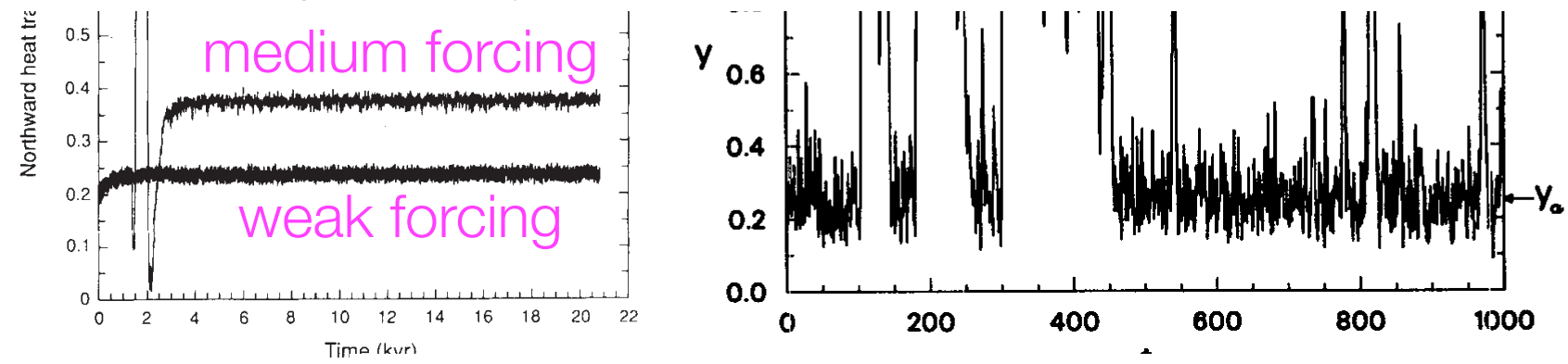


FIG. 5. A typical time series of y solution of (2.8b). At every time step, of size $dt = 3.33 \times 10^{-3}$, the stochastic forcing is randomly picked from a Gaussian distribution with zero mean and standard deviation $\sigma = 3.3$. The values of \bar{p} and μ^2 are as in Fig. 2. The salinity difference y spends most of the time in the neighborhood of the stable states y_a and y_c .

Weaver and Hughes 1994, Cessi 1994

AMOC variability: stochastic resonance

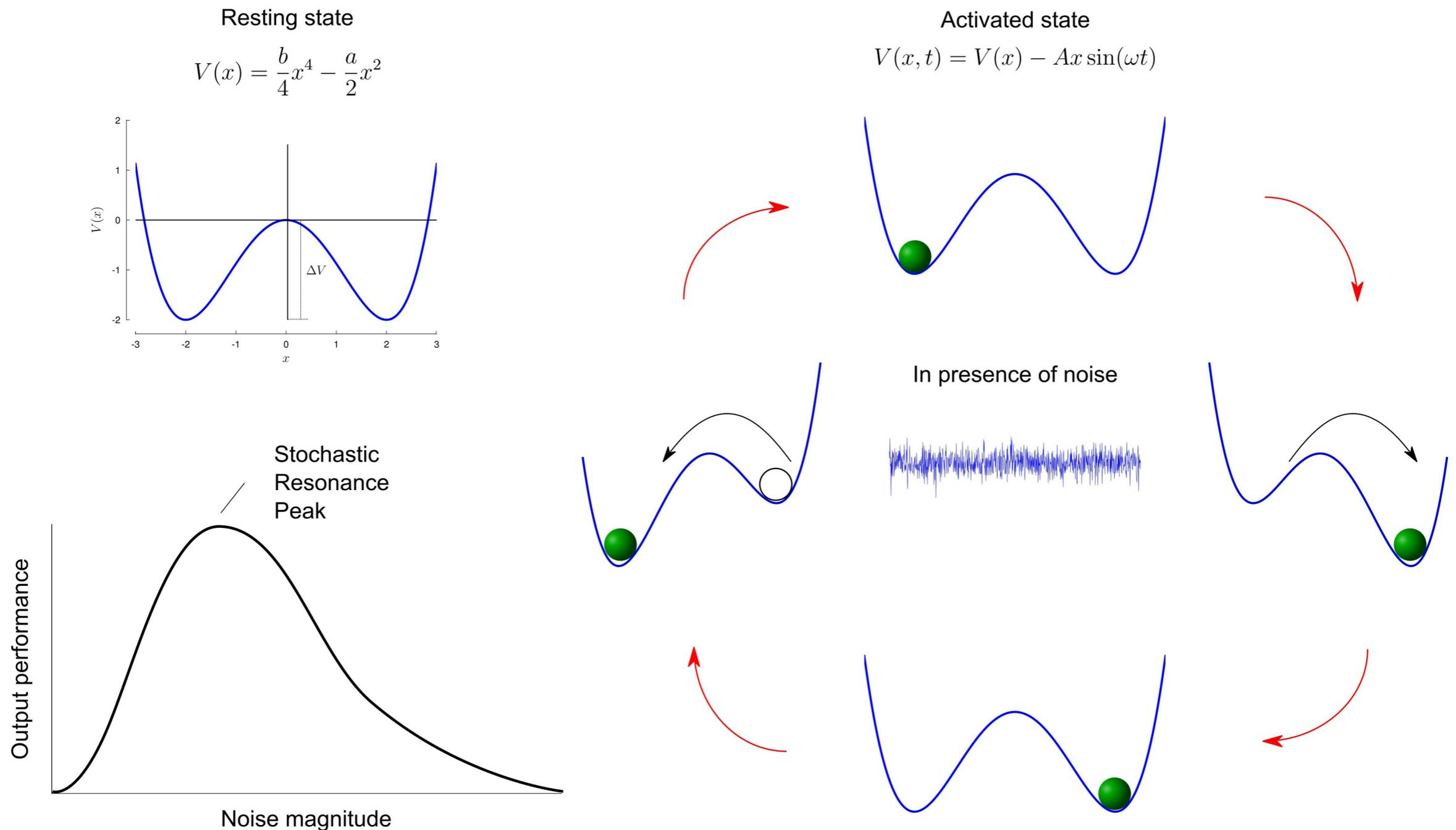
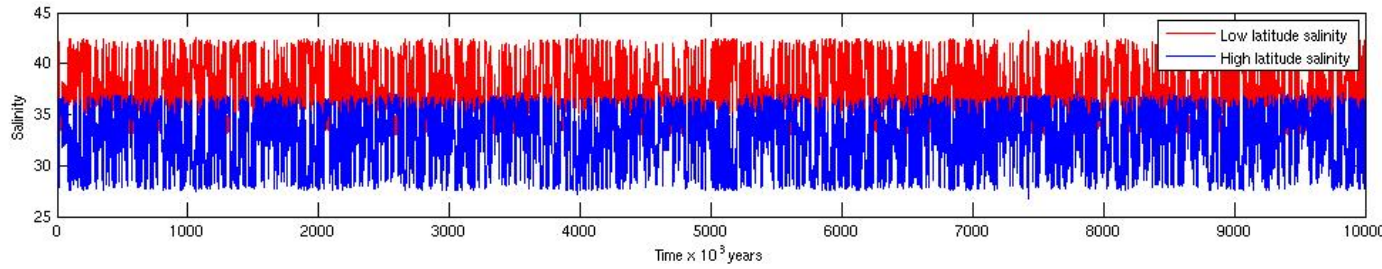
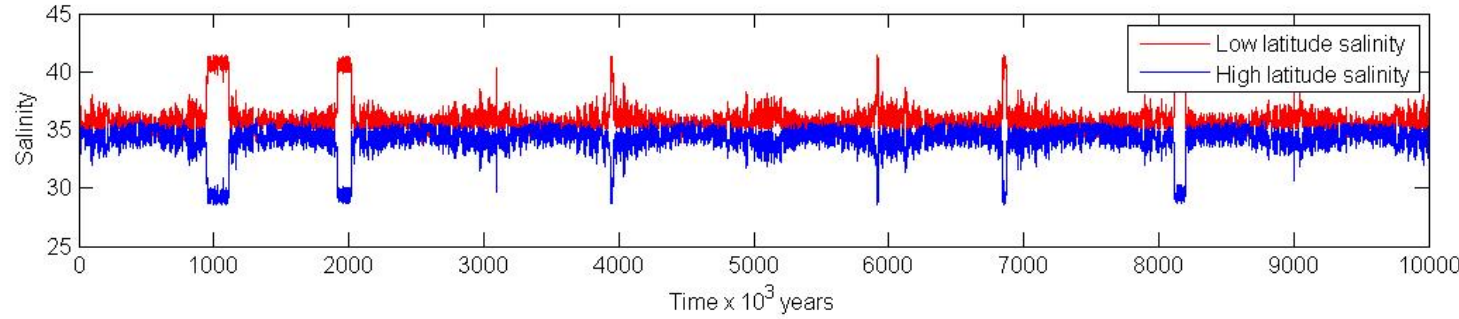
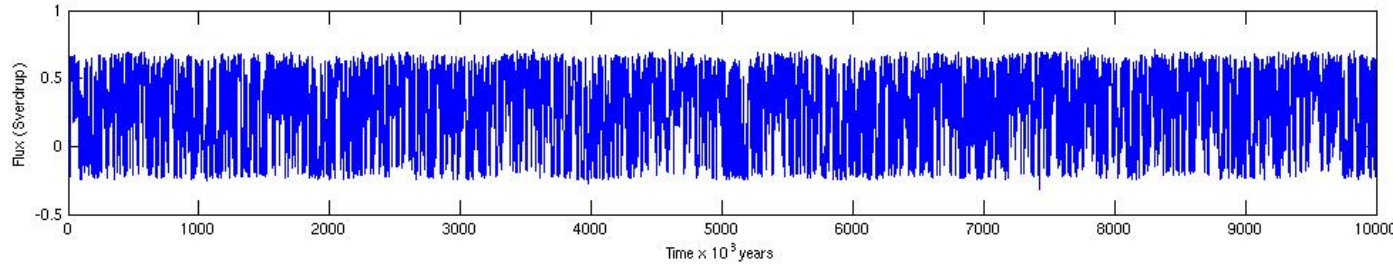


FIGURE 1 | Mechanism of stochastic resonance. **(A)** Sketch of a double well potential $V(x)$. In this example, the values a and b are set to 2 and 0.5, respectively. The minima are located at $x = \pm\sqrt{\frac{a}{b}}$ and are separated by a barrier potential $\Delta V = \frac{a^2}{4b}$. **(B)** In the presence of periodic driving, the height of the potential barrier oscillates through an antiphase lowering and raising of the wells. The cyclic variations are depicted in the cartoon. A suitable dose of noise (represented by the central white noise plot) will allow the marble to hop to the globally stable state. **(C)** Typical curve of output performance versus input noise magnitude, for systems capable of stochastic resonance. For small and large noise, the performance metric is very small, while some intermediate non-zero noise level provides optimal performance. Panels **A,B** adapted from Gammaitoni et al. (1998).

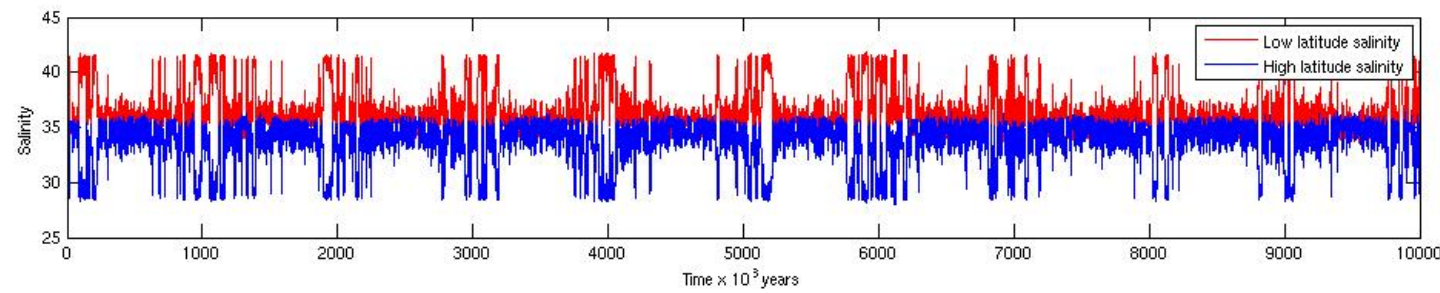
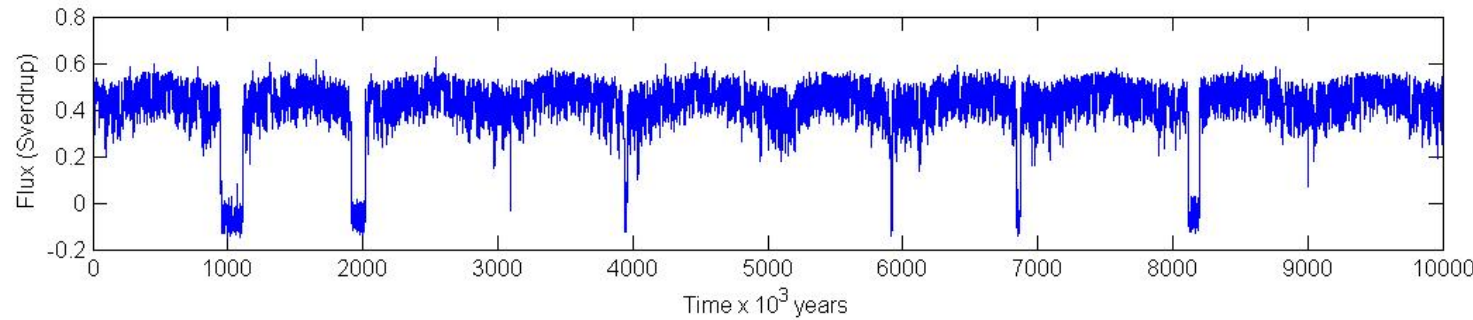
AMOC variability: stochastic resonance



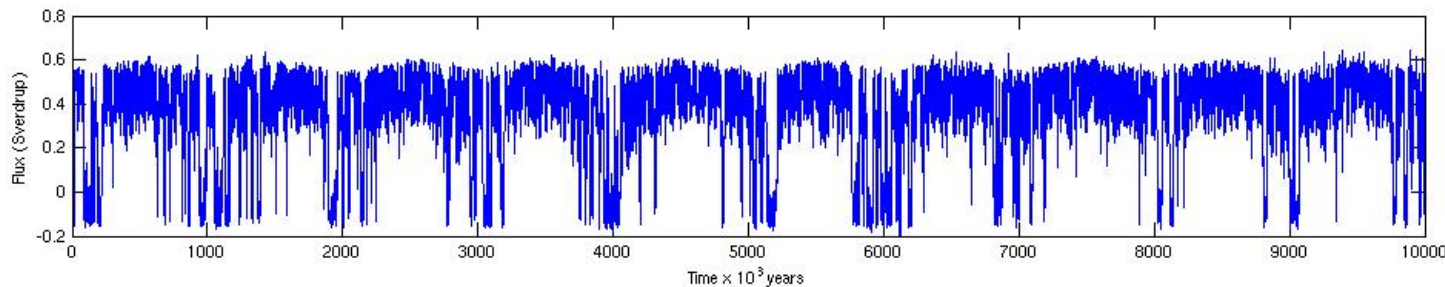
strong forcing,
frequent
transitions



weak forcing,
rare transitions



‘optimal’ forcing,
periodic
transitions



Stommel model under periodic+stochastic FW forcing

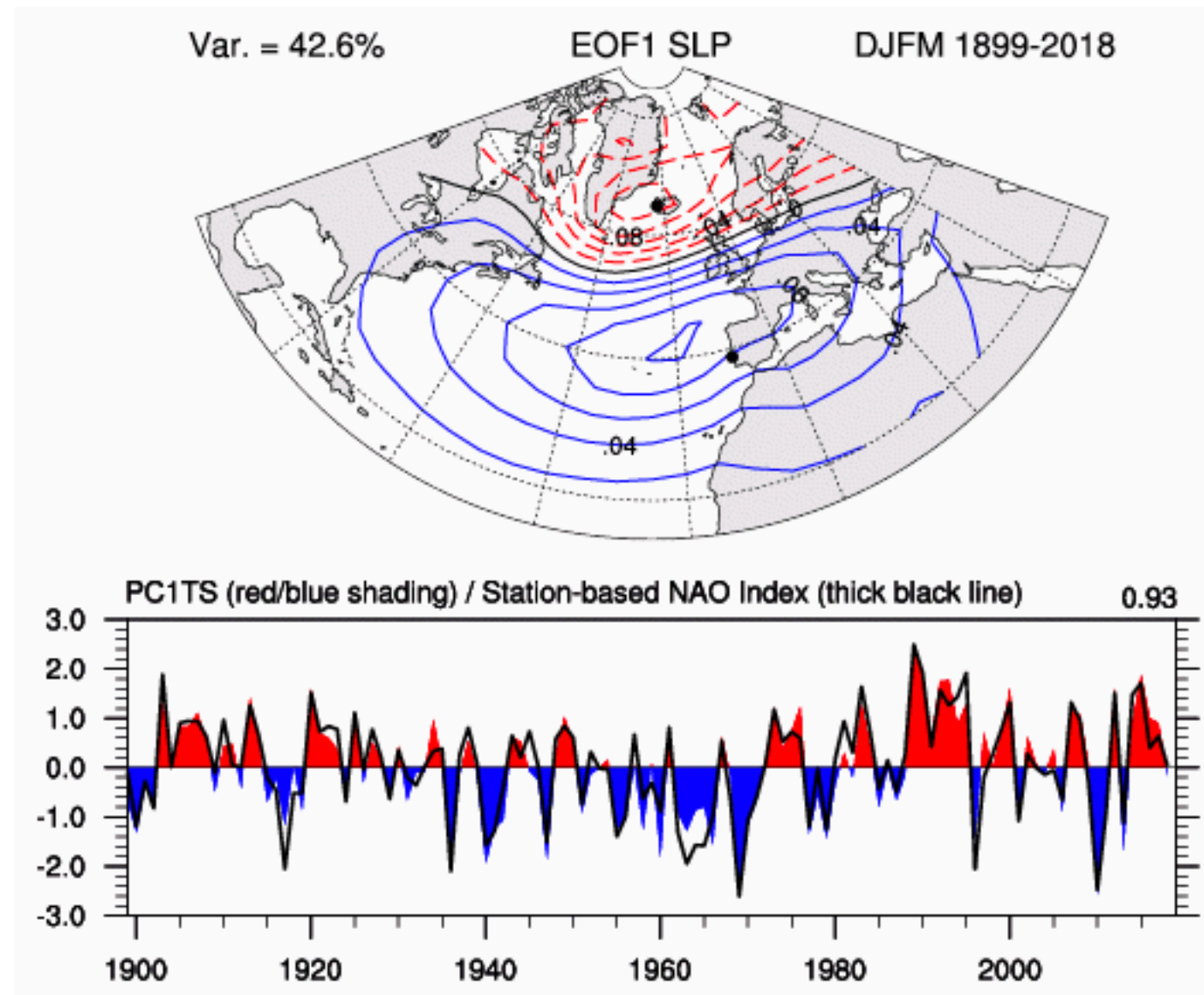
graduate level

notes: stochastic AMOC variability:

1. Hasselmann
2. stochastically forced damped oscillator
3. reminder: transient non-normal growth
4. stochastic optimals

what is this stochastic forcing? e.g. NAO, next 2 slides

Stochastic forcing of AMOC variability by NAO



NAO index time series is defined as:

Sea Level Pressure (SLP) at Lisbon, Portugal, minus Reykjavik, Iceland, Dec–Mar mean

or

The time series of the first EOF (principal component) of SLP over the Atlantic sector that is shown above

Stochastic forcing of AMOC variability by NAO

1. NAO index time series: SLP from Lisbon, Portugal, minus Reykjavik, Iceland, Dec–Mar mean
2. calculate composite air-sea fluxes for +/- NAO phases
3. create anomalous fluxes w/NAO spatial pattern & sine amplitude, periods 2, 5, 10, 20, 50, 100 yrs.

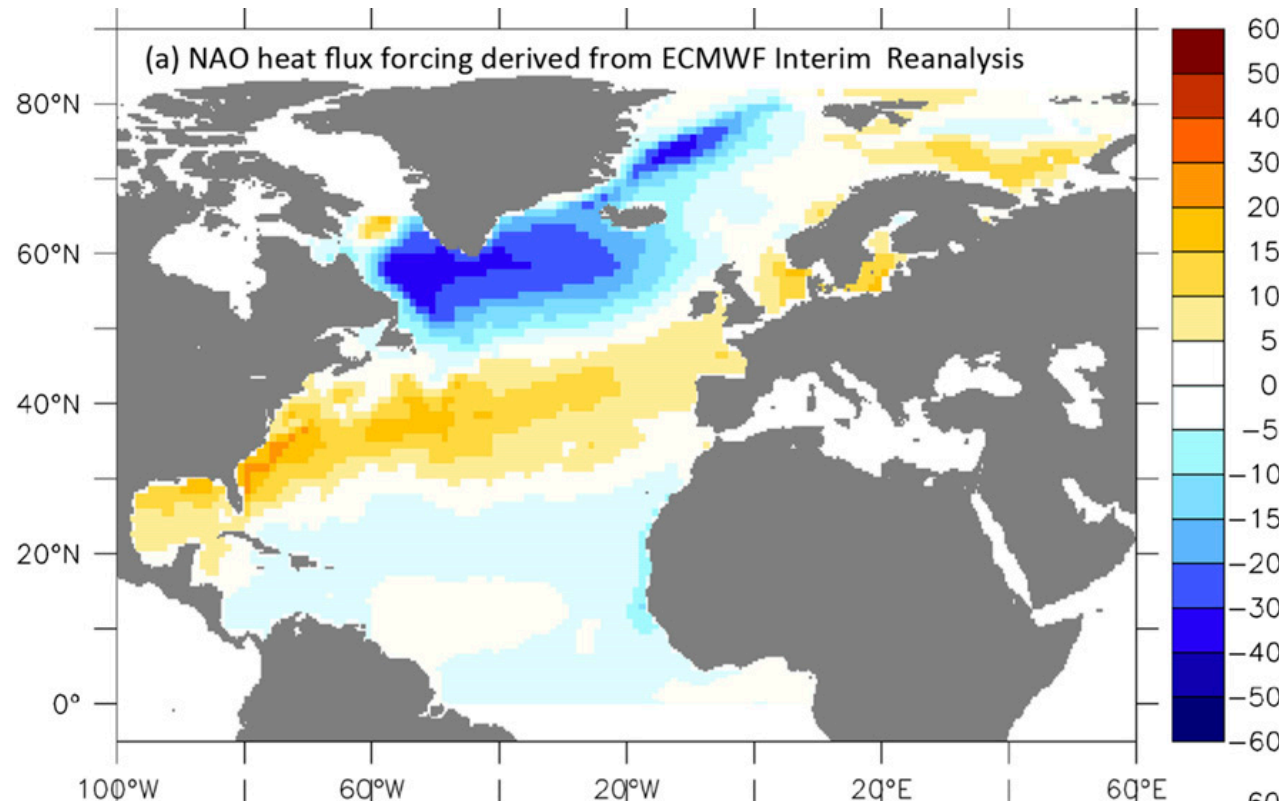


FIG. 1. Spatial pattern of heat flux anomalies (W/m^2) used as model forcing. Negative = ocean cooling. From ERA-Interim, avg over Dec–Mar, corresponding to a 1-std of NAO.

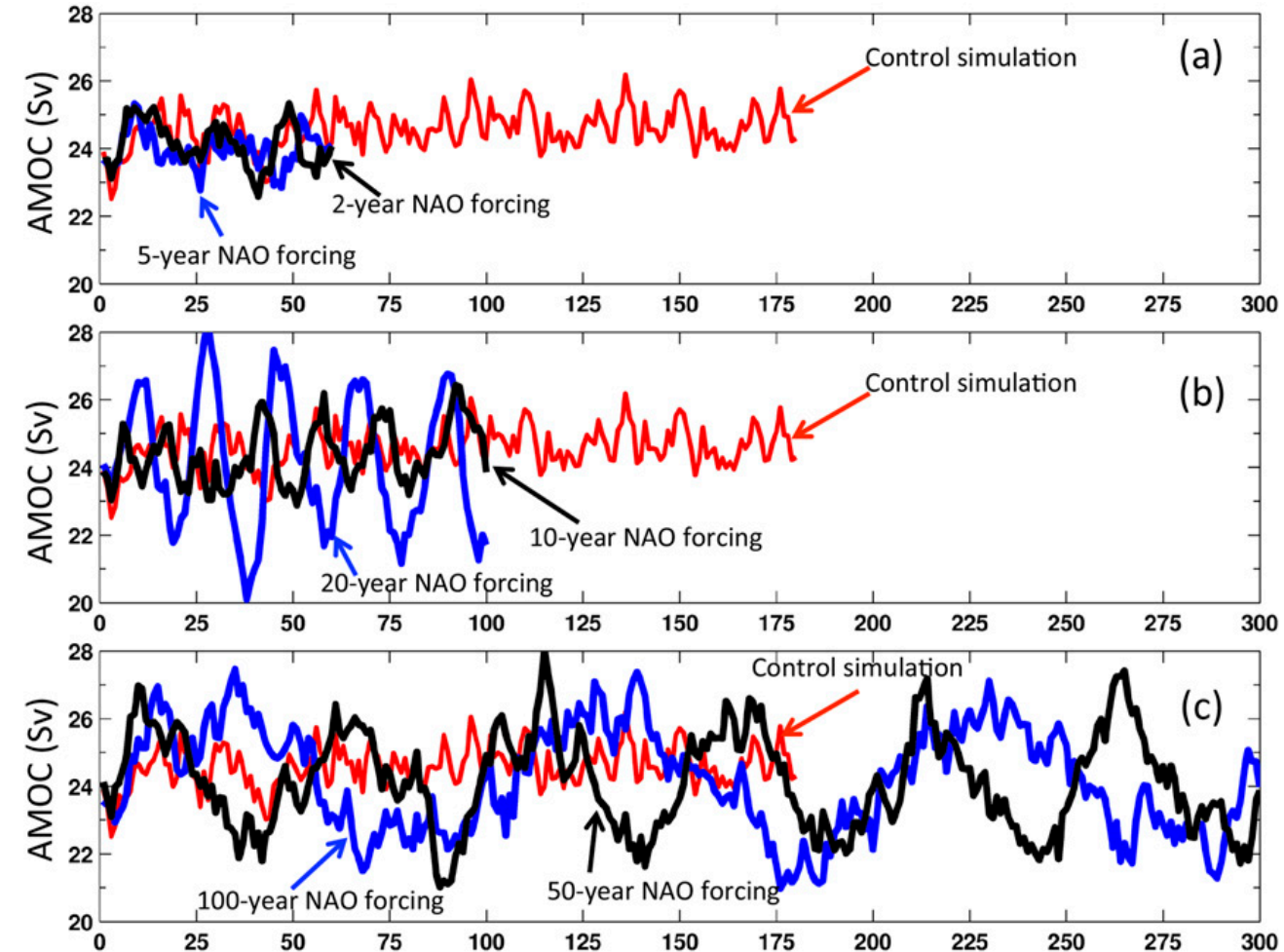


FIG. 5. AMOC response to periodic forcing. 10-member ensemble averages.

➡ Longer NAO time scale leads to a larger amplitude AMOC response, up to a limit.
Stochastic response not explored yet

Delworth & Zeng 2016

graduate level

Summary

- AMOC transports significant heat poleward; affects high latitude climate; not necessarily the dominant factor; see atmospheric jet meanders

Summary

- AMOC transports significant heat poleward; affects high latitude climate; not necessarily the dominant factor; see atmospheric jet meanders
- Drivers: T&S, air-sea heat&FW fluxes, interior mixing, Southern Ocean wind

Summary

- AMOC transports significant heat poleward; affects high latitude climate; not necessarily the dominant factor; see atmospheric jet meanders
- Drivers: T&S, air-sea heat&FW fluxes, interior mixing, Southern Ocean wind
- Interior mixing via internal wave breaking, energy due to tides & topography

Summary

- AMOC transports significant heat poleward; affects high latitude climate; not necessarily the dominant factor; see atmospheric jet meanders
- Drivers: T&S, air-sea heat&FW fluxes, interior mixing, Southern Ocean wind
- Interior mixing via internal wave breaking, energy due to tides & topography
- Diabatic vs an adiabatic picture of the circulation

Summary

- AMOC transports significant heat poleward; affects high latitude climate; not necessarily the dominant factor; see atmospheric jet meanders
- Drivers: T&S, air-sea heat&FW fluxes, interior mixing, Southern Ocean wind
- Interior mixing via internal wave breaking, energy due to tides & topography
- Diabatic vs an adiabatic picture of the circulation
- Multiple equilibria and hysteresis, Stommel box model

Summary

- AMOC transports significant heat poleward; affects high latitude climate; not necessarily the dominant factor; see atmospheric jet meanders
- Drivers: T&S, air-sea heat&FW fluxes, interior mixing, Southern Ocean wind
- Interior mixing via internal wave breaking, energy due to tides & topography
- Diabatic vs an adiabatic picture of the circulation
- Multiple equilibria and hysteresis, Stommel box model
- Variability mechanisms

Summary

- AMOC transports significant heat poleward; affects high latitude climate; not necessarily the dominant factor; see atmospheric jet meanders
- Drivers: T&S, air-sea heat&FW fluxes, interior mixing, Southern Ocean wind
- Interior mixing via internal wave breaking, energy due to tides & topography
- Diabatic vs an adiabatic picture of the circulation
- Multiple equilibria and hysteresis, Stommel box model
- Variability mechanisms
 - Self-sustained vs. damped and stochastically-driven, Hopf bifurcation.

Summary

- AMOC transports significant heat poleward; affects high latitude climate; not necessarily the dominant factor; see atmospheric jet meanders
- Drivers: T&S, air-sea heat&FW fluxes, interior mixing, Southern Ocean wind
- Interior mixing via internal wave breaking, energy due to tides & topography
- Diabatic vs an adiabatic picture of the circulation
- Multiple equilibria and hysteresis, Stommel box model
- Variability mechanisms
 - Self-sustained vs. damped and stochastically-driven, Hopf bifurcation.
 - Convective oscillations, Welander flip-flop mechanism, self-sustained variability, relaxation oscillations

Summary

- AMOC transports significant heat poleward; affects high latitude climate; not necessarily the dominant factor; see atmospheric jet meanders
- Drivers: T&S, air-sea heat&FW fluxes, interior mixing, Southern Ocean wind
- Interior mixing via internal wave breaking, energy due to tides & topography
- Diabatic vs an adiabatic picture of the circulation
- Multiple equilibria and hysteresis, Stommel box model
- Variability mechanisms
 - Self-sustained vs. damped and stochastically-driven, Hopf bifurcation.
 - Convective oscillations, Welander flip-flop mechanism, self-sustained variability, relaxation oscillations
 - Oscillations due to advection of salinity, advective instability mechanism

Summary

- AMOC transports significant heat poleward; affects high latitude climate; not necessarily the dominant factor; see atmospheric jet meanders
- Drivers: T&S, air-sea heat&FW fluxes, interior mixing, Southern Ocean wind
- Interior mixing via internal wave breaking, energy due to tides & topography
- Diabatic vs an adiabatic picture of the circulation
- Multiple equilibria and hysteresis, Stommel box model
- Variability mechanisms
 - Self-sustained vs. damped and stochastically-driven, Hopf bifurcation.
 - Convective oscillations, Welander flip-flop mechanism, self-sustained variability, relaxation oscillations
 - Oscillations due to advection of salinity, advective instability mechanism
 - Stochastically forced damped oscillatory mode, with phase lags between T,S and a role for the advective feedback.

Summary

- AMOC transports significant heat poleward; affects high latitude climate; not necessarily the dominant factor; see atmospheric jet meanders
- Drivers: T&S, air-sea heat&FW fluxes, interior mixing, Southern Ocean wind
- Interior mixing via internal wave breaking, energy due to tides & topography
- Diabatic vs an adiabatic picture of the circulation
- Multiple equilibria and hysteresis, Stommel box model
- Variability mechanisms
 - Self-sustained vs. damped and stochastically-driven, Hopf bifurcation.
 - Convective oscillations, Welander flip-flop mechanism, self-sustained variability, relaxation oscillations
 - Oscillations due to advection of salinity, advective instability mechanism
 - Stochastically forced damped oscillatory mode, with phase lags between T,S and a role for the advective feedback.
 - A role for non-normal noise amplification, stochastic optimals.

Summary

- AMOC transports significant heat poleward; affects high latitude climate; not necessarily the dominant factor; see atmospheric jet meanders
- Drivers: T&S, air-sea heat&FW fluxes, interior mixing, Southern Ocean wind
- Interior mixing via internal wave breaking, energy due to tides & topography
- Diabatic vs an adiabatic picture of the circulation
- Multiple equilibria and hysteresis, Stommel box model
- Variability mechanisms
 - Self-sustained vs. damped and stochastically-driven, Hopf bifurcation.
 - Convective oscillations, Welander flip-flop mechanism, self-sustained variability, relaxation oscillations
 - Oscillations due to advection of salinity, advective instability mechanism
 - Stochastically forced damped oscillatory mode, with phase lags between T,S and a role for the advective feedback.
 - A role for non-normal noise amplification, stochastic optimals.
 - Noise-driven jumps between steady states

Summary

- AMOC transports significant heat poleward; affects high latitude climate; not necessarily the dominant factor; see atmospheric jet meanders
- Drivers: T&S, air-sea heat&FW fluxes, interior mixing, Southern Ocean wind
- Interior mixing via internal wave breaking, energy due to tides & topography
- Diabatic vs an adiabatic picture of the circulation
- Multiple equilibria and hysteresis, Stommel box model
- Variability mechanisms
 - Self-sustained vs. damped and stochastically-driven, Hopf bifurcation.
 - Convective oscillations, Welander flip-flop mechanism, self-sustained variability, relaxation oscillations
 - Oscillations due to advection of salinity, advective instability mechanism
 - Stochastically forced damped oscillatory mode, with phase lags between T,S and a role for the advective feedback.
 - A role for non-normal noise amplification, stochastic optimals.
 - Noise-driven jumps between steady states
 - Stochastic resonance

The End